

Gauge Theory Bootstrap: Pion amplitudes and low energy parameters

Yifei He¹, Martin Kruczenski² *

¹ Laboratoire de Physique de l'École Normale Supérieure, ENS, Université PSL,
CNRS, Sorbonne Université, Université Paris Cité, F-75005 Paris, France

² Department of Physics and Astronomy and PQSEI[†]
Purdue University, West Lafayette, IN 47907, USA.

September 17, 2024

Abstract

Following the Gauge Theory Bootstrap method proposed in our previous work [1], we compute pion scattering phase shifts for all partial waves with angular momentum $\ell \leq 3$ up to 2 GeV and calculate the low energy χ PT coefficients $\bar{\ell}_{1,2,4,6}$. The method looks for the most general S-matrix that matches at low energy the tree level amplitudes of the non-linear sigma model and at high energy, QCD sum rules and form factors. This is a theoretical/numerical calculation that uses as only data the pion mass m_π , pion decay constant f_π and the QCD parameters $N_c = 3$, $N_f = 2$, m_q and α_s . All results are in reasonable agreement with experiment. In particular, we find the $\rho(770)$, $f_2(1270)$ and $\rho(1450)$ resonances and some initial indication of particle production near the resonances. The interplay between the UV gauge theory and low energy pion physics is an example of a general situation where we know the microscopic theory as well as the effective theory of long wavelength fluctuations but we want to solve the strongly coupled dynamics at intermediate energies. The bootstrap builds a bridge between the low and high energy by determining the consistent S-matrix that matches both and provides, in this case, a new direction to understand the strongly coupled physics of gauge theories.

*E-mail: yifei.he@ens.fr, markru@purdue.edu.

[†]Purdue Quantum Science and Engineering Institute

Contents

1	Introduction	4
2	Summary of the gauge theory bootstrap	8
2.1	S-matrix/form factor bootstrap	8
2.2	Chiral symmetry breaking	10
2.3	SVZ sum rules and form factor asymptotics	12
2.4	Allowed space and extremal amplitudes	15
2.5	Unitarization and unitarity (un)saturation	17
2.6	Comment on the condensates	18
3	Phase shifts for $I = 0, 1, 2$ and $\ell \leq 3$ up to 2 GeV	19
3.1	Forward amplitudes	21
4	Low energy parameters	21
4.1	Scattering lengths and effective range parameters	22
4.2	Low energy expansion of form factors	23
4.3	Chiral Lagrangian coefficients	23
5	Resonances	25
5.1	Scalar form factor	25
5.2	The ρ meson	25
5.2.1	Pole in the $P1$ wave	26
5.2.2	Vector form factor	26
5.2.3	The $\rho(1450)$	30
5.3	The gravitational form factor and the f_2 meson	31
6	Form factors	33
6.1	Definitions	34
6.1.1	Angular momentum ℓ	34
6.1.2	The gravitational form factor	35
6.2	Asymptotic form	36
6.2.1	The gravitational form factor	40
6.2.2	Scalar form factor	41
7	Two point functions	42
7.1	Definitions	42
7.2	Asymptotic form	42

7.2.1	Two quark operators of arbitrary ℓ	43
7.2.2	Energy momentum tensor	44
7.2.3	Four quark scalar current	45
8	Numerical method	48
8.1	Kernels for partial wave computations	49
8.2	Mapping to the circle	53
8.3	Interpolation points	55
8.4	Numerical gauge theory bootstrap	58
8.5	Unitarization	63
9	Conclusions	64
10	Acknowledgements	65
A	Scattering lengths from chiral Lagrangian coefficients	66
B	Test on numerical parameters M, L	67
C	Form factors asymptotics	68
D	Some integrals	68
D.1	Feynman type integrals	68
D.2	Multi-ball integrals	69

1 Introduction

We recently proposed the Gauge Theory Bootstrap [1] a method to address the important problem of computing pion scattering amplitudes in the strongly coupled regime of asymptotically free gauge theories under the assumption that they undergo confinement and chiral symmetry breaking. In QCD language, ignoring all other interactions, the pion and the nucleons are the only stable particles. Pions, in particular, can be thought as the pseudo-Goldstone bosons of chiral symmetry breaking. Their interactions are severely restricted by symmetry considerations and their low energy effective field theory is a non-linear sigma model with coupling f_π (pion decay constant) and pion mass m_π . In pion scattering, nucleons can be ignored below the nucleon anti-nucleon threshold ~ 2 GeV. Thus, we have a UV description of the theory in terms of weakly coupled quarks and gluons and a low energy effective field theory (EFT) description in terms of weakly coupled pions. However, this is *not sufficient* to compute pion scattering since the effective pion coupling increases with the energy and the EFT description breaks down before we reach the asymptotically free regime.

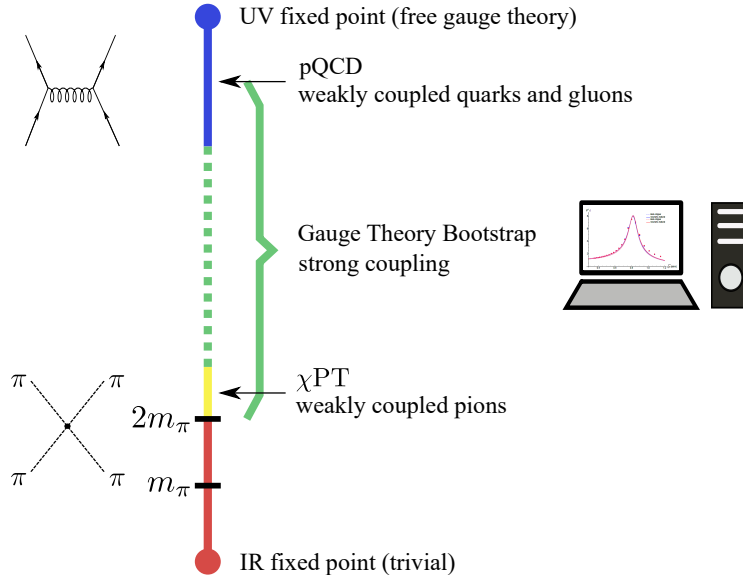


Figure 1: The Gauge Theory Bootstrap builds a (strongly coupled) bridge between the weakly coupled QCD at high energies and a weakly coupled EFT of pions at low energy.

In this intermediate regime, both the gauge theory and the theory of pions are

strongly coupled, making it an ideal target for bootstrap methods. The situation is sketched in fig.1. The Gauge Theory Bootstrap [1] addresses this problem by looking for the most general S-matrix that matches the low and high energy theories. This is done in three steps. First we parameterize the space of S-matrices and form factors that satisfy the general conditions of analyticity, crossing, unitarity and global symmetries. In order to do that we use bootstrap ideas [2, 3] as recently reformulated for the S-matrix by Paulos, Penedones, Toledo, van Rees and Vieira [4–7] and augmented by Karateev, Kuhn and Penedones [8] to incorporate form factors and current spectral densities (or vacuum polarizations).

Second, we consider that pions are the pseudo-Goldstone of chiral symmetry breaking and are described at low energy by a non-linear sigma model (Weinberg model [9]). Thus, we require that the partial waves match (within a tolerance) the tree level predictions of the non-linear sigma model. This drastically reduces the space of S-matrices and produces partial waves that, in some channels, display properties similar to experiment. A notable exception is the absence of a ρ meson resonance in the $P1$ channel, showing that pion scattering is not just a result of chiral dynamics but requires a deeper understanding of its relation to the high energy gauge theory.

Therefore, the third and final step is to introduce information about the high energy gauge theory by using the SVZ sum rules (Shifman, Vainshtein, Zakharov) [10–16] together with the high energy behavior of the form factors (from Brodsky and Lepage [17, 18]).

All these ingredients together allow to set up a numerical procedure to search for the S-matrix and compute the phase shifts of pion scattering. A Schematic of the Gauge Theory Bootstrap is depicted in fig. 2.

It is clear that, if enough conditions are imposed, we should *inevitably* find, from all S-matrices allowed by the basic constraints, the unique S-matrix that corresponds to the given UV theory. Perhaps surprisingly in the previous paper [1] we found that a small set of IR and UV constraints drastically reduce the space of allowed S-matrices leading to partial waves that qualitatively and quantitatively match the experimental results. Notice that other than symmetries and gauge theory parameters, the only input are the values of m_π and f_π . Since no experimental input on pion scattering is used, the bootstrap numerical calculation can be considered a *first principles calculation* from the pion physics point of view.

It is useful to recall how an effective field theory calculation would address the same problem. Initially we can attempt a standard perturbative calculation and start by computing tree level amplitudes using the lowest order chiral Lagrangian (sigma model). Since tree level amplitudes do not satisfy unitarity we have to incorporate

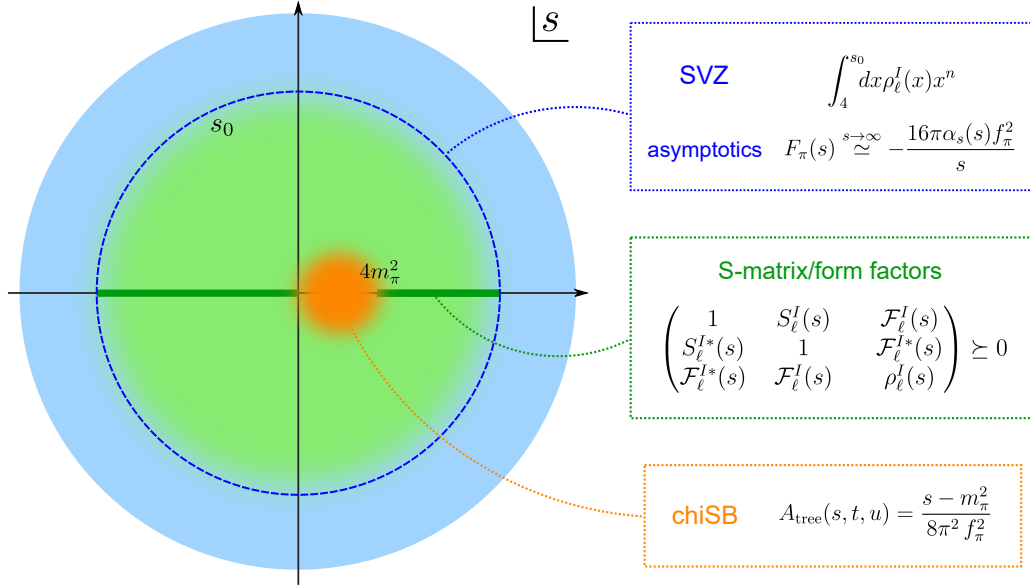


Figure 2: Schematic of the Gauge Theory Bootstrap.

loops. However the theory is non-renormalizable and we also have to add more and more counter-terms with new couplings that we do not know. In other words the UV completion is not unique. However the ambiguity is removed if we require that the theory matches QCD at high energy since the gauge theory provides the UV completion. The bootstrap shortcuts this procedure by focusing on the physically meaningful S-matrix, and allows us to pick out the one that corresponds to the given UV gauge theory. Moreover, the numerical implementation of this idea does not require expensive computations, in fact, computing the partial waves requires only a few minutes on an average PC.

In understanding why this method works and how it connects to other approaches, it is important to keep in mind that general considerations of analyticity, crossing and unitarity have played a significant role in studying pion scattering since the early days [2] and have motivated various bootstrap approaches to the problem. Indeed, phenomenological studies by Pelaez and Yndurain [19, 20] using conformal mapping and by Colangelo, Gasser and Leutwyler [21] using Roy equations have shown that the experimental phase shifts can be described in terms of analytic functions satisfying crossing and unitarity. More recently, the low energy effective field theory was extensively studied with the S-matrix bootstrap in order to put generic bounds on its parameters. In the case of massive and massless pions in [22, 23] the allowed parameter space was determined using the full constraints of unitarity, crossing and

analyticity. There is also a number of interesting related work on the large N_c limit of the effective theory using bootstrap [24–28]. For example, using the large N_c QCD positivity bootstrap, [28] found a point in the space of S-matrices that displays a full Regge trajectory. Another related topic is that the hadronic vacuum polarization or spectral densities that we consider are related to the $g - 2$ experiment (see *e.g.* the review [29]), although we cannot yet compute them with the required precision to compete for example with lattice calculations [30].

What seems particularly interesting is that, by using UV theory information, our method allows to identify the low energy S-matrix corresponding to a specific gauge theory, in some sense going back to the roots of the bootstrap program [2] which was to *compute* the S-matrix of the strong interactions. An important consequence of having such a method is that it allows a numerical exploration of different gauge theories (number of colors, quark masses, etc.) and also of different phenomena in the same theory. By including and removing constraints we can determine what physics is given by chiral symmetry alone (seemingly the S_0 and S_2 partial waves) and which is a consequence of QCD dynamics (like the ρ meson). For example removing the P_1 sum rules eliminates the ρ meson but removing the D_0 sum rule does not completely eliminate the f_2 resonance in that channel. These naive explorations that the method allow may become an important tool in understanding the interplay between the non-linear sigma model and the gauge theory.

Organization of the paper:

In section 2 we review the main idea of the method and give a short summary of its implementation. The main results are described in section 3, namely, the scattering phase shifts for partial waves with angular momentum $\ell \leq 3$ up to a center of mass energy $\sqrt{s} = 2 \text{ GeV}$. Analyzing those results in more detail allow the computation of the scattering lengths, effective range parameter, charge radii of the pion and finally the chiral Lagrangian coefficients usually denoted as \bar{l}_j following Gasser and Leutwyler [31, 32]. The results are presented in section 4. In the following section 5, we study the resonances that are evident in the phase shifts, *i.e.* $\rho(770)$, $f_2(1270)$ and $\rho(1450)$, find their masses and widths as well as couplings to pions and form factors. This completes the description of the results. For the reader interested in the perturbative QCD calculations, we include section 6 where we review the computation of the asymptotic form factor pioneered by Brodsky and Lepage [17, 18] and section 7 where we review the calculation of the two point functions that we use in the SVZ sum rules [10]. For the readers interested in the numerical procedure and reproducing the results, we provide a detailed description in section 8 and

accompanying Mathematica and Matlab notebooks with this submission.¹ Finally we give our conclusions in section 9. In the appendices we include a recalculation of the scattering lengths based on the χ PT parameters \bar{l}_j , a more detailed example of a Feynman diagram that contributes to the asymptotic form factors and some analytical integrals that are useful in the main text.

2 Summary of the gauge theory bootstrap

The basic idea of the gauge theory bootstrap is to find the S-matrix (here we concentrate on the elastic $2 \rightarrow 2$ S-matrix) of pion scattering that agrees with lowest order chiral perturbation theory at low energy and perturbative QCD at high energy. To implement this idea we follow the procedure already described in [1] but extend it to a larger range of energy and several more partial waves. In this section, we describe the main ideas of this approach and give a brief summary of its implementation. A more detailed description of the numerical method is given in section 8.

2.1 S-matrix/form factor bootstrap

We start with the basic setup where we parameterize the scattering amplitudes and form factors so that all linear constraints of analyticity, crossing and global symmetries are satisfied. Unitarity, a non-linear constraint is imposed later numerically. Thus, we consider a scattering amplitude analytic in the Mandelstam variables (s, t, u) and assume maximal (or Mandelstam) analyticity which means that we only consider singularities required by physical reasons. Those can be poles due to stable bound states (that we do not have here) and two-particle (and other multi-particle) cuts. Under this conditions we write the $2 \rightarrow 2$ pion scattering amplitude as

$$\begin{aligned}
A(s, t, u) = & T_0 + \frac{1}{\pi} \int_4^\infty dx \frac{\sigma_1(x)}{x-s} + \frac{1}{\pi} \int_4^\infty dx \sigma_2(x) \left[\frac{1}{x-t} + \frac{1}{x-u} \right] \\
& + \frac{1}{\pi^2} \int_4^\infty dx \int_4^\infty dy \frac{\rho_1(x, y)}{x-s} \left[\frac{1}{y-t} + \frac{1}{y-u} \right] \\
& + \frac{1}{\pi^2} \int_4^\infty dx \int_4^\infty dy \frac{\rho_2(x, y)}{(x-t)(y-u)}
\end{aligned} \tag{2.1}$$

¹The Mathematica program computes the coefficients needed to setup the bootstrap maximization problem. Having those, the matlab program takes ~ 20 min on an average laptop to find the partial waves.

where $s + t + u = 4$ (setting $m_\pi = 1$). The amplitude is parametrized by a constant T_0 , two single spectral densities $\sigma_{1,2}$ and two double spectral densities $\rho_{1,2}$. It satisfies the crossing condition $A(s, t, u) = A(s, u, t)$ by requiring $\rho_2(x, y) = \rho_2(y, x)$. In each isospin channel $I = 0, 1, 2$ the amplitude reads:

$$T^{I=0}(s, t, u) = 3A(s, t, u) + A(t, s, u) + A(u, t, s) \quad (2.2a)$$

$$T^{I=1}(s, t, u) = A(t, s, u) - A(u, t, s) \quad (2.2b)$$

$$T^{I=2}(s, t, u) = A(t, s, u) + A(u, t, s) \quad (2.2c)$$

Projecting onto fixed angular momentum we find the partial waves

$$f_\ell^I(s) = \frac{1}{4} \int_{-1}^1 d\cos\theta P_\ell(\cos\theta) T^I(s, t), \quad \ell = \begin{cases} \text{even}, & I = 0, 2 \\ \text{odd} & I = 1 \end{cases} \quad (2.3)$$

with

$$t = \frac{(s - 4)(1 - \cos\theta)}{2} \quad (2.4)$$

The partial waves (2.3) are analytic functions of s with cuts for $s \in (-\infty, 0) \cup (4, \infty)$. Finally, unitarity is imposed on the partial waves

$$S_\ell^I(s^+) = 1 + i\pi \sqrt{\frac{s-4}{s}} f_\ell^I(s) = \eta_\ell^I(s) e^{2i\delta_\ell^I(s)}, \quad s \in \mathbb{R}_{\geq 4} \quad (2.5)$$

as

$$\eta_\ell^I(s) = |S_\ell^I(s^+)| \leq 1, \quad s \in \mathbb{R}_{>4}, \quad \forall I, \ell \quad (2.6)$$

In addition to the scattering amplitudes, we consider the 2-particle form factors associated with gauge theory local operators \mathcal{O}_ℓ^I with same quantum numbers I, ℓ that we are considering for the partial wave (see for e.g. (2.17a), (2.18a), (2.19a) with quantum numbers $S0, P1, D0$). The form factors $F_\ell^I = \langle \pi\pi | \mathcal{O}_\ell^I | 0 \rangle$ (see more details in section 6.1) are analytic functions of one complex variable with a cut on the real axis $(4, \infty)$. Assuming convergence with one subtraction, the form factors can be parametrized by their imaginary part on the real axis

$$F_\ell^I(s) = 1 + \frac{1}{\pi} \int_4^\infty dx \left(\frac{1}{x-s} - \frac{1}{x} \right) \text{Im} F_\ell^I(x) \quad (2.7)$$

where we use the condition $F_\ell^I(0) = 1$ (otherwise we change the constant). The two point function, i.e., vacuum polarization $\Pi_\ell^I(s)$ of the operator \mathcal{O}_ℓ^I itself has the same analytic structure with a cut $s \geq 4$ and the discontinuity across the cut defines the spectral density $\rho_\ell^I(x), x \in (4, \infty)$. See section 7.1 for more details.

As initially discussed by Karateev, Kuhn and Penedones [8] (see also [1] in this context), the amplitudes $S_\ell^I(s)$, the rescaled form factors $\mathcal{F}_\ell^I(s)$ (see section 6.1) and the spectral density $\rho_\ell^I(s)$ obey the positivity condition

$$\begin{pmatrix} 1 & S_\ell^I(s) & \mathcal{F}_\ell^I(s) \\ S_\ell^{I*}(s) & 1 & \mathcal{F}_\ell^{I*}(s) \\ \mathcal{F}_\ell^{I*}(s) & \mathcal{F}_\ell^I(s) & \rho_\ell^I(s) \end{pmatrix} \succeq 0, \quad s > 4, \quad \forall \ell, I \quad (2.8)$$

Thus, we define the variables of the gauge theory bootstrap procedure:

$$\{T_0, \sigma_{\alpha=1,2}(x), \rho_{\alpha=1,2}(x, y), \text{Im}F_\ell(x), \rho_\ell^I(x)\}, \quad x, y \in (4, \infty), \forall \ell, I \quad (2.9)$$

For implementation, we choose a discrete set of points $x_{j=1\dots M}$ and define a discrete set of $\mathbf{M} \sim M^2$ real variables

$$[T_0, \sigma_{\alpha=1,2}(x_j), \rho_{\alpha=1,2}(x_{j_1}, x_{j_2}), \text{Im}F_\ell^I(x_j), \rho_\ell^I(x_j)] \in \mathbb{R}^{\mathbf{M}} \quad (2.10)$$

for some \mathbf{M} usually large ($\sim 5,000$ in our numerics). The set of constraints defines a convex space in $\mathbb{R}^{\mathbf{M}}$ of scattering amplitudes, form factors and spectral densities that satisfy the most generic constraints; a space that we want to explore. We give the detailed numerical method for this implementation in section 8.

2.2 Chiral symmetry breaking

The low energy description of QCD is in terms of a theory of pions, the pseudo Goldstone bosons of chiral symmetry breaking. It should be noted that, in our calculation, we only use as input the Weinberg model [9] that gives an amplitude $A(s, t, u) = \frac{s-m_\pi^2}{8\pi^2 f_\pi^2}$. However, it is useful to set up the calculation in the context of the full chiral perturbation theory framework initiated by Gasser and Leutwyler [31] to better understand the results and the relation to other approaches.

At lowest order in derivatives, the chiral Lagrangian with sources is

$$\mathcal{L}_2 = \frac{f_\pi^2}{4} \text{Tr}[D_\mu U D^\mu U^\dagger] + \frac{f_\pi^2}{4} \text{Tr}(\chi U^\dagger + U \chi^\dagger) \quad (2.11)$$

where $U(x) = e^{\frac{i\pi_a \tau_a}{f_\pi}} \in SU(2)$ parameterizes a 3-sphere, the coset space $SU(2)_L \times SU(2)_R / SU(2)_V$. At this level, the only low energy parameters are the pion decay constant f_π and the pion mass m_π that is introduced by taking $\chi = m_\pi \mathbb{1}_{2 \times 2}$. The pion decay constant f_π is defined in terms of the matrix element of the axial current

$$\langle 0 | j_5^{I,\mu}(x) | \pi^{I'}(p) \rangle = -ip^\mu f_\pi \delta^{II'} e^{-ipx} \quad (2.12)$$

and can therefore be determined independently from weak pion decay. If one goes to higher energy, new terms appear such as

$$\begin{aligned}
\mathcal{L}_4 = & \frac{l_1}{4} \{ \text{Tr}[D_\mu U (D^\mu U)^\dagger] \}^2 + \frac{l_2}{4} \text{Tr}[D_\mu U (D_\nu U)^\dagger] \text{Tr}[D^\mu U (D^\nu U)^\dagger] \\
& + \frac{l_3}{16} [\text{Tr}(\chi U^\dagger + U \chi^\dagger)]^2 + \frac{l_4}{4} \text{Tr}[D_\mu U (D^\mu \chi)^\dagger + D_\mu \chi (D^\mu U)^\dagger] \\
& + l_5 \left[\text{Tr}(f_{\mu\nu}^R U f_L^{\mu\nu} U^\dagger) - \frac{1}{2} \text{Tr}(f_{\mu\nu}^L f_L^{\mu\nu} + f_{\mu\nu}^R f_R^{\mu\nu}) \right] \\
& + i \frac{l_6}{2} \text{Tr}[f_{\mu\nu}^R D^\mu U (D^\nu U)^\dagger + f_{\mu\nu}^L (D^\mu U)^\dagger D^\nu U] \\
& - \frac{l_7}{16} [\text{Tr}(\chi U^\dagger - U \chi^\dagger)]^2
\end{aligned} \tag{2.13}$$

as described in [31,33] that the reader can consult for a more detailed description. Let us just note that we omitted contact terms that do not depend on U and that $f_{\mu\nu}^{R,L}$ are the field strengths associated with the external spectator gauge fields (sources). In the usual approach the couplings $l_{1...7}$ are determined from experiment, for example $l_{1,2}$ are related to the scattering lengths of the D -waves and $l_{4,6}$ to the scalar and vector charge radius of the pion. More recently, positivity methods have been used to put generic bounds on those parameters (see *e.g.* [24]). On the other hand, in our gauge theory bootstrap approach, these parameters are *calculable*. In this paper we determine $\bar{l}_{1,2,4,6}$, the renormalized values of the couplings (l_j in \mathcal{L}_4 are divergent bare couplings).

Being able to compute (approximately) the low energy couplings is already quite interesting progress. However, the EFT becomes strongly coupled as we increase the energy and predictions become unreliable long before we reach the asymptotically free regime. For example the ρ resonance in the $P1$ channel will not appear from the EFT. In fact, the main purpose of this and the previous paper [1] is to find the phase shifts in that region by using gauge theory input.

We want to emphasize that, from the point of view of pion physics, the bootstrap calculation is a *first principles* calculation of pion scattering. Usually what that means is that we compute pion scattering starting from a given Lagrangian or Hamiltonian. In this case the Lagrangian is \mathcal{L}_2 that contains the pion mass m_π and coupling f_π . Using this Lagrangian, however, is not sufficient since it has to be supplemented by an infinite number of higher derivative terms with unknown couplings that have to be measured. Instead of doing that, we use the information that pions describe the low-energy dynamics of a gauge theory (QCD). In that way we do not require any extra experimental input for the computation.

Now let's see how we incorporate the Lagrangian \mathcal{L}_2 in the bootstrap. At tree level \mathcal{L}_2 determines the function $A(s, t, u)$ in (2.1) to be

$$A_{\text{tree}}(s, t, u) = \frac{s - m_\pi^2}{8\pi^2 f_\pi^2} \quad (2.14)$$

This was already derived by Weinberg [9] and later confirmed by experiment even before the advent of QCD [34]. In our case we want to consider amplitudes that satisfy the generic constraints of the previous subsection and that match this low energy behavior. It turns out to be more convenient to put the constraints in terms of the partial waves that we want to compute. We also expect this tree level computation (linearized approximation) to be better at small values of s , in particular in the unphysical region $0 < s < 4$ where the partial waves are real. The only non-zero tree level partial waves are (see *e.g.* [35]):

$$f_{0,\text{tree}}^0(s) = \frac{2}{\pi} \frac{2s - m_\pi^2}{32\pi f_\pi^2}, \quad f_{1,\text{tree}}^1(s) = \frac{2}{\pi} \frac{s - 4m_\pi^2}{96\pi f_\pi^2}, \quad f_{0,\text{tree}}^2(s) = \frac{2}{\pi} \frac{2m_\pi^2 - s}{32\pi f_\pi^2} \quad (2.15)$$

To implement this low energy match, we choose a small set of points s_j in the very low energy unphysical region $0 < s \leq 2$, and require that

$$\begin{aligned} \|f_0^0(s_j) - R_{01}^{\text{tree}}(s_j)f_1^1(s_j)\| &\leq \epsilon^\chi, \\ \|f_0^2(s_j) - R_{21}^{\text{tree}}(s_j)f_1^1(s_j)\| &\leq \epsilon^\chi, \\ R_{01}^{\text{tree}} &= \frac{f_{0,\text{tree}}^0}{f_{1,\text{tree}}^1}, \quad R_{21}^{\text{tree}} = \frac{f_{0,\text{tree}}^2}{f_{1,\text{tree}}^1} \end{aligned} \quad (2.16)$$

with some norm and a tolerance ϵ^χ . Note that the expressions 2.16 use only the ratios of the tree level partial waves which eliminate the f_π so the matching applies to arbitrary f_π . For each given tolerance this drastically reduces the convex space of amplitudes inside $\mathbb{R}^{\mathbf{M}}$ defined by the generic constraints in the previous step. Finally, we use the physical value of $f_\pi = 92$ MeV to choose an appropriate tolerance ϵ^χ for our computation. The precise description of how to implement these constraints is given in section 8.

2.3 SVZ sum rules and form factor asymptotics

Even after significantly reducing the allowed space using low energy information, there is still a large number of allowed S-matrices, each of which may (or may not) correspond to (different) consistent UV completions. For our purpose of determining

the strongly coupled dynamics of the gauge theory, we need to incorporate high energy information, and this is done by constraining spectral densities and form factors variables in (2.10). In order to do that we choose a scale s_0 where we assume the theory is properly described at least approximately² by perturbative QCD. In our previous paper we took $\sqrt{s_0} = 1.2 \text{ GeV}$ and here we take $\sqrt{s_0} = 2 \text{ GeV}$. An important test of the method is that, below 1.2 GeV the phase shifts agree with the previously computed ones. If $\sqrt{s_0}$ were setting the energy scale of all features (*e.g.* resonances), a factor of almost 2 in $\sqrt{s_0}$ should be quite noticeable.

Having chosen s_0 , we impose constraints on the spectral density given by a finite energy version of the Shifman, Vainshtein, Zakharov (SVZ) sum rules [10] and constraints on the asymptotic behavior of the form factors as given by Brodsky and Lepage [17]. Notice that this asymptotic behavior of the form factors should be reached at very high energies and therefore we use it for initial guidance as described in the numerical section 8. Below, we give a brief summary of the form factors and spectral densities with quantum numbers $S0$ (scalar current), $P1$ (vector current) and $D0$ (energy momentum tensor) we use in this paper. The relevant quantities are properly defined in more detail later in sections 6.1 and 7.1. Here we simply present the definitions of the current $j_\ell^I(x)$, their two-particle form factor $F_\ell^I(s)$ with definite angular momentum and rescaled form factor \mathcal{F}_ℓ^I with definite angular momentum and isospin. We also present the large s (short distance) expansion of the two-point function $\Pi_\ell^I(s)$ leading to the SVZ sum rules on ρ_ℓ^I as well as the asymptotic form of the form factors. The detailed computations are given in sections 6 and 7³.

$S0$

$$j_0^0 = m_q(\bar{u}u + \bar{d}d) \quad (2.17a)$$

$$\langle \pi^+(p_1) \pi^-(p_2) | j_0^0 | 0 \rangle = F_0^0(s) \quad (2.17b)$$

$$F_0^0(0) = 1 \quad (2.17c)$$

$$\langle I=0, P\ell\sigma | j_0^0 | 0 \rangle = \delta_{\ell 0} \delta_{\sigma 0} \mathcal{F}_0^0(s) \quad (2.17d)$$

$$\mathcal{F}_0^0(s) = \frac{\sqrt{6}\pi}{16\pi^3} \frac{1}{s^{\frac{1}{4}}} \left(\frac{s-4}{4} \right)^{\frac{1}{4}} F_0^0(s) \quad (2.17e)$$

$$\Pi_0^0(s) \simeq -\frac{N_f m_q^2}{(2\pi)^4} \frac{3}{8\pi^2} \left(1 + \frac{13}{3} \frac{\alpha_s}{\pi} \right) s \ln \left(-\frac{s}{\mu^2} \right) \quad (2.17f)$$

²Since going to very large energies is challenging numerically due to the larger number of interpolation points required, we make a compromise in choosing s_0 .

³We were not able to find in the literature the computation of the scalar form factor so we include a crude estimate (up to numerical factors).

$$\frac{1}{s_0^{n+2}} \int_4^{s_0} \rho_0^0(x) x^n dx \simeq \frac{N_f m_q^2}{(2\pi)^4} \frac{3}{4\pi(n+2)} \left(1 + \frac{13}{3} \frac{\alpha_s}{\pi}\right), \quad n \geq 0 \quad (2.17g)$$

$$|F_0^0(s)| \sim 4\pi\alpha_s f_\pi^2 \frac{m_q^2}{s} \ln\left(\frac{s}{m_\pi^2}\right), \quad (s \rightarrow \infty) \quad (2.17h)$$

P1

$$j_1^1 = \frac{1}{2}(\bar{u}\gamma_+ u - \bar{d}\gamma_+ d) \quad (2.18a)$$

$$\langle \pi^+(p_1) \pi^-(p_2) | j_{1,\mu}^1 | 0 \rangle = (p_{2,\mu} - p_{1,\mu}) F_1^1(s) \quad (2.18b)$$

$$F_1^1(0) = 1 \quad (2.18c)$$

$$\langle I = 1, P\ell\sigma | j_1^1 | 0 \rangle = \delta_{\ell 1} \delta_{\sigma 1} \mathcal{F}_1^1(s) \quad (2.18d)$$

$$\mathcal{F}_1^1(s) = \sqrt{\frac{4\pi}{3}} \frac{1}{8\pi^3} \frac{1}{s^{\frac{1}{4}}} \left(\frac{s-4}{4}\right)^{\frac{3}{4}} F_1^1(s) \quad (2.18e)$$

$$\Pi_1^1(s) \simeq -\frac{1}{(2\pi)^4} \frac{1}{8\pi^2} \left(1 + \frac{\alpha_s}{\pi}\right) s \ln\left(-\frac{s}{\mu^2}\right) \quad (2.18f)$$

$$\frac{1}{s_0^{n+2}} \int_4^{s_0} \rho_1^1(x) x^n dx \simeq \frac{1}{(2\pi)^4} \frac{1}{4\pi(n+2)} \left(1 + \frac{\alpha_s}{\pi}\right), \quad n \geq -1 \quad (2.18g)$$

$$|F_1^1(s)| \simeq 16\pi \frac{\alpha_s f_\pi^2}{s}, \quad (s \rightarrow \infty) \quad (2.18h)$$

D0

$$j_2^0 = T^{++}(0) \quad (2.19a)$$

$$\langle \pi^+(p_1) \pi^-(p_2) | j_2^0 | 0 \rangle = 4|\vec{p}_1|^2 \sqrt{\frac{2\pi}{15}} Y_{22}(\hat{p}_1) F_2^0(s) \quad (2.19b)$$

$$F_2^0(s) = 1 \quad (2.19c)$$

$$\langle I = 0, P\ell\sigma | j_2^0 | 0 \rangle = \delta_{\ell 2} \delta_{\sigma 2} \mathcal{F}_2^0(s) \quad (2.19d)$$

$$\mathcal{F}_2^0(s) = \frac{1}{4\pi^3} \sqrt{\frac{3\pi}{15}} \frac{1}{s^{\frac{1}{4}}} \left(\frac{s-4}{4}\right)^{\frac{5}{4}} F_2^0(s) \quad (2.19e)$$

$$\Pi_2^0(s) \simeq -\frac{1}{(2\pi)^4} \frac{1}{8\pi^2} \left(\frac{11}{10} - \frac{17}{18} \frac{\alpha_s}{\pi}\right) s^2 \ln\left(-\frac{s}{\mu^2}\right) \quad (2.19f)$$

$$\frac{1}{s_0^{n+3}} \int_4^{s_0} \rho_2^0(x) x^n dx \simeq \frac{1}{(2\pi)^4} \frac{1}{4\pi} \frac{1}{n+3} \left(\frac{11}{10} - \frac{17}{18} \frac{\alpha_s}{\pi} \right), \quad n \geq -2 \quad (2.19g)$$

$$|F_2^0(s)| \simeq \frac{48\pi\alpha_s f_\pi^2}{s}, \quad (s \rightarrow \infty) \quad (2.19h)$$

In these formulas, $+$ indicates the component of a vector $v_+ = \frac{1}{\sqrt{2}}(v_1 - iv_2)$, also $P = p_1 + p_2$ and $s = P^2$. Equivalently, as we do later, we can contract all currents with a vector $\Delta = \frac{1}{\sqrt{2}}(0, 1, i, 0)$.

We implement the SVZ sum rules (2.17g), (2.18g), (2.19g) as constraints on the spectral densities. It is worth noting that the SVZ expansion of the two point functions contains expectation values (condensates) of higher order operators that we do not include in (2.17f), (2.18f), (2.19f) because they are suppressed by the large energy scale s_0 . We comment on this further in section 2.6. The precise implementation of the sum rules is described in section 8.

For the numerical computation to work we have to take into account that the form factors vanish at infinity as predicted by QCD. In practice, we require that the form factors above the energy scale s_0 are small, with an initial estimate of their value following from the asymptotic forms (2.17h), (2.18h) and (2.19h). More details of this are given in section 8.

2.4 Allowed space and extremal amplitudes

We started by discretizing the variables and parameterizing the amplitudes/form factors by a point in $\mathbb{R}^{\mathbf{M}}$ for some large $\mathbf{M} \sim 5,000$. After imposing many constraints, the dimension and volume of such space is considerably reduced. At this point we hope that the set of remaining points describe similar S-matrices but how do we focus on one? A common practice of the bootstrap is to project the space onto a lower dimensional subspace [36], for example a plane. In that subspace we plot the “shadow” or projection of the higher dimensional space. Intuitively, the edges or boundaries of the shadow will lift to unique points on the boundary of the higher dimensional space. Such a point corresponds to a set of bootstrap variables that describe a particular extremal amplitudes/form factors living on the boundary of the space. Finding the boundary of the region can be done by maximizing linear functionals of the bootstrap variables. While this idea was used extensively in the pure S-matrix bootstrap to put generic bounds on certain physical quantities, here we do not consider these linear functionals to carry specific physical meanings, but we use

them simply as a way to access scattering amplitudes/form factors on the boundary of the allowed space under constraints. The naive belief is that given enough physical conditions from low energy and high energy, there is eventually a unique (within errors) physical amplitude that matches these physical requirement as well as bootstrap consistency conditions. Although, ideally, the specific functional used to find this amplitude should be irrelevant, in practice we have to choose functionals that include relevant physical information and lead to a well defined numerical problem. In this work, we consider two linear functionals (related to the forward amplitudes):⁴

$$\mathfrak{F}_0 = 2(f_0^0(s=3) + 5f_2^0(s=3)), \quad \mathfrak{F}_1 = 2(3f_1^1(s=3) + 7f_3^1(s=3)) \quad (2.20)$$

Preliminary tests on other similar functionals give similar results and we hope to report on a full exploration of this aspect in the future. The space of amplitudes projected out on the two dimensional space characterized by (2.20) is given in figure 3. The region inside the green shape is allowed by the constraints but no specific amplitude is associated with the interior points (there are many for each point). On the other hand, each green dot at the boundary *is* associated with a particular extremal amplitude/form factor and therefore we choose among them the one that we expect to represent the correct amplitude. In order to do that we use the physical value $f_\pi = 92 \text{ MeV}$ as follows: The black line indicates the values of $\mathfrak{F}_0, \mathfrak{F}_1$ for the Weinberg model or χ PT tree level amplitudes (2.15) evaluated for different values of f_π . The black dot corresponds to $f_\pi = 92 \text{ MeV}$, namely the initial approximation we start with. Using this input it is then natural to focus on the points closest to the black dot (the blue and red points) and take the corresponding amplitudes as the result of our computation. It is worth pointing out that the points at the lower edge could be alternative candidates but these amplitudes appear to display numerical instabilities where the sum rules are satisfied by discontinuous jumps near threshold. This could indicate that the sum rules cannot be satisfied with smooth functions and these points might be excluded from a more involved numerical implementation. In any case, the upper edge points (blue and red) do not seem to suffer from that problem and satisfy the sum rules by displaying resonances as physically expected. For that reason, from now on, we concentrate on the S-matrices associated with the blue and red points on the upper edge and continue our analysis in the following sections. For future improvement, we expect that a more precise identification can be made by evaluating f_π for each of the boundary points, potentially by incorporating

⁴This is a slight modification of the functionals $f_0^0(s=3), f_1^1(s=3)$ we used in previous work [1] to include some contributions from the D and F partial waves.

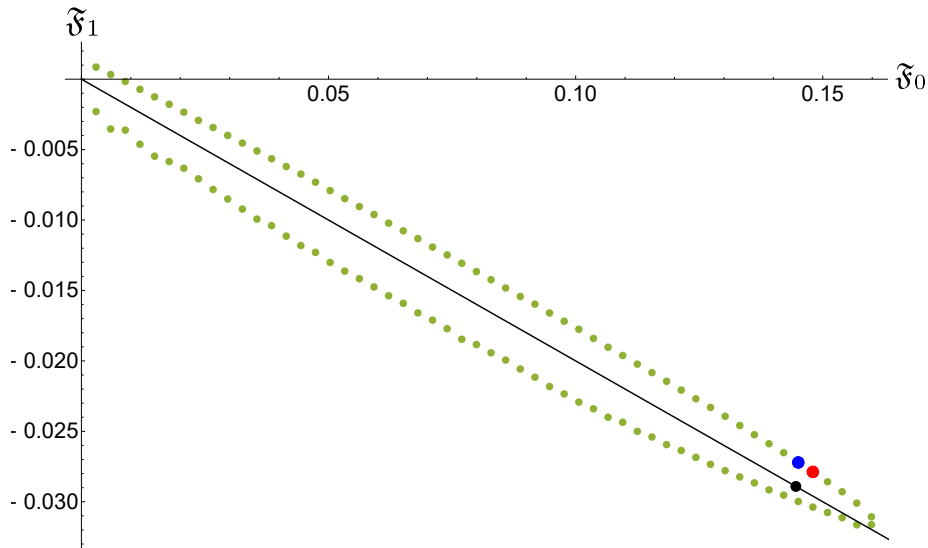


Figure 3: The projected space of amplitudes characterized by two linear functionals (2.20) in the gauge theory bootstrap. The black line indicates the two functionals evaluated using tree level amplitudes whereas the black dot is for the physical value $f_\pi = 92$ MeV, the initial approximation we start with. We take two points (blue and red) on the boundary of the allowed space closest to the black point.

the matrix element of the axial current (2.12) into the bootstrap setup. We leave this interesting exploration for later work.

2.5 Unitarization and unitarity (un)saturation

The bootstrap procedure looks for S-matrices that are at the boundary of the allowed space. Since the boundary is given by unitarity saturation, the S-matrices that we find normally saturate unitarity. When the problem is more complex, as in this case, the maximization can stop before the partial waves saturate unitarity. If that is the case, we perform one extra step that we call unitarization. This procedure was already done in [37] in the case of 2d models. It consists in writing a new functional based on linearized unitarity constraint and perform one last optimization, which we will describe in detail in section 8. It is relatively easy to see that this last step moves the partial waves closer to saturate unitarity. In some cases unitarity non-saturation still remains and we consider that an indication that the actual theory does not saturate unitarity and there is particle production. Below, in section 3, we will see this happens near the f_2 resonance in the $D0$ channel.

Note that, experimentally, elastic pion scattering saturates unitarity up to energies of order 1.2 GeV. Although it is not completely clear why this is so, it agrees very nicely with the results obtained from the bootstrap. It is also interesting to consider that particle production can happen through an intermediate resonance. The ρ meson for example decays into two pions basically 100% of the time but the $f_2(1270)$ resonance decays into two pions only 84% of the time and then mostly into four pions. Going higher in energy we have for example the $\rho_3(1690)$ in the $F1$ channel ⁵ that decays into 2 pions only 24% of the time and the rest mostly into four pions. Going to this higher energy regime would then require understanding particle production, something that we leave for later work.

2.6 Comment on the condensates

One important point of the original SVZ proposal was the existence of the quark condensate $m_q \langle 0 | \bar{q}q | 0 \rangle$ and gluon condensate or equivalently expectation value of the trace of the energy momentum tensor $\langle 0 | T_\mu^\mu | 0 \rangle$ that contribute to the sum rules. This was taken into account by using the OPE of the currents:

$$T\{j(x)j(0)\} = C_{\mathbb{1}}(x) \mathbb{1} + \sum_{\mathcal{O}} C_{\mathcal{O}}(x) \mathcal{O}(0) \quad (2.21)$$

and realizing that, when taking expectation value in the symmetry broken vacuum, other operators contribute. Thus, the SVZ expansion is

$$\langle 0 | T\{j(x)j(0)\} | 0 \rangle = C_{\mathbb{1}}(x) + C_{\bar{q}q}(x) \langle 0 | j_S(0) | 0 \rangle + C_{G^2}(x) \langle 0 | \frac{\alpha_s}{\pi} G_{\mu\nu}^a G^{a\mu\nu} | 0 \rangle + \dots \quad (2.22)$$

where $j_S = m_q(\bar{u}u + \bar{d}d)$. The expectation value $\langle 0 | \frac{\alpha_s}{\pi} G_{\mu\nu}^a G^{a\mu\nu} | 0 \rangle$ can be written in terms of the quark condensate and the trace of $T_{\mu\nu}$. These condensates play an important role in the SVZ approach similar to the low energy EFT coefficients l_j do in chiral perturbation theory, they have to be determined from experiment (or lattice). However, in the finite energy sum rules that we used in the bootstrap their contribution is suppressed by inverse powers of the QCD matching scale s_0 and we ignore them in the computational setup. The idea is the same as for l_j , namely that fitting the high energy to the bootstrap we should find that corrections are required and thus the condensates should be *calculable* in the bootstrap. At the moment our precision is not enough for that so we leave this interesting topic for future work. Notice that this is an improvement on paper [1] where we used condensate values as parameters taken from the literature (although they did not affect the numerics).

⁵that we do not yet see in our numerics due to lack of resolution at higher energy.

3 Phase shifts for $I = 0, 1, 2$ and $\ell \leq 3$ up to 2 GeV

Now we apply the procedure to QCD. In this case we consider an $SU(3)$ gauge theory with two quarks of the same mass much lower than the QCD scale. We extend the energy range from 1.2 GeV in our previous paper [1] to 2 GeV in this paper. Keep in mind that at 2 GeV, our input from perturbative QCD for the form factors and spectral densities should be more precise. As described in section 2.4, we take two points (blue and red) in figure 3 near the black dot that indicates the Weinberg model (tree level χ PT) and examine the corresponding six partial waves $S0$, $D0$, $S2$, $D2$, $P1$, and $F1$. The results for the phase shifts δ_ℓ^I and inelasticity η_ℓ^I are plotted in fig.4, where the blue and red points correspond to the points in fig. 3 of the same color. We also plot together the experimental data (gray dots) from [38–40] and phenomenological fits (gray lines) from [19] for comparison. In this figure, the horizontal axis indicates the center of mass energy \sqrt{s} in GeV.

In addition to the reasonable overall agreement with experiments, it is worth noting several points. First, the experimental data in the $S0$ channel includes Kaon production leading to a rise of the phase shift around 1 GeV which we do not expect to reproduce as we are not considering the strange quark. Therefore, the phenomenological fit plot for $S0$ is done using the parametrization [19] with the Kaon production removed. Second, note that although the energy range was extended from 1.2 GeV to 2 GeV, the SVZ sum rules and the form factor asymptotics still determine the $\rho(770)$ meson to be near its physical value. This is further confirmation that our framework does not rely on the s_0 scale we choose. With this extension to 2 GeV, we now see a clear $f_2(1270)$ meson resonance in the $D0$ channel. Moreover, the $P1$ channel contains another phase rise at $\simeq 1.6$ GeV (the phase shift values are plotted modulo π) corresponding to another resonance which should be identified with $\rho(1450)$. See section 5.2.3 below for more details. It is interesting to notice also the potential particle productions at the energy of the $f_2(1270)$ ($D0$ channel) and $\rho(1450)$ ($P1$ channel), in agreement with experiments. Away from threshold the agreement in the $D2$ and $F1$ channels is poor but the phase shifts are small and the experimental data on these channels is confusing.

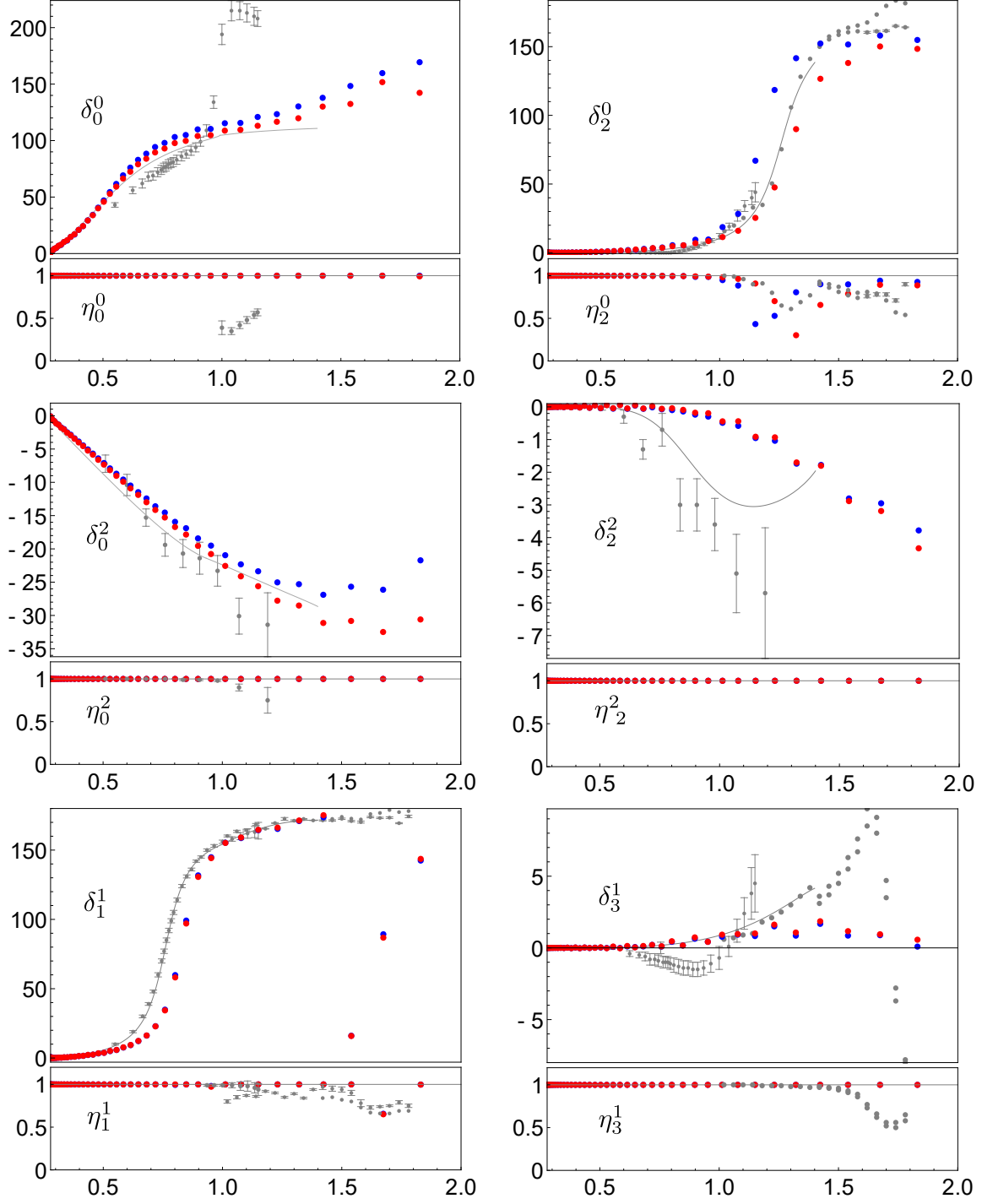


Figure 4: Phase shifts δ_ℓ^I and inelasticity η_ℓ^I from GTB comparing with experiments [38–40] and phenomenological fit [19]. Horizontal axis is \sqrt{s} in GeV. See text.

3.1 Forward amplitudes

The forward amplitudes (zero scattering angle or $t = 0$) combine all partial waves and presumably display Regge behavior at larger energies than the ones considered here. In fig. 5 we plot the amplitudes $T_{0+}(s, 0)$, $T_{00}(s, 0)$, $T^{I_t=1}(s, 0)$ that are $s \leftrightarrow u$ symmetric (or anti-symmetric). In terms of the fixed isospin amplitudes they read

$$T_{0+} \equiv T(\pi^0 \pi^+ \rightarrow \pi^0 \pi^+) = \frac{1}{2} T^{I_s=1} + \frac{1}{2} T^{I_s=2} \quad (3.1a)$$

$$T_{00} \equiv T(\pi^0 \pi^0 \rightarrow \pi^0 \pi^0) = \frac{1}{3} T^{I_s=0} + \frac{2}{3} T^{I_s=2} \quad (3.1b)$$

$$T^{I_t=1} = \frac{1}{3} T^{I_s=0} + \frac{1}{2} T^{I_s=1} - \frac{5}{6} T^{I_s=2} \quad (3.1c)$$

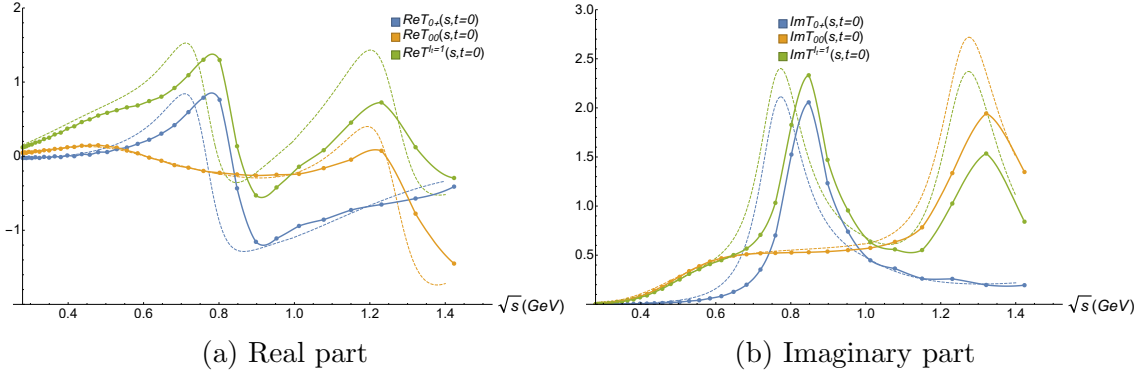


Figure 5: Real and Imaginary parts of the forward amplitudes corresponding to the red point in fig.3 (points and solid interpolating lines) and the phenomenological analysis of Pelaez and Yndurain (dashed) [19] with Kaon production removed.

4 Low energy parameters

In the previous section we showed that we find good agreement between the computed phase shifts and the experimental ones. Thus we might expect that all quantities agree. Although this way of thinking is generically correct, low energy parameters like scattering lengths a_ℓ^I , effective range parameters b_ℓ^I and higher order chiral Lagrangian coefficients \bar{l}_j have sensitive dependence on the detail structure of the amplitudes near threshold and might not necessarily agree with experiment. In this section we analyze these quantities in detail.

4.1 Scattering lengths and effective range parameters

Near threshold, the scattering is usually characterized by the scattering length and the effective range parameters defined through an expansion of the real part of the partial waves:

$$\text{Re}f_\ell^I(s) \stackrel{k \rightarrow 0}{\simeq} k^{2\ell}(a_\ell^I + b_\ell^I k^2 + \dots), \quad k = \frac{\sqrt{s - 4m_\pi^2}}{2} \quad (4.1)$$

One success of the Weinberg model (2.14) was that it gave reasonable values for the S_0 , S_2 and P_1 scattering lengths. However, as explained in section 2.2 the gauge theory bootstrap does not impose matching with the Weinberg model very close to threshold and therefore, the scattering lengths for those and the other partial waves resulting from the computation may or may not agree with experimental values. We displayed the results in table 1 that includes the Weinberg model (W) (2.14), the Gauge Theory Bootstrap (GTB), and the phenomenological results of Colangelo, Gasser and Leutwyler (CGL) [21], and Pelaez and Yndurain (PY) [19]. The blue and red colors correspond to results from the blue and red points depicted in fig.3.

	W	GTB	CGL	PY
$a_0^{(0)}$	0.16	0.178, 0.182	0.220 ± 0.005	0.230 ± 0.010
$a_0^{(2)}$	-0.046	-0.0369, -0.0378	-0.0444 ± 0.0010	-0.0422 ± 0.0022
$b_0^{(0)}$	0.18	0.287, 0.290	0.280 ± 0.001	0.268 ± 0.010
$b_0^{(2)}$	-0.092	-0.064, -0.066	-0.080 ± 0.001	-0.071 ± 0.004
$a_1^{(1)}$	31	28.0, 28.4	37.0 ± 0.13	$38.1 \pm 1.4 (\times 10^{-3})$
$b_1^{(1)}$	0	2.86, 3.37	5.67 ± 0.13	$4.75 \pm 0.16 (\times 10^{-3})$
$a_2^{(0)}$	0	12.6, 12.3	17.5 ± 0.3	$18.0 \pm 0.2 (\times 10^{-4})$
$a_2^{(2)}$	0	2.87, 2.81	1.70 ± 0.13	$2.2 \pm 0.2 (\times 10^{-4})$

Table 1: Scattering lengths and effective range parameters in units of m_π . Red and blue correspond to the amplitudes at points in fig.3 with the same color and the others are phenomenological results as described in the text.

4.2 Low energy expansion of form factors

Since the gauge theory bootstrap also computes the form factors, it is interesting to obtain their low energy expansion given by

$$F_0^0(s) = F_0^0(0) \left[1 + \frac{1}{6} s \langle r^2 \rangle_S^\pi + \dots \right] \quad (4.2)$$

$$F_1^1(s) = 1 + \frac{1}{6} s \langle r^2 \rangle_V^\pi + \dots \quad (4.3)$$

where $\langle r^2 \rangle_{S,V}^\pi$ are the scalar and vector charge radius of the pion. Recall that $F_0^0(0) = 1$ in our units where $m_\pi = 1$. The result for the charge radius is displayed in table 2 together with the values derived from experiment [21, 41, 42].

	GTB	Exp. fits
$\langle r^2 \rangle_S^\pi$	0.64, 0.61	$0.61 \pm 0.04 \text{ fm}^2$
$\langle r^2 \rangle_V^\pi$	0.388, 0.381	$0.439 \pm 0.008 \text{ fm}^2$

Table 2: Pion scalar $\langle r^2 \rangle_S^\pi$ and vector $\langle r^2 \rangle_V^\pi$ (or electromagnetic) radii.

4.3 Chiral Lagrangian coefficients

As mentioned in section 2.2, the EFT method provides a compact way to organize the results in terms of the coefficients of the most general Lagrangian compatible with the symmetries (2.13). Usually, these coefficients are determined by comparison with experiment. More recently there has been a large effort in using positivity methods to put generic bounds on them. With the gauge theory bootstrap we have a scheme to actually compute such coefficients based on self-consistency conditions (bootstrap) and gauge theory input. The results are given in table 3. As described in the previous subsections, we have obtained the D -waves scattering lengths and the pion scalar and vector radii. Therefore, we can obtain the chiral Lagrangian coefficients $\bar{l}_{1,2,4,6}$ from

the formulas [31, 33]

$$a_{D0} = \frac{1}{1440\pi^3 f_\pi^4} \left\{ \bar{l}_1 + 4\bar{l}_2 - \frac{53}{8} \right\} + \dots \quad (4.4)$$

$$a_{D2} = \frac{1}{1440\pi^3 f_\pi^4} \left\{ \bar{l}_1 + \bar{l}_2 - \frac{103}{40} \right\} + \dots \quad (4.5)$$

$$F_0^0(s) = 1 + \frac{s}{16\pi^2 f_\pi^2} \left(\bar{l}_4 - \frac{13}{12} \right) + \dots \quad (4.6)$$

$$F_1^1(s) = 1 + \frac{s}{96\pi^2 f_\pi^2} (\bar{l}_6 - 1) + \dots \quad (4.7)$$

With the values shown in table 1 and table 2, we find

	GTB	GL	Bij	CGL
\bar{l}_1	0.92, 0.93	-2.3 ± 3.7	-1.7 ± 1.0	-0.4 ± 0.6
\bar{l}_2	4.1, 4.0	6.0 ± 1.3	6.1 ± 0.5	4.3 ± 0.1
\bar{l}_4	4.7, 4.6	4.3 ± 0.9	4.4 ± 0.3	4.4 ± 0.2
\bar{l}_6	14.3, 14.1	16.5 ± 1.1	$16.0 \pm 0.5 \pm 0.7$	

Table 3: Low energy parameters computed using gauge theory bootstrap (GTB) and phenomenological values (see text). The coefficient \bar{l}_1 is challenging to evaluate and very sensitive to the D -wave scattering lengths.

These values may be used to recompute the scattering lengths and effective range parameters to compare with the ones directly extracted in table 1 as a consistency check. See appendix A. In table 3, we also displayed the results compiled in [33] from Gasser and Leutwyler (GL) [31], Bijmans et al. (Bij) [43–45] and Colangelo et al. (CGL) [21]. As we can see, the phenomenological determination of these parameters is also not too precise but there is reasonable agreement except for \bar{l}_1 that is challenging to determine. At this stage our procedure is not precise enough to give very accurate figures but it is satisfying that it is within expected values. The main point is, as we mentioned, that we have a scheme to *calculate* the EFT parameters.

5 Resonances

As we have seen in section 3 fig.4, the $P1$, $D0$ and potentially $S0$ channels display resonances. In this section we study their properties more closely.

5.1 Scalar form factor

In fig. 4, the $S0$ channel phase shift exhibits a sharp rise starting from threshold as also seen in the phenomenological fits. Correspondingly we see, at ~ 500 MeV a peak in the scalar form factor plotted in fig.6 corresponding to the blue and red points in fig. 3.

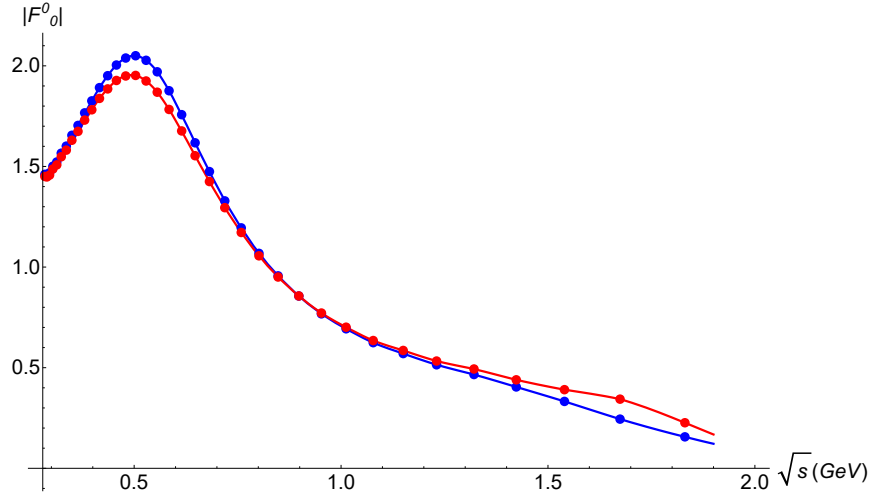


Figure 6: Pion scalar form factor.

This broad peak can be interpreted as the σ resonance but our current numerics is not precise enough to see a pole far from the real axis.

5.2 The ρ meson

In our previous work [1], we found the ρ meson as a resonance in the $P1$ channel. In this paper we see that its properties remain largely unchanged after increasing the QCD matching energy s_0 from $\sqrt{s_0} = 1.2$ GeV in the previous paper to $\sqrt{s_0} = 2$ GeV in this one. This is a good test of the consistency of the procedure in particular because the ρ meson is a signature of QCD and is determined, in this approach, by

the gauge theory dynamics imposed at s_0 . Let us now study its properties in more detail.

5.2.1 Pole in the $P1$ wave

The unitarity saturation condition on the $4 < s < 16$ region of the real axis (or any larger region) for a given partial wave can be written as

$$S_\ell^I(s)(S_\ell^I(\bar{s}))^* = 1 \quad (5.1)$$

Written in this way, the left hand side is an analytic function of s and therefore, if it is equal to 1 in a segment, it is equal to 1 for any value of s . Notice however that this means that if s is in the lower half plane, below the cut, \bar{s} has to be above but crossing under the cut, namely on the second sheet. This also explains why $|S(s)|^2 = 1$ is not valid on the real axis for $s < 4$ since s and \bar{s} are on different sheets and neither has to be for $s > 16$ since a new cut appears there. In any case, what (5.1) implies is that a pole in the second sheet appears as a zero in the first sheet. In fig.7 we plot the modulus of the scattering amplitude $S_1^1(s)$ analytically continued to the second sheet using (5.1). A pole is clearly visible in the plot. We extract the position of this pole and the comparison with experiments is given in table (4).

	GTB	PDG
$\text{Re}(\sqrt{s_\rho})$	829, 832	$761 - 765 \pm 0.23 \text{ MeV}$
$\text{Im}(\sqrt{s_\rho})$	63, 64	$71 - 74 \pm 0.8 \text{ MeV}$

Table 4: Position of the ρ meson T-matrix pole s_ρ in MeV.

5.2.2 Vector form factor

Next, we fit the $P1$ form factor that we obtained from the bootstrap by assuming it is dominated by a ρ -meson pole, namely it is of the Breit-Wigner form [41]:

$$F_1^1(s) = -\frac{m_\rho^2}{s - m_\rho^2 + im_\rho \Gamma_\rho \theta(s - 4m_\pi^2)} \quad (5.2)$$

where the function $\theta(x) = 1$ if $x > 0$ and zero otherwise, ensuring that it is real for $s < 4$ and $F_1^1(0) = 1$. This is a very convenient form since it is given by only two

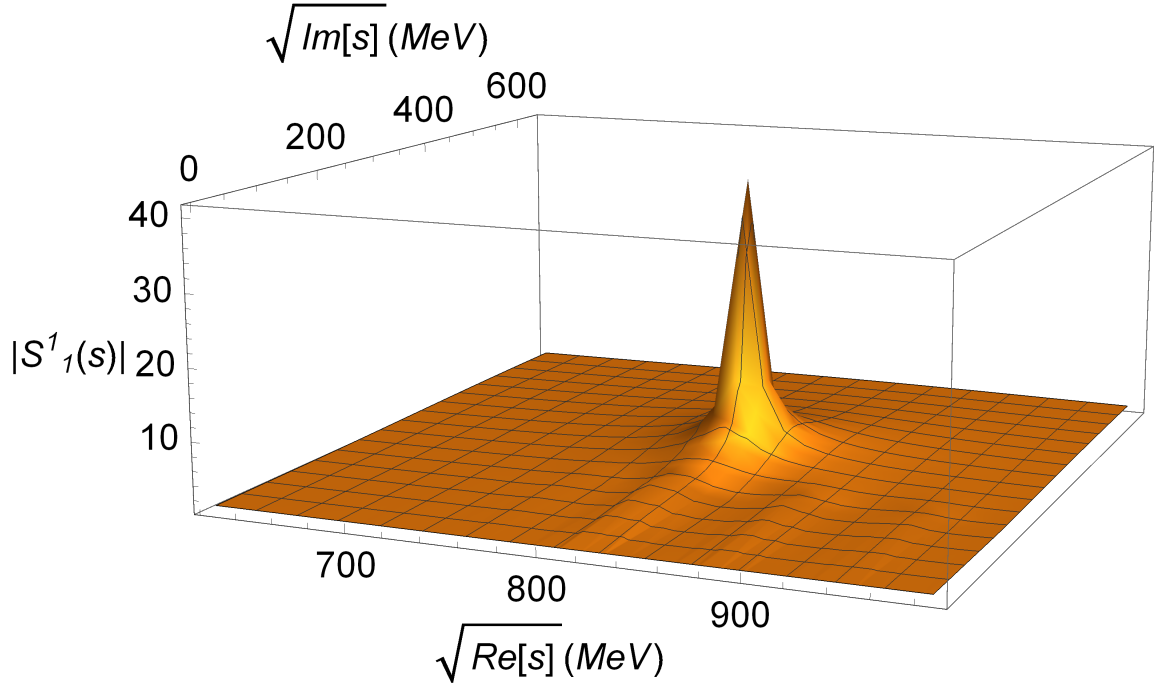


Figure 7: S-matrix pole on the second sheet corresponding to the ρ meson.

parameters (m_ρ, Γ_ρ) that we can fit. For each of the blue and red points considered (in fig. 3) we fit the form factor as shown in figure 8 using a Breit-Wigner shape (dashed line). The agreement is reasonable but can be improved. In fact it was noted long ago that the ρ is not of the Breit-Wigner type. Using general considerations of elastic unitarity and analyticity, a better formula was developed by Gounaris and Sakurai [46] resulting in

$$F_1^1(s) = \frac{m_\rho^2[1 + d\Gamma_\rho/m_\rho]}{(m_\rho^2 - s) - im_\rho\Gamma_\rho(q/q_\rho)^3(m_\rho/\sqrt{s})} \quad (5.3)$$

where $q = \sqrt{\frac{s-4}{4}}$ and

$$d = \frac{3}{\pi} \frac{1}{q_\rho^2} \ln \left(\frac{m_\rho + 2q_\rho}{2} \right) + \frac{m_\rho}{2\pi q_\rho} - \frac{m_\rho}{\pi q_\rho^3}. \quad (5.4)$$

Notice that we still have only two constants (m_ρ, Γ_ρ) to fit. With this formula we fit the form factor again and find a better agreement on the low energy side of the peak (the Gounaris-Sakurai form takes into account the correct threshold behavior).

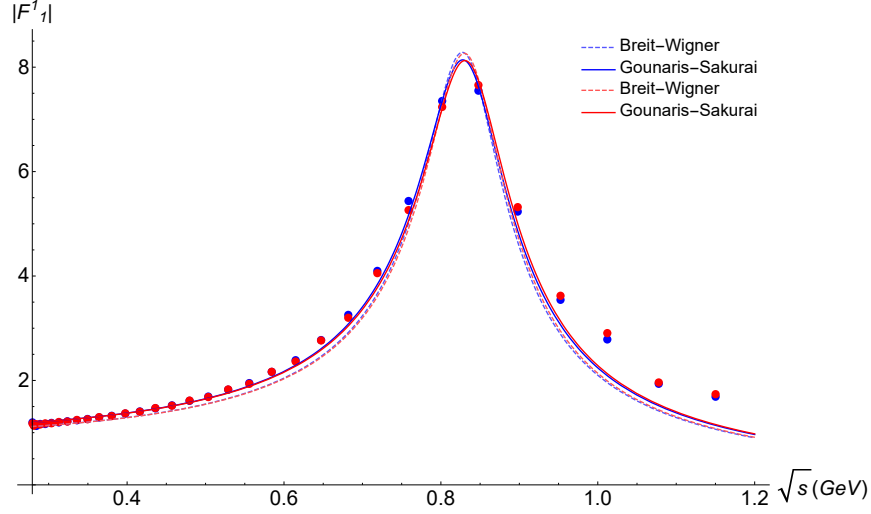


Figure 8: ρ resonance in the vector form factor. The peak is fit with a Breit-Wigner resonance (dashed line) and a Gounaris-Sakurai shape (solid line) that gives a better fit on the low energy side. From here we obtain the mass and width of the ρ meson.

As a result we obtain for the ρ mass and width for each of the two curves compared to the experimental value in table 5. It is interesting to note that the associated spectral density is related [47, 48] to the so called hadronic ratio $R = \frac{\sigma(e^+e^- \rightarrow \text{hadrons})}{\sigma(e^+e^- \rightarrow \mu^+\mu^-)}$ that can be measured very precisely (and for example plays an important role in $g - 2$ computations). For completeness we include a plot in fig. 9.

	GTB	PDG
m_ρ	836, 839	$775 \pm 0.23 \text{ MeV}$
Γ_ρ	111, 111	$149.1 \pm 0.8 \text{ MeV}$

Table 5: ρ meson mass and width in MeV compared to the data [49].

Having determined the ρ mass m_ρ and width Γ_ρ and given that ρ decays into two pions, we can use these values to determine the $g_{\rho\pi\pi}$ coupling through the formula [34]:

$$\Gamma_\rho = g_{\rho\pi\pi}^2 \frac{m_\rho}{48\pi} \left[1 - \frac{4m_\pi^2}{m_\rho^2} \right]^{\frac{3}{2}} \quad (5.5)$$

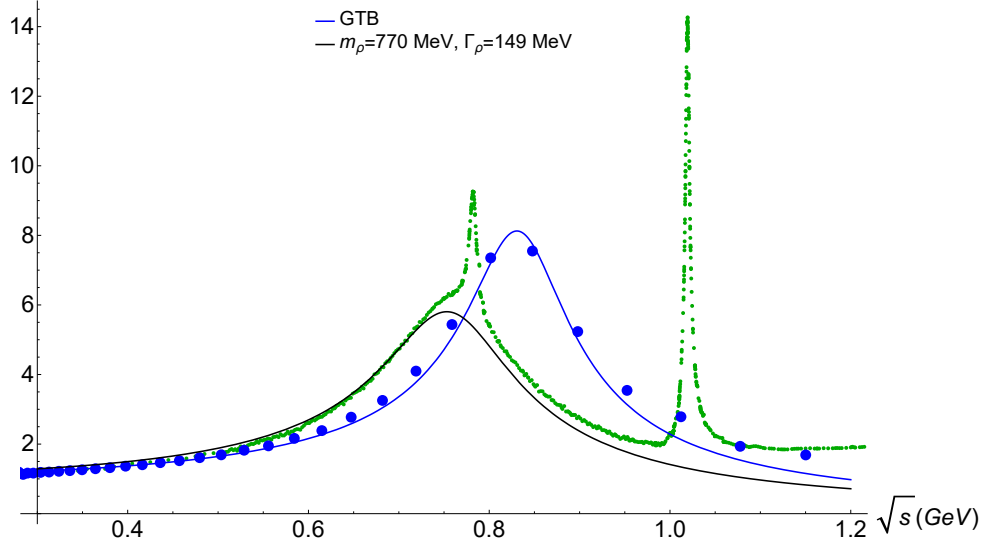


Figure 9: We compare one of the fits (blue) in fig.8 with the Gounaris-Sakurai form using the PDG data (black). The green curve represents the cross section of $e^+ + e^- \rightarrow \text{hadrons}$ (from PDG) properly rescaled to be compared to the form factor of j_V . This last one displays two extra narrow peaks, the ω and ϕ resonances that do not appear in the $P1$ channel for $SU(2)$ flavor.

We find

$$g_{\rho\pi\pi} = 4.9, \quad 4.9 \quad (5.6)$$

compared to the value $g_{\rho\pi\pi} = 6$ computed similarly from the PDG values $m_\rho = 775\text{MeV}$ and $\Gamma_\rho = 149\text{MeV}$. This simply reflects that we have a somewhat narrower resonance.

Another important constant associated with the ρ meson is g_ρ defined through

$$\langle 0 | j_V^\mu | \rho \rangle = \frac{m_\rho^2}{g_\rho} \epsilon^\mu \quad (5.7)$$

where ϵ is the polarization of the ρ meson. It determines the electromagnetic decay width for $\rho \rightarrow e^+ + e^-$. We can compute g_ρ using (the $(2\pi)^{-4}$ is because of our normalization):

$$\int_{\rho \text{ peak}} dx \frac{|\mathcal{F}_1^1(x)|^2}{x} \simeq \frac{1}{(2\pi)^4} \frac{m_\rho^2}{2} \frac{4\pi}{g_\rho^2} \quad (5.8)$$

giving $\frac{4\pi}{g_\rho^2} \simeq 0.55, \quad 0.55$ to be compared with $\frac{4\pi}{g_\rho^2} = 0.507 \pm 0.011$ [50]. Equivalently

$g_\rho = 4.8 \simeq g_{\rho\pi\pi}$. Historically [51], an early model of the ρ meson consider it to be a gauge boson in which case $g_\rho = g_{\rho\pi\pi}$ was the universal gauge coupling. Alternatively, the same equality can be understood from the Vector Meson Dominance (VMD) hypothesis stating that the photon couples to hadrons mainly through the ρ meson and therefore the ρ meson pole dominates the electromagnetic form factor of the pion even far from the resonance. Our results are in agreement with that hypothesis since the fit in fig.8 is good all the way down to threshold.

5.2.3 The $\rho(1450)$

Although the vector form factor \mathcal{F}_1^1 that we obtained (see Fig.8) is dominated by the $\rho(770)$ meson resonance, at larger energy $\simeq 1.6$ GeV another, smaller, peak becomes visible. It is also apparent in fig. 4 as a second rise in the $P1$ phase shift around the same energy. From the PDG meson table [49], it is natural to identify it with the $\rho(1450)$ resonance that has the correct quantum numbers. We take this identification as preliminary and leave more precise calculations for future work. In fig. 10 we fit the form factor we obtained with a a sum of two Breit-Wigner resonances:

$$F_1^1(s) = \frac{-A_1 m_1^2}{s - m_1^2 + im_1 \Gamma_1 \theta(s - 4m_\pi^2)} + \frac{A_2 m_2^2}{s - m_2^2 + im_2 \Gamma_2 \theta(s - 4m_\pi^2)} \quad (5.9)$$

where $\theta(x)$ is the step function that ensures the form factor is real for $s < 4m_\pi^2$. The fit parameters are given in table 6, together with the estimate given by PDG. Note that the fit parameters give

$$A_1 - A_2 = 1.04, 1.01 \quad (5.10)$$

agreeing nicely with the normalization for the form factor $F_1^1(0) = 1$. Assuming that mesons fall into Regge trajectories, we have found the starting point of two distinct Regge trajectories one beginning with the $\rho(770)$ and the second with the $\rho(1450)$. Asymptotically ($s \rightarrow \infty$) the form factor (5.9) behaves as

$$F_1^1(s) \simeq \frac{-A_1 m_1^2 + A_2 m_2^2}{s} \quad (5.11)$$

showing that the asymptotic behavior (2.18h) should be the result of cancellations among several resonances.

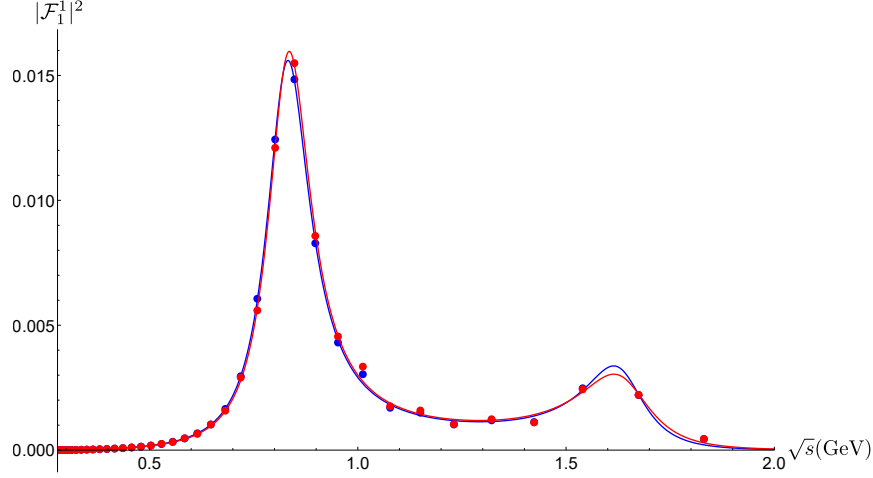


Figure 10: The fit of the bootstrap results of the rescaled form factor $|\mathcal{F}_1^1(s)|^2$ up to 2 GeV with two Breit-Wigner resonances (5.9). In addition to the sharper peak we already saw in fig. 8 identified with $\rho(770)$, we find a peak at higher energy which we preliminarily identify with $\rho(1450)$.

	GTB	PDG
m_1	825, 828	775 ± 0.23 MeV
Γ_1	128, 126	149.1 ± 0.8 MeV
m_2	1632, 1636	1465 ± 25 MeV
Γ_2	180, 210	400 ± 60 MeV
A_1	1.23, 1.21	
A_2	0.19, 0.20	

Table 6: the mass and width in MeV of the $\rho(770)$ meson (m_1, Γ_1) and $\rho(1450)$ meson (m_2, Γ_2) compared to the data [49].

5.3 The gravitational form factor and the f_2 meson

The $D0$ wave has isospin 0 and angular momentum $\ell = 2$, the same quantum numbers as the energy momentum tensor and the graviton. Hypothetically gravity could

couple to hadrons through the f_2 meson resonance in the $D0$ channel as the photon couples through the ρ meson in the $P1$ channel. In this section we study the form factor of the energy momentum tensor a.k.a the gravitational form factor.

The phase shift and form factor of the $D0$ wave clearly show a strong resonance near 1.2 GeV that we naturally identify with the $f_2(1270)$ meson. Fitting the form factor with a Breit-Wigner form (fig. 11) we determine the mass and width as in table 7.

	GTB	PDG
m_{f_2}	1165, 1283	1275.4 ± 0.6 MeV
Γ_{f_2}	151, 201	186.6 ± 2.3 MeV

Table 7: f_2 meson mass and width in MeV compared to the data [49].

It should be noted that the $f_2(1270)$ meson decay fraction to $\pi\pi$ is $(84.3^{+2.9}_{-0.9})\%$ with the rest of the time decaying to $\pi\pi\pi\pi$ (10.5%) and $K\bar{K}$ (4.6%). This is in constrast to the ρ that decays $\sim 100\%$ into $\pi\pi$. Therefore one has particle production through the resonance. One can see this experimentally as depicted in fig.4. In the bootstrap, as mentioned before we carry out a unitarization step to saturate unitarity and reach the boundary of the allowed space. It is curious that, even after this step, we do not find unitarity saturation in the $D0$ wave. Neither in the $P1$ wave near the $\rho(1450)$ resonance. We believe that this is a hint that we are starting to find pion production ($\pi\pi \rightarrow \pi\pi\pi\pi$) in the gauge theory bootstrap. At least there seems to be a clear indication that such production might happen through the resonances ($\pi\pi \rightarrow f_2 \rightarrow \pi\pi\pi\pi$) and therefore can be more under control.

Now, using the formula [50]⁶

$$\Gamma(f_2 \rightarrow \pi^0\pi^0) = \frac{1}{2}\Gamma(f_2 \rightarrow \pi^+\pi^-) = \frac{m_{f_2}}{960\pi} |g_{f_2\pi\pi}|^2 \left(\frac{m_{f_2}}{M_0}\right)^2 \left(1 - \frac{4m_\pi^2}{m_{f_2}^2}\right)^{\frac{5}{2}} \quad (5.12)$$

we find

$$g_{f_2\pi\pi} = 10.5, \quad 10.3 \quad (5.13)$$

if we assume 100% decay into $\pi\pi$. However, since we saw a hint of particle production, assuming 84% decay into $\pi\pi$ (that we have no way to compute at the moment) we

⁶The f_2 pion coupling is a dimension five operator of the schematic form $\mathcal{L} \sim \frac{g_{f_2\pi\pi}}{M_0} \phi \partial \pi \partial \pi$. In [50] a reference mass $M_0 = 1$ GeV is introduced to define a dimensionless coupling.

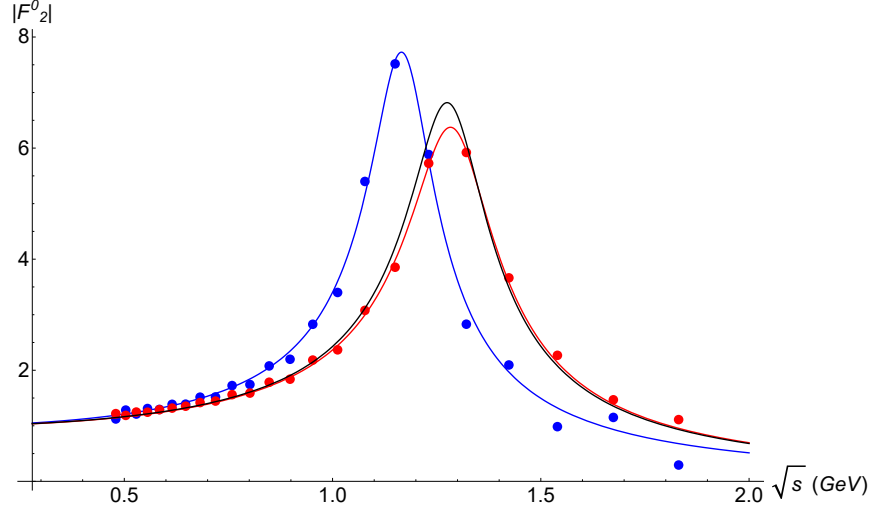


Figure 11: Gravitational form factor, fit with a Breit Wigner form (blue and red), compared to the Breit-Wigner form using PDG data on f_2 (black).

get

$$g_{f_2\pi\pi} = 9.66, \quad 9.52 \quad (5.14)$$

closer to the value $g_{f_2\pi\pi} = 9.26$ from [50].

6 Form factors

The form factors are an important part of the numerical method. Given that the results needed for the numerical computation are available in the literature, this section mostly provides some useful definitions and normalizations. It also provides some computations that can be useful in further implementations of the gauge theory bootstrap with more partial waves. The reader may omit sections 6 and 7 initially.

To each partial wave we associate a gauge theory operator with the same quantum numbers I, ℓ (isospin and angular momentum). The operators we choose for $I = 0, 1$

are

$$\begin{aligned}
I = 0, \ell = 0 & \quad j_S = m_q \bar{\psi} \psi \\
I = 1, \ell = 1 & \quad j_V^{\Delta, I} = \frac{1}{2} \tau_{AB}^I \bar{\psi}_A \not{\Delta} \psi_B \\
I = 0, \ell = 2 & \quad j_2^{\Delta, I} = T^{\mu\nu} \Delta_\mu \Delta_\nu \\
I = 0, \ell > 2, \text{ even} & \quad j_\Delta = \bar{\psi}_A \not{\Delta} D_\Delta^{\ell-1} \psi_A \\
I = 1, \ell > 2, \text{ odd} & \quad j_\Delta^I = \frac{1}{2} \tau_{AB}^I \bar{\psi}_A \not{\Delta} D_\Delta^{\ell-1} \psi_B
\end{aligned} \tag{6.1}$$

where $\Delta = \frac{1}{\sqrt{2}}(0, 1, i, 0)$ is used to consider the operator with largest projection in the direction $x^+ = \frac{1}{\sqrt{2}}(x + iy)$ and ensure the angular momentum is ℓ . The Pauli matrices τ_{AB}^I are used to project to isospin 1. The covariant derivative is $D_\Delta = \Delta^\mu (\partial_\mu - ig A_\mu)$. In the present paper we only use the first three in the list: scalar and vector currents and the energy momentum tensor. They have been extensively studied in the literature [17, 18, 30, 41, 52–58] and we only review their properties. For recent bootstrap applications of form factors specially in 2d systems see [8, 59–62]. For the $\ell > 2$ case we give computations that we think will be useful in future implementations of the gauge theory bootstrap. Finally, operators with $I = 2$ require at least four quarks, we discuss an example in the next section.

6.1 Definitions

6.1.1 Angular momentum ℓ

In the center of mass frame where $p_1 = (\epsilon, \vec{p})$ and $p_2 = (\epsilon, -\vec{p})$ we define the form factor $F_\ell(s)$ for an operator of angular momentum ℓ as:

$$\begin{aligned}
\langle p_1 p_2 | j_\Delta^{(\ell)} | 0 \rangle &= (p_1 \cdot \Delta)^\ell F_\ell(s) \\
&= (-\sin \theta)^\ell e^{i\ell\phi} |\vec{p}|^\ell F_\ell(s) \\
&= 2^\ell \ell! \sqrt{\frac{4\pi}{(2\ell+1)!}} Y_{\ell\ell}(\hat{p}_1) |\vec{p}|^\ell F_\ell(s)
\end{aligned} \tag{6.2}$$

where $\Delta = \frac{1}{\sqrt{2}}(0, 1, i, 0)$ and (θ, ϕ) are polar angles for $\vec{p} = |\vec{p}|(\sin \theta \cos \phi, \sin \theta \sin \phi, \cos \theta)$. For center of mass momentum $P = p_1 + p_2$ and angular momentum and isospin eigen-

states we get

$$\langle P\ell\sigma, I=0 | j_{\Delta}^{I'\ell} | 0 \rangle = \sqrt{\frac{3}{2}} \delta_{\sigma\ell} \mathcal{F}_{\ell}^{I=0}(s) \quad (6.3)$$

$$\langle P\ell\sigma, I=1 | j_{\Delta}^{(\ell)} | 0 \rangle = \delta_{\sigma\ell} \mathcal{F}_{\ell}^{I=1}(s) \quad (6.4)$$

$$\mathcal{F}_{\ell}^I(s) = \frac{1}{16\pi^3} \left(\frac{s-4}{4} \right)^{\frac{2\ell+1}{4}} \frac{1}{s^{\frac{1}{4}}} 2^{\ell} \ell! \sqrt{\frac{4\pi}{(2\ell+1)!}} F_{\ell}^I(s) \quad (6.5)$$

6.1.2 The gravitational form factor

In the case of the $D0$ wave we need an operator with spin 2 and isospin 0. We can use $\mathcal{O} = \bar{\psi}_a \gamma^+ D^+ \psi_a$. However that operator mixes with a gluonic one. A particular linear combination is the energy momentum tensor that we are going to use in this case. From energy momentum conservation we can write (the upper index in the form factor is the isospin)

$$\langle \pi_{p_1}^+ | T^{\mu\nu}(x) | \pi_{p_2}^+ \rangle = e^{i(p_1-p_2)x} \left\{ \frac{1}{2} F_2^0(t) (p_1 + p_2)^{\mu} (p_1 + p_2)^{\nu} + \right. \quad (6.6)$$

$$\left. \tilde{F}(t) (t \eta^{\mu\nu} - (p_1 - p_2)^{\mu} (p_1 - p_2)^{\nu}) \right\} \quad (6.7)$$

with $t = (p_1 - p_2)^2$. Also given that the Hamiltonian is $H = \int d^3x T^{00}(x)$ and that $H | \pi_{p_2}^+ \rangle = \epsilon_{p_2} | \pi_{p_2}^+ \rangle$ we find

$$\langle \pi_{p_1}^+ | \int d^3x T^{00}(x) | \pi_{p_2}^+ \rangle = \epsilon_{p_2} \langle \pi_{p_1}^+ | \pi_{p_2}^+ \rangle = 2\epsilon_{p_1}^2 (2\pi)^3 \delta^{(3)}(\vec{p}_1 - \vec{p}_2) \quad (6.8)$$

Comparing with (6.6) we find

$$F_2^0(0) = 1 \quad (6.9)$$

From (6.6) and using crossing symmetry we obtain

$$\text{out} \langle \pi_{p_1}^+ \pi_{p_2}^- | T^{\mu\nu}(0) | 0 \rangle = \frac{1}{2} F_2^0(s) (p_1 - p_2)^{\mu} (p_1 - p_2)^{\nu} + \tilde{F}(s) (s \eta^{\mu\nu} - (p_1 + p_2)^{\mu} (p_1 + p_2)^{\nu}) \quad (6.10)$$

and in particular

$$\text{out} \langle \pi_{p_1}^+ \pi_{p_2}^- | T^{++}(0) | 0 \rangle = 4 |\vec{p}_1|^2 F_2^0(s) \sqrt{\frac{2\pi}{15}} Y_{22}(\hat{p}_1) \quad (6.11)$$

where $Y_{\ell\sigma}(\hat{p}_1)$ are the usual spherical harmonics evaluated in the direction of \vec{p}_1 . Now it follows that

$$\langle P\ell\sigma | T^{++}(0) | 0 \rangle = \mathcal{F}_2^0(s) \delta_{\ell 2} \delta_{\sigma 2} \quad (6.12)$$

$$\mathcal{F}_2^0(s) = \frac{1}{4\pi^3} \sqrt{\frac{3\pi}{15}} \frac{1}{s^{\frac{1}{4}}} \left(\frac{s-4}{4} \right)^{\frac{5}{4}} F_2^0(s) \quad (6.13)$$

6.2 Asymptotic form

The computation of asymptotic form factors is well known since the pioneering work of Brodsky and Lepage [17] on exclusive QCD processes. In this section we give a simple presentation of the subject that allows to compute the case of general ℓ at lowest order. Physically, for large momentum, the form factor is very small since it gives the amplitude for a rare process where a (virtual) particle (*e.g.* photon) strikes a pion and the pion absorbs the particle without being destroyed. It can be computed in the parton model by considering that the particle strikes a parton that has to interchange gluons with the other partons so that all partons move in the new direction. The largest contribution comes from the part of the wave function with smallest number of partons, in this case 2. The results depend on the parton distribution function and are also valid at large energies $\sqrt{s} \gg \Lambda_{QCD}$. Since this is the only available result from QCD we use it with some caveats as discussed in section 8. In this section we describe the computation of the generic ℓ case thinking that it might help to extend the method to higher energies and angular momenta. We start by considering a generic current contracted with a vector Δ as

$$j_{B'A'}^\ell = \bar{\psi}_{B'} \not{\Delta} D_{\Delta}^{\ell-1} \psi_{A'} \quad (6.14)$$

where A' and B' are flavor indices that should be contracted with Pauli matrices $\tau_{B'A'}^I$ for isospin 1 and $\delta_{A'B'}$ for isospin 0. We then take a simple “pion state” in QCD as a superposition of two free quarks (we follow the normalization in [47])

$$|\pi^I(p)\rangle = \int_0^1 dx \int d^2 k_\perp X_{s_1 s_2} \psi(x, k_\perp) \frac{1}{2} \tau_{AB}^I \sqrt{2\omega_k} \sqrt{2\omega_{p-k}} a_{aAs,k}^\dagger b_{aBs,p-k}^\dagger |0\rangle \quad (6.15)$$

where $k = xp + k_\perp$, $k' = x'p' + k'_\perp$. In all calculations we take the large energy limit where $s = q^2 = (p-p')^2 \simeq -2pp' \rightarrow \infty$ and we drop all terms involving k_\perp , k'_\perp . This is explained in more detail in appendix C where we compute one Feynman diagram for pedagogical reasons. The wave function $\psi(x, k_\perp)$ is a low energy quantity. We sum over spin assuming a choice $v_p = -\gamma_5 u_p$ such that $u_p^s \bar{v}_p^s = (\not{p} + m_q) \gamma_5$ as required to match the one piece of information we have from the axial current form factor

$$\langle 0 | j_\mu^{I,5}(0) | \pi^{I'}(p) \rangle = -i \delta^{II'} p_\mu f_\pi \quad (6.16)$$

It also requires the normalization

$$\int_0^1 dx \int d^2 k_\perp \sqrt{x(1-x)} \psi(x, k_\perp) = -\frac{i}{2N_c} f_\pi \quad (6.17)$$

From [17] we take, for very high energy, in our normalization

$$\sqrt{x(1-x)}\psi(x, k_\perp) = -\frac{i}{2N_c} f_\pi \phi(x) \tilde{\psi}(k_\perp), \quad \int d^2 k_\perp \tilde{\psi}(k_\perp) = 1 \quad (6.18)$$

where $\phi(x)$ is usually taken to be $\phi(x) = 6x(1-x)$ [17]. The calculation for the insertion of a current (6.14) follows, at lowest order in perturbation theory from the Feynman diagrams (a) and (b) in fig. 13 using the vertices of fig. 12. For the contribution of all four diagrams of type (a), *i.e.* inserting the current in any of the fermion lines, we get (see appendix for one of the diagrams)

$$\mathbb{T}_{ABCD A' B'}^{(a)} = \frac{16ig^2}{s} C_2(N_c) (-ip\Delta)^\ell \frac{x^{\ell-1}}{(1-x)(1-x')} [\delta_{AB'} \delta_{A'C} \delta_{BD} + (-)^\ell \delta_{A'B} \delta_{AC} \delta_{B'D}] \quad (6.19)$$

with $C_2(N_c) = \frac{N_c^2-1}{2}$. Similarly we find (two diagrams of type (b) inserting the current on the top or bottom lines)

$$\mathbb{T}_{ABCD A' B'}^{(b)} = \frac{8ig^2}{s} C_2(N_c) (-ip\Delta)^\ell \frac{x'^{\ell-1} - x^{\ell-1}}{(1-x)(1-x')(x'-x)} [\delta_{AB'} \delta_{A'C} \delta_{BD} + (-)^\ell \delta_{A'B} \delta_{AC} \delta_{B'D}] \quad (6.20)$$

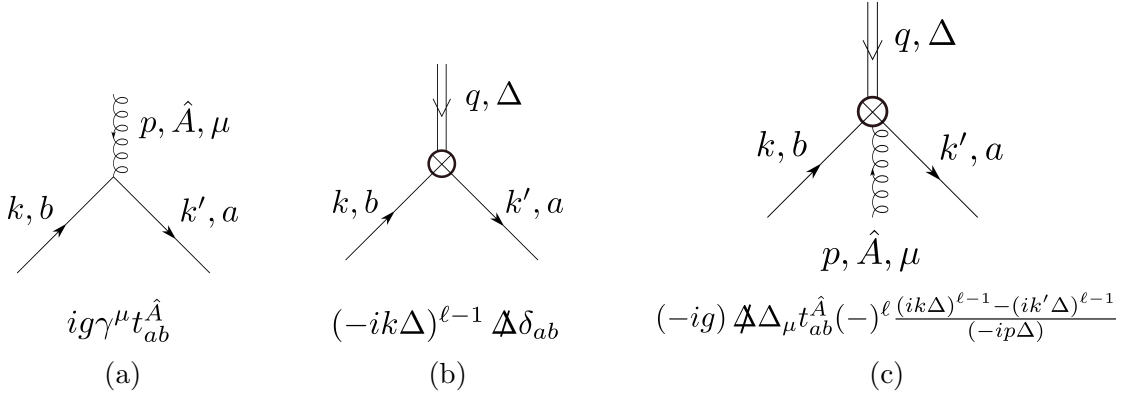


Figure 12: Vertices to compute the current propagators and the asymptotic form factors. (a) standard gauge theory vertex (b) Current insertion. (c) Current insertion with one gluon from the covariant derivatives.

resulting in the form factor

$$\langle \pi_p^{I''} | j_{B'A'}^\ell | \pi_p^I \rangle = \frac{f_\pi^2}{4N_c^2} \int_0^1 \int_0^1 dx dx' \phi(x) \phi^*(x') \frac{1}{4} \tau_{BA}^I \tau_{CD}^{I''} \mathbb{T}_{ABCD A' B'} \quad (6.21)$$

where $\phi(x) = 6x(1-x)$ and $\mathbb{T} = \mathbb{T}^{(a)} + \mathbb{T}^{(b)}$. We find ($\alpha_s = g^2/(4\pi)$.)

$$\langle \pi_{p'}^{I''} | j_{B'A'}^\ell | \pi_p^I \rangle = \frac{72i\pi\alpha_s f_\pi^2}{t} \frac{C_2(N_c)}{N_c^2} (-ip\Delta)^\ell \left[\tau^{I''} \tau^I + (-)^\ell \tau^I \tau^{I''} \right]_{A'B'} \left\{ \frac{1}{\ell+1} + \frac{2(H_\ell-1)}{\ell+2} \right\} \quad (6.22)$$

where we introduced the harmonic numbers $H_\ell = \sum_{p=1}^\ell \frac{1}{p}$. Two cases have to be considered now.

Isospin 1:

We take the current to be

$$j_\ell^I = \frac{1}{2} \tau_{B'A'}^I j_{B'A'}^\ell \quad (6.23)$$

We define the form factor $F_\ell^I(s)$ from the equation:

$$\langle \pi_{p'}^{I''} | j_{\ell,\Delta}^{I'} | \pi_p^I \rangle = -2(-ip\Delta)^\ell \epsilon^{I''I'I} F_\ell^1(t = (p-p')^2) \quad (6.24)$$

Using (6.21) and performing the integrals we obtain (for ℓ odd, it vanishes for ℓ even):

$$F_\ell^1(t) \simeq_{t \rightarrow \infty} -\frac{72\pi\alpha_s f_\pi^2}{t} \frac{C_2(N_c)}{N_c^2} \left\{ \frac{1}{\ell+1} + \frac{2(H_\ell-1)}{\ell+2} \right\} \quad (6.25)$$

with $H_\ell = \sum_{p=1}^\ell \frac{1}{p}$. Setting $\ell = 1$ and $N_c = 3$ in the previous formula ($C_2(N_c) = \frac{N_c^2-1}{2}$) we find

$$F_1^1(t) \simeq_{s \rightarrow \infty} -\frac{16\pi\alpha_s f_\pi^2}{t} \quad (6.26)$$

in agreement with Brodsky-Lepage [17, 18]. The higher values of ℓ are not used in this paper but they could be useful for later reference.

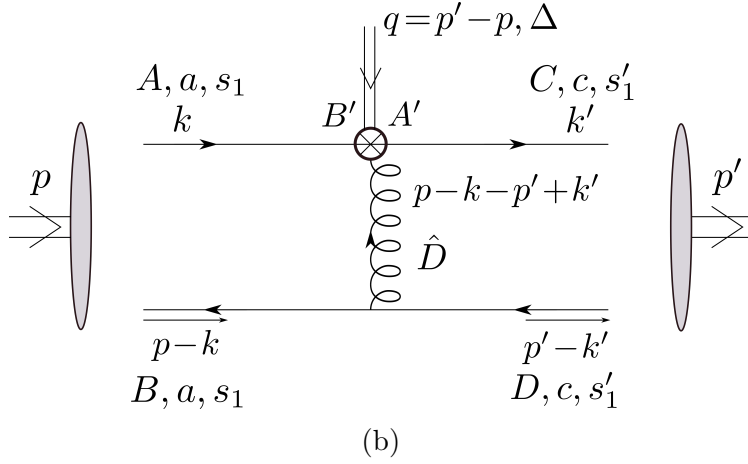
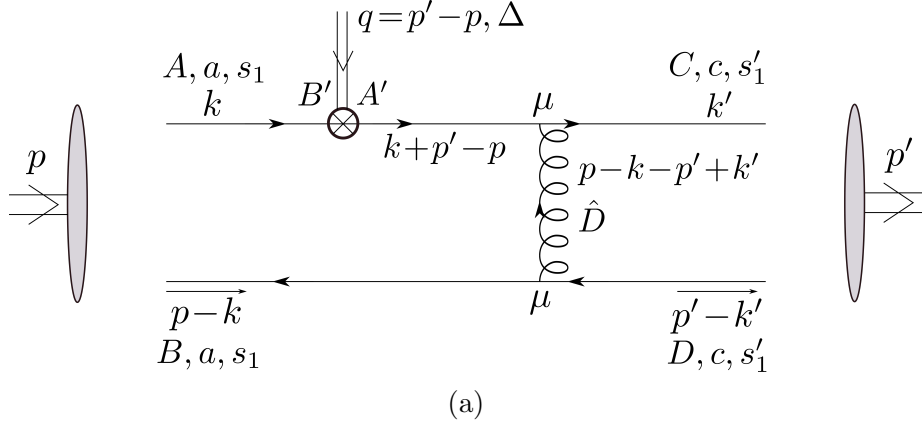


Figure 13: Standard Feynman diagrams with on-shell external particles contributing to the asymptotic pion form factor in the parton model. The grey blobs represent a linear combination of free fermions as in (6.15). The indices A, B, C, D, A', B' indicate flavor, a, c color, s_1, s'_1 polarization, and \hat{D} are in the adjoint representation of the gauge group.

Isospin 0:

We take the current to be

$$j_{\ell, \Delta} = \delta_{B'A'} j_{B'A'}^{\ell} \quad (6.27)$$

We define the form factor $F_{\ell}^I(s)$ from the equation:

$$\langle \pi_{p'}^{I'} | j_{\ell, \Delta} | \pi_p^I \rangle = -2(-ip\Delta)^{\ell} \delta^{I'I} F_{\ell}^0(t = (p - p')^2) \quad (6.28)$$

Using (6.21) and performing the integrals we obtain (for ℓ even, it vanishes for ℓ odd):

$$F_\ell^0(t) \simeq_{t \rightarrow \infty} -\frac{144i\pi\alpha_s f_\pi^2}{t} \frac{C_2(N_c)}{N_c^2} \left\{ \frac{1}{\ell+1} + \frac{2(H_\ell-1)}{\ell+2} \right\} \quad (6.29)$$

with $H_\ell = \sum_{p=1}^{\ell} \frac{1}{p}$. The case $\ell = 2$, is relevant for the gravitational form factor:

$$F_{2q}^0(t) \simeq_{t \rightarrow \infty} -\frac{84i\pi\alpha_s f_\pi^2}{t} \frac{C_2(N_c)}{N_c^2} \quad (6.30)$$

where we added the subindex q to indicate it comes from the quark part.

6.2.1 The gravitational form factor

The gravitational form factor is the form factor associated with the energy momentum tensor

$$T^{\mu\nu} \Delta_\mu \Delta_\nu = -F^{a\mu\alpha} F^{a\nu}{}_\alpha \Delta_\mu \Delta_\nu + \bar{\psi}_A \not{\Delta} i D_\Delta \psi_A \quad (6.31)$$

The kernels were computed in [53]. Since in that paper the final integral with the parton distribution was not performed, to avoid problems with different normalization we recompute the result here. In fact, up to a factor i the quark part was already computed in the previous subsection. The gluonic part can be computed from the diagram in fig.14 giving

$$\mathbb{T}_{ABCD} = -\frac{8g^2}{t} C_2(N_c) (-ip\Delta)^2 \left\{ \frac{1}{x(1-x)} + \frac{1}{x'(1-x')} \right\} \delta_{AC} \delta_{BD} \quad (6.32)$$

and thus

$$\langle \pi_p^{I'} | -F^{a\mu\alpha} F^{a\nu}{}_\alpha \Delta_\mu \Delta_\nu | \pi_p^I \rangle \simeq_{t \rightarrow \infty} -\frac{48\pi\alpha_s f_\pi^2}{t} \frac{C_2(N_c)}{N_c^2} (-ip\Delta)^2 \delta^{II'} \quad (6.33)$$

and, from (6.28):

$$F_{2g}^0(t) \simeq_{t \rightarrow \infty} \frac{24\pi\alpha_s f_\pi^2}{t} \frac{C_2(N_c)}{N_c^2} \quad (6.34)$$

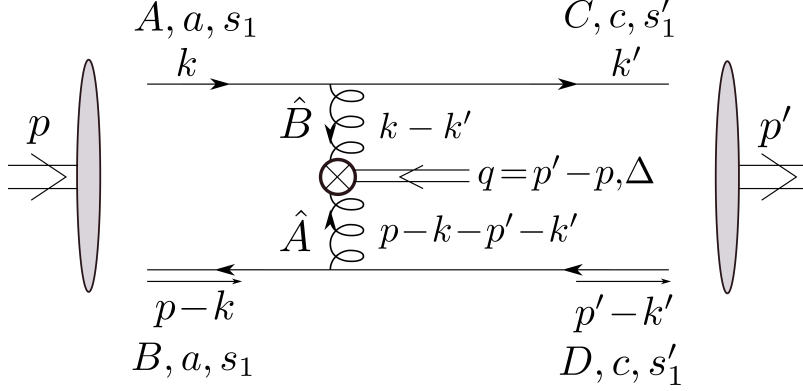


Figure 14: Feynman diagrams contributing energy momentum asymptotic pion form factor (gluon contribution).

Putting both together we find

$$F_2^0(t) = F_{2g}^0(t) + iF_{2q}^0(t) \simeq_{t \rightarrow \infty} \frac{108\pi\alpha_s f_\pi^2 C_2(N_c)}{t N_c^2} \quad (6.35)$$

For the case $N_c = 3$ of interest here we find

$$F_2^0(t) \simeq_{t \rightarrow \infty} \frac{48\pi\alpha_s f_\pi^2}{t} \quad (6.36)$$

As explained more in section 8, it turns out that around $s \sim 2 \text{ GeV}$ this estimate is somewhat low due to the f_2 resonance so only the order of magnitude is relevant.

6.2.2 Scalar form factor

We were not able to find much information about the asymptotic form of the scalar form factor in the literature. A calculation similar to the one for the vector form factor vanishes in the chiral limit since one gets the trace of a product of an odd number of Dirac matrices. The subleading term contains a power of the quark mass m_q . Namely, the scalar current changes the chirality of the fermion and we need a mass insertion to restore it. The resulting computation has a divergence at the ends of the interval $x \rightarrow 0, 1$. The fermion propagator regulates it at an energy $p^2 = p'^2 = m_\pi^2$. These qualitative arguments suggest a behavior

$$F_0^0(t) \sim_{t \rightarrow \infty} 4\pi\alpha_s f_\pi^2 \frac{m_q^2}{t} \frac{C_2(N_c)}{N_c^2} \ln \left(\frac{s}{m_\pi^2} \right) \quad (6.37)$$

up to a numerical factor. The other power of m_q is from the definition of the current. This is too small for the precision of our numerics where we use another estimate.

7 Two point functions

In this section we consider the two point functions of various currents discussed in the previous section. Since the results needed for the numerical computations of the paper are available in the literature, this section can be omitted in a first read of the paper. It contains calculations that can be useful in future implementations of the bootstrap with more partial waves. The leading term in the expansion of the two point functions comes from the free theory, namely the UV fixed point of the theory but the results are already not trivial at this order since we are considering composite operators and renormalization is required.

7.1 Definitions

Given an arbitrary local operator or current $j(x)$ we define an integrated operator:

$$\mathcal{O}(P) = \int \frac{d^4x}{(2\pi)^4} e^{-iPx} j(x) \quad (7.1)$$

The two currents correlator, or vacuum polarization is defined as

$$\Pi(s) = i \int \frac{d^4x}{(2\pi)^4} e^{iP(x-y)} \langle 0 | \hat{T} \{ j(x)^\dagger j(y) \} | 0 \rangle \quad (7.2)$$

and the spectral density as

$$\rho(s) = 2 \text{Im} \Pi(s + i\epsilon) = \int \frac{d^4x}{(2\pi)^4} e^{iPx} \langle 0 | j(x)^\dagger j(0) | 0 \rangle \quad (7.3)$$

where $s = P^2$. Notice that

$$\langle 0 | (\mathcal{O}(P'))^\dagger \mathcal{O}(P) | 0 \rangle = \delta^{(4)}(P' - P) \rho(s) \quad (7.4)$$

which is the identity required by the form factor bootstrap.

7.2 Asymptotic form

As in the case of the form factors, the calculation requires the asymptotic form of the the two current correlator for $|s| \rightarrow \infty$. Here $|s| = s_0 = 2 \text{ GeV}$ and we make the assumption that the asymptotic form given by the free theory (Feynman diagram in fig.15) is already dominant.

7.2.1 Two quark operators of arbitrary ℓ

Consider the current and operator

$$j_{\ell,AB}^{\Delta}(x) = \bar{\psi}_{Aa}(x) \not{D}_{\Delta}^{\ell-1} \psi_{Ba}(x) \quad (7.5)$$

$$\mathcal{O}_{q,AB}^{\Delta} = \int \frac{d^4x}{(2\pi)^4} e^{-iqx} j_{\ell,AB}^{\Delta}(x) \quad (7.6)$$

where A, B and a, b are flavor and color indices respectively and $\Delta = \frac{1}{\sqrt{2}}(0, 1, i, 0)$. This implies $\Delta^2 = 0 = \bar{\Delta}^2$, $\Delta\bar{\Delta} = -1$ and also, in the center of mass where q is time-like, $q\Delta = 0 = q\bar{\Delta}$. A standard one loop diagram (fig.15) using the vertex (b) of fig.12 gives, in the free theory:

$$\begin{aligned} \Pi(s)_{\ell,ABCD}^{\Delta} &= i \int \frac{d^d x}{(2\pi)^d} e^{iP(x-y)} \langle 0 | \hat{T} \{ (j_{\ell,AB}^{\Delta}(x))^{\dagger} j_{\ell,CD}^{\Delta}(y) \} | 0 \rangle \\ &= -\frac{N_c}{(2\pi)^4} \frac{\delta_{AC}\delta_{BD}}{2\pi^2} \frac{\ell+1}{2^{\ell}\ell} B(\ell+1, \ell+1) s^{\ell} \ln\left(-\frac{s}{\mu^2}\right) \end{aligned} \quad (7.7)$$

Also $B(a, b) = \frac{\Gamma(a)\Gamma(b)}{\Gamma(a+b)}$. From here we find

$$\rho(s)_{\ell,ABCD}^{\Delta} = 2\text{Im}\Pi(s+i\epsilon)_{\ell,ABCD}^{\Delta} = \frac{N_c}{(2\pi)^4} \frac{\delta_{AC}\delta_{BD}}{\pi} \frac{\ell+1}{2^{\ell}\ell} B(\ell+1, \ell+1) s^{\ell} \quad (7.8)$$

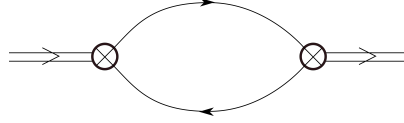


Figure 15: Standard Feynman diagrams contributing to the two point function of the current at lowest order.

and the generic sum rule

$$\frac{1}{s_0^{n+\ell+1}} \int_4^{s_0} \rho(x)_{\ell,ABCD}^{\Delta} x^n dx = \frac{N_c}{(2\pi)^4} \frac{\delta_{AC}\delta_{BD}}{\pi} \frac{\ell+1}{2^{\ell}\ell} \frac{B(\ell+1, \ell+1)}{n+\ell+1}, \quad n \geq 0 \quad (7.9)$$

It might be interesting to note that for $\ell \gg 1$ a standard Stirling approximation shows that the right hand side is very small

$$\frac{1}{s_0^{n+\ell+1}} \int_4^{s_0} \rho(x)_{\ell,ABCD}^{\Delta} x^n dx \simeq \frac{N_c}{(2\pi)^4} \frac{\delta_{AC}\delta_{BD}}{\pi} \sqrt{\frac{\pi}{l}} \frac{1}{2^{3\ell+1}} \frac{1}{n+\ell+1}, \quad n \geq 0, \ell \gg 1 \quad (7.10)$$

This is a reasonable approximation even if ℓ is small.

7.2.2 Energy momentum tensor

The energy momentum tensor is one of the most studied operators in Quantum Field Theory. For recent results in QCD see [63] and also the very recent paper [64] that uses energy momentum tensor correlators to study glueballs. Now we are interested in the vacuum polarization

$$\Pi_2(s) = i \int \frac{d^4x}{(2\pi)^4} e^{iqx} \langle 0 | \hat{T} \{ T^{--}(x) T^{++}(0) \} | 0 \rangle \quad (7.11)$$

From [65] we find

$$i \int d^4x e^{iqx} \langle 0 | \hat{T} \{ T^{\mu\nu}(x) T^{\rho\sigma}(0) \} | 0 \rangle \simeq C_0^T(s) \left\{ P^{\mu\rho} P^{\nu\sigma} + P^{\mu\sigma} P^{\nu\rho} - \frac{2}{3} P^{\mu\nu} P^{\rho\sigma} \right\} + C_0^S(s) P^{\mu\nu} P^{\rho\sigma} \quad (7.12)$$

with

$$P^{\mu\nu} = q^2 \eta^{\mu\nu} - q^\mu q^\nu \quad (7.13)$$

$$\begin{aligned} C_0^T(s) &= \frac{1}{16\pi^2} \left[-\frac{n_g}{10} - \frac{1}{20} n_f d_R + \frac{\alpha_s}{\pi} \left\{ \frac{1}{18} C_A n_g - \frac{7}{144} n_f T_F n_g \right\} \right] \ln \left(-\frac{s}{\mu^2} \right) \\ &= \frac{1}{16\pi^2} \left(-\frac{11}{10} + \frac{17}{18} \frac{\alpha_s}{\pi} \right) \ln \left(-\frac{s}{\mu^2} \right) \end{aligned} \quad (7.14)$$

From here, and working in the frame where $q = (\sqrt{s}, 0, 0, 0)$ we obtain

$$\Pi_2(s) = \frac{1}{(2\pi)^4} s^2 C_0^T(s) \quad (7.15)$$

Notice that the power s^2 is determined by the symmetry and conservation law, therefore also appears as $s \rightarrow 0$ implying that $\frac{1}{s^2} \Pi_2(s)$ is analytic. For $SU(N_c)$ gauge theory with n_f flavors in the fundamental we have $d_R = N_c$, $n_g = N_c^2 - 1$, $C_A = 2T_F N_c$, $C_F = \frac{T_F n_g}{N_c}$, $T_F = \frac{1}{2}$. If we set $n_f = 0$ these results agree with those of [64]. In any case, for $N_c = 3$ and $n_f = 2$, the results of [65] reduce to

$$\Pi_2(s) = \frac{1}{(2\pi)^4} \frac{1}{8\pi^2} \left(-\frac{11}{10} + \frac{17}{18} \frac{\alpha_s}{\pi} \right) s^2 \ln \left(-\frac{s}{\mu^2} \right) + \dots \quad (7.16)$$

namely

$$\rho_2(s) \underset{s \rightarrow \infty}{=} \frac{1}{(2\pi)^4} \frac{1}{4\pi} \left(\frac{11}{10} - \frac{17}{18} \frac{\alpha_s}{\pi} \right) s^2 \ln \left(-\frac{s}{\mu^2} \right) \quad (7.17)$$

giving the FESR

$$\frac{1}{s_0^{n+3}} \int_4^{s_0} \rho_2(x) x^n dx = \frac{1}{(2\pi)^4} \frac{1}{4\pi} \frac{1}{n+3} \left(\frac{11}{10} - \frac{17}{18} \frac{\alpha_s}{\pi} \right), \quad n \geq -2 \quad (7.18)$$

that we impose for $n = -2, -1$.

7.2.3 Four quark scalar current

Consider the scalar current relevant for the isospin $I = 2$ case

$$j_{ABCD} = (\bar{\psi}_A \psi_B)(\bar{\psi}_C \psi_D) \quad (7.19)$$

where the fields in parenthesis are color singlets. The indices $A, B, C, D = 1 \dots N_f$ are flavor indices. We are interested in the correlator

$$\Pi(s) = i \int \frac{d^d x}{(2\pi)^d} e^{-iPx} \langle 0 | \hat{T} \{ (j_{A'B'C'D'}(x))^\dagger j_{ABCD}(0) \} \rangle \quad (7.20)$$

where $s = P^2$. Using Wick's theorem, in the free theory, namely the Feynman diagrams of fig.16 where the blobs represent current insertions, we find

$$\begin{aligned} \Pi(s) = i \int \frac{d^d x}{(2\pi)^d} e^{-iPx} \times \\ \{ N_c^2 (\delta_{AA'} \delta_{BB'} \delta_{CC'} \delta_{DD'} + \delta_{AC'} \delta_{CA'} \delta_{BD'} \delta_{DB'}) \text{Tr}[\Delta_F(-x) \Delta_F(x)] \text{Tr}[\Delta_F(-x) \Delta_F(x)] \\ - N_c (\delta_{AC'} \delta_{CA'} \delta_{BB'} \delta_{DD'} + \delta_{AA'} \delta_{CC'} \delta_{BD'} \delta_{DB'}) \text{Tr}[\Delta_F(-x) \Delta_F(x) \Delta_F(-x) \Delta_F(x)] \} \end{aligned} \quad (7.21)$$

where $\Delta_F(x)$ is the fermion propagator

$$\Delta_F(x) = \int \frac{d^d k}{(2\pi)^d} \frac{i(\not{k} + m)}{k^2 - m^2 + i\epsilon} e^{-ikx} = (i\not{\partial}_x + m)\Delta(x) \quad (7.22)$$

where $\Delta(x)$ is the scalar propagator. This results in

$$\begin{aligned} \Pi(s) = i \int \frac{d^d x}{(2\pi)^d} e^{-iPx} [\partial_\mu \Delta(x) \partial^\mu \Delta(x) + m^2 \Delta(x)^2] \times \\ \{ 16 N_c^2 (\delta_{AA'} \delta_{BB'} \delta_{CC'} \delta_{DD'} + \delta_{AC'} \delta_{CA'} \delta_{BD'} \delta_{DB'}) \\ - 4 N_c (\delta_{AC'} \delta_{CA'} \delta_{BB'} \delta_{DD'} + \delta_{AA'} \delta_{CC'} \delta_{BD'} \delta_{DB'}) \} \end{aligned} \quad (7.23)$$

Since we consider the case of light quarks, we ignore the quark mass and use the massless propagator and the general formula

$$\int \frac{d^d k}{(2\pi)^d} \frac{e^{-ikx}}{(k^2 + i\epsilon)^a} = i \frac{\Gamma(\frac{d}{2} - a)}{\Gamma(a)} \frac{(-1)^a}{4^a \pi^{\frac{d}{2}} (-x^2)^{\frac{d}{2} - a}} \quad (7.24)$$

we obtain

$$\int \frac{d^d x}{(2\pi)^d} e^{-iPx} [\partial_\mu \Delta(x) \partial^\mu \Delta(x)]^2 = -i \frac{\Gamma(\frac{d}{2})^4 \Gamma(2 - \frac{3}{2}d)}{16\pi^{2d} \Gamma(2d - 2)} \frac{1}{4^{2d-2} \pi^{\frac{d}{2}} (-P^2 - i\epsilon)^{2 - \frac{3}{2}d}} \quad (7.25)$$

Replacing $d = 4 - \epsilon$, expanding in ϵ and renormalizing we get

$$\begin{aligned} \Pi(s) &= i \int \frac{d^4 x}{(2\pi)^4} e^{-iPx} \langle 0 | \hat{T} \{ (j_{A'B'C'D'}(x))^\dagger j_{ABCD}(0) \} \\ &= - \left\{ 16N_c^2 (\delta_{AA'} \delta_{BB'} \delta_{CC'} \delta_{DD'} + \delta_{AC'} \delta_{CA'} \delta_{BD'} \delta_{DB'}) \right. \\ &\quad \left. - 4N_c (\delta_{AC'} \delta_{CA'} \delta_{BB'} \delta_{DD'} + \delta_{AA'} \delta_{CC'} \delta_{BD'} \delta_{DB'}) \right\} \\ &\quad \frac{1}{(2\pi)^4} \frac{1}{2^{18} 3^2 5 \pi^6} s^4 \ln \left(-\frac{s}{\mu^2} \right) \end{aligned} \quad (7.26)$$

One check is that for the currents $j_\pm = \frac{1}{\sqrt{2}} \sum_{\Gamma=1, \gamma_5} (\bar{s}\Gamma s) (\bar{u}\Gamma u \pm \bar{d}\Gamma d)$ we get

$$\Pi(s) = -2 \frac{16N_c^2}{(2\pi)^4} \frac{1}{2^{18} 3^2 5 \pi^6} s^4 \ln \left(-\frac{s}{\mu^2} \right) = -\frac{1}{(2\pi)^4} \frac{1}{40960 \pi^6} s^4 \ln \left(-\frac{s}{\mu^2} \right) \quad (7.27)$$

in agreement with [63, 66]

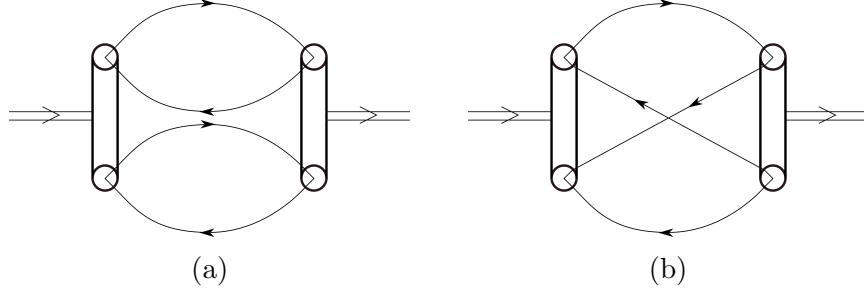


Figure 16: Standard Feynman diagrams contributing to the two point function of the four fermion current at lowest order.

In our case we are interested in

$$j(x) = (\bar{u}(x)d(x)) (\bar{u}(x)d(x)) \quad (7.28)$$

$$\mathcal{O}(P) = \int \frac{d^4 x}{(2\pi)^4} e^{-iPx} j(x) \quad (7.29)$$

which gives

$$\begin{aligned}
\Pi(s) &= i \int \frac{d^4x}{(2\pi)^4} e^{-iqx} \langle 0 | \hat{T} \{ j(x) j(0) \} | 0 \rangle \\
&= -8N_c(4N_c - 1) \frac{1}{(2\pi)^4} \frac{1}{2^{18} 3^2 5} s^4 \ln\left(-\frac{s}{\mu^2}\right) \\
&= -\frac{1}{(2\pi)^4} \frac{11}{491520 \pi^6} s^4 \ln\left(-\frac{s}{\mu^2}\right)
\end{aligned} \tag{7.30}$$

and from here

$$\rho(s) = 2\text{Im}\Pi(s + i\epsilon) = \frac{1}{(2\pi)^4} \frac{11}{245760 \pi^5} s^4 \tag{7.31}$$

One may suspect that the result may have some ambiguity from renormalization, but that is not the case since $\rho(s)$ should be finite. To check that, one can alternatively compute

$$\mathcal{O}_q|0\rangle = \int \prod_{j=1}^4 \frac{d^3k_j}{(2\pi)^3 \sqrt{2\omega_j}} \delta^{(4)}\left(\sum_{j=1}^4 k_j - q\right) \sum_{s_1, s_2, s_3, s_4} (\bar{u}_{k_1}^{s_1} v_{k_2}^{s_2}) (\bar{u}_{k_3}^{s_3} v_{k_4}^{s_4}) a_{k_1 s_1 a}^\dagger b_{k_2 s_2 a}^\dagger a_{k_3 s_3 b}^\dagger b_{k_4 s_4 b}^\dagger |0\rangle \tag{7.32}$$

where $a_{k_1 s_1 a}^\dagger$ creates a u -quark with momentum k_1 polarization s_1 and color index a , and $b_{k_1 s_1 a}^\dagger$ does the same for an anti d -quark. Notice that the time part of the delta function (total energy fixed) implies that $|\vec{k}_j| < q^0$ and therefore the integrals are over finite size balls giving a finite value to $\rho(s)$ in

$$\langle 0 | \mathcal{O}^\dagger(P') \mathcal{O}(P) | 0 \rangle = \rho(P^2) \delta^{(4)}(P' - P) \tag{7.33}$$

Using the “multi-ball integrals” in the appendix one can evaluate $\rho(s)$ from this last equation giving

$$\begin{aligned}
\rho(s) &= \frac{8N_c(4N_c - 1)}{(2\pi)^{12}} \int \prod_{j=1}^4 \frac{d^3k_j}{(2\pi)^3 2\omega_j} \delta^{(4)}\left(\sum_{j=1}^4 k_j - q\right) (k_1 k_2) (k_3 k_4) \\
&= \frac{1}{(2\pi)^4} \frac{11}{245760 \pi^5} s^4
\end{aligned} \tag{7.34}$$

in agreement with eq.(7.31). Now, using the value of $\Pi(s)$ we can write the sum rule

$$\frac{1}{s_0^{n+5}} \int_4^{s_0} \rho_{S2}(x) x^n dx = \frac{1}{(2\pi)^4} \frac{11}{245760 \pi^5} \frac{1}{n+5}, \quad n \geq 0 \tag{7.35}$$

8 Numerical method

In section 2, we have explained the main ideas of the gauge theory bootstrap and now we are going to describe their numerical implementation. This section is perhaps better read in conjunction with the mathematica and matlab programs provided with this paper. Let us briefly recall the steps involved in this framework:

- We find an (approximate) parameterization of the space of all S-matrices that satisfy the constraints of analyticity, crossing and global symmetries in terms of a large but finite number of real parameters. Within that space we identify a finite volume convex set of all S-matrices that satisfy the unitarity constraints.
- We require that the partial waves, in the Mandelstam region, approximate the Weinberg model (χ PT at tree level) within a certain tolerance. This reduces the allowed space of amplitudes to a much smaller one.
- We introduce information of the UV gauge theory (QCD) through the sum rules and asymptotic form factors. The allowed space of amplitudes is further reduced, with the amplitudes on the boundary displaying behaviors (phase shifts, form factors) agreeing with experiments.

To understand the resulting convex space we maximize linear functionals using tools of convex optimization, and examine the extremal amplitudes/form factors living on the boundary of the allowed space. The idea is that given enough physical constraints from low energy and high energy, the allowed space of amplitudes consistent with the bootstrap constraints should become a very small set consisting of amplitudes with similar behavior, and eventually allowing to identify a unique theory. In principle, the maximization functional should be irrelevant in achieving this. In practice, we focus on functionals given by linear combinations of partial waves evaluated in the unphysical region (Mandelstam triangle) to carry out this projection, and use the low energy physical information $f_\pi = 92$ MeV to identify the theory that we wish to compute. It would however be interesting for future work to check different functionals for this purpose.

In this section, we describe in detail the numerical method to carry out the gauge theory bootstrap computation. We have also provided a Mathematica notebook `GTB_numerics.nb` that implements the numerical computation described in this section, as well as a Matlab notebook `GTB_numerics.m` that contains the optimization program for the bootstrap. To carry out the optimization, we use CVX [67–69], a package for specifying and solving convex programs [67, 68]. Interested readers

can download the notebooks, install the CVX package⁷, and run the programs to reproduce the results we present in this paper.

8.1 Kernels for partial wave computations

To impose the unitarity condition (2.6), evaluate the maximization functionals (2.20), and imposing the low energy matching (2.15), we need to evaluate the partial waves $f_\ell^I(s)$ from the bootstrap variables $\{T_0, \sigma_{1,2}, \rho_{1,2}\}$. In this section, we compute such expression:

$$\begin{aligned} f_\ell^I(s) = & \hat{\Phi}_\ell^I(s)T_0 + \int_4^\infty dx \Phi_{\ell,1}^I(s, x)\sigma_1(x) + \int_4^\infty dx \Phi_{\ell,2}^I(s, x)\sigma_2(x) \\ & + \int_4^\infty dxdy \tilde{\Phi}_{\ell,1}^I(s, x, y)\rho_1(x, y) + \int_4^\infty dxdy \tilde{\Phi}_{\ell,2}^I(s, x, y)\rho_2(x, y) \end{aligned} \quad (8.1)$$

where $f_\ell^I(s)$ is an analytic function of s with cut $s > 4, s < 0$.

To arrive at the expression (8.1), the idea is to compute the partial waves projection of different parts of the amplitudes (single and double dispersion analytic functions of the variables s, t, u) and combine them into the appropriate combinations with fixed isospins.

We start by rewriting the Mandelstam representation of the amplitude (2.1) as

$$A(s, t, u) = T_0 + H_1(s) + H_2(t) + H_2(u) + \tilde{H}_1(s, t) + \tilde{H}_1(s, u) + \tilde{H}_2(t, u) \quad (8.2)$$

with

$$\begin{aligned} H_i(\nu) &= \frac{1}{\pi} \int_4^\infty dx \left[\frac{1}{x - \nu} - \frac{1}{x - \nu_0} \right] \sigma_i(x) \\ \tilde{H}_i(\nu_1, \nu_2) &= \frac{1}{\pi^2} \int_4^\infty dxdy \left[\left(\frac{1}{x - \nu_1} - \frac{1}{x - \nu_0} \right) \left(\frac{1}{y - \nu_2} - \frac{1}{y - \nu_0} \right) \right] \rho_i(x, y) \end{aligned} \quad (8.3)$$

where we simply subtracted each integration kernel at a point $s, t, u = \nu_0$ and redefined the bootstrap variables $\{T_0, \sigma_1, \sigma_2, \rho_1, \rho_2\}$. Keep in mind the symmetry $\rho_2(x, y) = \rho_2(y, x)$. Neglecting the indices i , let us consider the partial wave projection for each part of the amplitude (8.2) and write down the following Froissart-

⁷We use the MOSEK solver [70] for fast numerical optimizations.

Gribov type formula:

$$f_\ell^{(s)}(s) \equiv \frac{1}{4} \int_{-1}^1 d\mu P_\ell(\mu) H(s) dx = \frac{\delta_{l0}}{2} \mathcal{K}(s, x) \sigma(x) \quad (8.4a)$$

$$f_\ell^{(t)}(s) \equiv \frac{1}{4} \int_{-1}^1 d\mu P_\ell(\mu) H(t) dx = \int_4^\infty dx \mathcal{A}(s, x) \sigma(x) - \frac{\delta_{l0}}{2} \int dx \mathcal{W}_0(x) \sigma(x) \quad (8.4b)$$

$$f_\ell^{(u)}(s) \equiv \frac{1}{4} \int_{-1}^1 d\mu P_\ell(\mu) H(u) dx = (-1)^l \int_4^\infty dx \mathcal{A}(s, x) \sigma(x) - \frac{\delta_{l0}}{2} \int dx \mathcal{W}_0(x) \sigma(x) \quad (8.4c)$$

and

$$\begin{aligned} f_\ell^{(s,t)}(s) &\equiv \frac{1}{4} \int_{-1}^1 d\mu P_\ell(\mu) \tilde{H}(s, t) dx \\ &= \int_4^\infty dx dy \mathcal{A}(s, y) \mathcal{K}(s, x) \rho(x, y) - \frac{\delta_{l,0}}{2} \mathcal{K}(s, x) \mathcal{W}_0(y) \rho(x, y) \end{aligned} \quad (8.5a)$$

$$\begin{aligned} f_\ell^{(s,u)}(s) &\equiv \frac{1}{4} \int_{-1}^1 d\mu P_\ell(\mu) \tilde{H}(s, u) dx \\ &= (-1)^l \int_4^\infty dx dy \mathcal{A}(s, y) \mathcal{K}(s, x) \rho(x, y) - \frac{\delta_{l,0}}{2} \mathcal{K}(s, x) \mathcal{W}_0(y) \rho(x, y) \end{aligned} \quad (8.5b)$$

$$\begin{aligned} f_\ell^{(t,u)}(s) &\equiv \frac{1}{4} \int_{-1}^1 d\mu P_\ell(\mu) \tilde{H}(t, u) dx \\ &= \int_4^\infty dx dy \mathcal{A}(s, y) \mathcal{W}(s, y, x) \rho(y, x) + (-1)^l \int_4^\infty dx dy \mathcal{A}(s, y) \mathcal{W}(s, y, x) \rho(x, y) \\ &\quad + \frac{\delta_{l,0}}{2} \mathcal{W}_0(x, y) \rho(x, y) \end{aligned} \quad (8.5c)$$

where on the LHS we use the superscripts to indicate the complex variables of the analytic functions H, \tilde{H} being projected. In the expressions (8.5) and (8.4), we have

defined the kernels:

$$\mathcal{A}(s, x) = \frac{1}{\pi(s-4)} Q_\ell \left(1 + \frac{2x}{s-4} \right) \quad (8.6a)$$

$$\mathcal{W}(s, y, x) = \frac{1}{\pi} \left[\frac{1}{x+y+s-4} - \frac{1}{x-\nu_0} \right] \quad (8.6b)$$

$$\mathcal{W}_{00}(x, y) = \frac{1}{\pi^2} \frac{1}{(x-\nu_0)(y-\nu_0)} \quad (8.6c)$$

$$\mathcal{W}_0(x) = \frac{1}{\pi} \frac{1}{x-\nu_0} \quad (8.6d)$$

$$\mathcal{K}(s, x) = \frac{1}{\pi} \left(\frac{1}{x-s} - \frac{1}{x-\nu_0} \right) \quad (8.6e)$$

with $x, y \in (4, \infty)$, s complex and Q_ℓ is the second Legendre function satisfying

$$Q_\ell(z) = \frac{1}{2} \int_{-1}^1 d\mu \frac{P_\ell(\mu)}{z-\mu} \quad (8.7)$$

Notice that the kernel \mathcal{K} in (8.6e) has an imaginary part for $s > 4$ and therefore will give rise to an imaginary part of the partial waves in the physical region.

The expressions (8.4) and (8.5) allow us to define the kernels

$$\begin{aligned} \Phi_\ell^{(s)}(s, x) &= \frac{\delta_{l0}}{2} \mathcal{K}(s, x) \\ \Phi_\ell^{(t)}(s, x) &= \mathcal{A}(s, x) - \frac{\delta_{l0}}{2} \mathcal{W}_0(x) \\ \Phi_\ell^{(u)}(s, x) &= (-1)^l \mathcal{A}(s, x) - \frac{\delta_{l0}}{2} \mathcal{W}_0(x) \end{aligned} \quad (8.8)$$

$$\begin{aligned} \tilde{\Phi}_\ell^{(s,t)}(s, x, y) &= \mathcal{A}(s, y) \mathcal{K}(s, x) - \frac{\delta_{l,0}}{2} \mathcal{K}(s, x) \mathcal{W}_0(y) \\ \tilde{\Phi}_\ell^{(s,u)}(s, x, y) &= (-1)^l \mathcal{A}(s, y) \mathcal{K}(s, x) - \frac{\delta_{l,0}}{2} \mathcal{K}(s, x) \mathcal{W}_0(y) \\ \tilde{\Phi}_\ell^{(t,u)}(s, x, y) &= \mathcal{A}(s, y) \mathcal{W}(s, y, x) \mathcal{T}_{x,y} + (-1)^l \mathcal{A}(s, y) \mathcal{W}(s, y, x) + \frac{\delta_{l,0}}{2} \mathcal{W}_0(x, y) \end{aligned} \quad (8.9)$$

where $\mathcal{T}_{x,y}$ interchanges the variables of a double spectral density $\rho(y, x) = \mathcal{T}_{x,y} \rho(x, y)$. Namely, integrating the spectral densities σ, ρ with these kernels (8.8), (8.9) give the partial waves (8.4) and (8.5) by projecting out different parts of the amplitudes to a definite angular momentum ℓ .

With these basic kernels, we can now make combinations which gives rise to kernels to be integrated with the spectral densities $\sigma_{1,2}$ and $\rho_{1,2}$ respectively. We have first the kernels for the single spectral densities:

$$\Phi_{\ell,1}^{(s)}(s, x) = \Phi_{\ell}^{(s)}(s, x) \quad (8.10a)$$

$$\Phi_{\ell,1}^{(t)}(s, x) = \Phi_{\ell}^{(t)}(s, x) \quad (8.10b)$$

$$\Phi_{\ell,1}^{(u)}(s, x) = \Phi_{\ell}^{(u)}(s, x) \quad (8.10c)$$

$$\Phi_{\ell,2}^{(s)}(s, x) = \Phi_{\ell}^{(t)}(s, x) + \Phi_{\ell}^{(u)}(s, x), \quad (8.10d)$$

$$\Phi_{\ell,2}^{(t)}(s, x) = \Phi_{\ell}^{(s)}(s, x) + \Phi_{\ell}^{(u)}(s, x), \quad (8.10e)$$

$$\Phi_{\ell,2}^{(u)}(s, x) = \Phi_{\ell}^{(s)}(s, x) + \Phi_{\ell}^{(t)}(s, x) \quad (8.10f)$$

where the subscript 1, 2 indicate the corresponding single spectral density $\sigma_{1,2}$. Similarly, we have

$$\tilde{\Phi}_{\ell,1}^{(s,t)}(s, x, y) = \tilde{\Phi}_{\ell}^{(s,t)}(s, x, y) + \tilde{\Phi}_{\ell}^{(s,u)}(s, x, y) \quad (8.11a)$$

$$\tilde{\Phi}_{\ell,1}^{(t,s)}(s, x, y) = \tilde{\Phi}_{\ell}^{(s,t)}(s, x, y)\mathcal{T}_{x,y} + \tilde{\Phi}_{\ell}^{(t,u)}(s, x, y) \quad (8.11b)$$

$$\tilde{\Phi}_{\ell,1}^{(u,t)}(s, x, y) = \tilde{\Phi}_{\ell}^{(t,u)}(s, x, y)\mathcal{T}_{x,y} + \tilde{\Phi}_{\ell}^{(s,u)}(s, x, y)\mathcal{T}_{x,y} \quad (8.11c)$$

$$\tilde{\Phi}_{\ell,2}^{(s,t)}(s, x, y) = \tilde{\Phi}_{\ell}^{(t,u)}(s, x, y) \quad (8.11d)$$

$$\tilde{\Phi}_{\ell,2}^{(t,s)}(s, x, y) = \tilde{\Phi}_{\ell}^{(s,u)}(s, x, y) \quad (8.11e)$$

$$\tilde{\Phi}_{\ell,2}^{(u,t)}(s, x, y) = \tilde{\Phi}_{\ell}^{(s,t)}(s, x, y)\mathcal{T}_{x,y} \quad (8.11f)$$

where again, the subscript 1, 2 indicate the corresponding double spectral density $\rho_{1,2}$ that it should be multiplied with. The superscript indicate the complex variables involves in the analytic function \tilde{H} before projecting out to a partial wave. For example, the superscript (t, s) arises from the integration kernel after projecting out a fixed angular momentum for analytic function $\tilde{H}(t, s)$. This switch of complex variables in the analytic functions \tilde{H} is due to the interchange of s, t, u variables in (2.2) for defining amplitudes of a fixed isospin.

The final kernels for computing the partial waves of fixed isospin from the spectral densities $\sigma_{1,2}, \rho_{1,2}$ is given by (we omit the variables s, x, y here)

$$\tilde{\Phi}_{\ell,i}^I = \begin{bmatrix} \tilde{\Phi}_{\ell,i}^0 \\ \tilde{\Phi}_{\ell,i}^1 \\ \tilde{\Phi}_{\ell,i}^2 \end{bmatrix} = \begin{bmatrix} 3\tilde{\Phi}_{\ell,i}^{(s,t)} + \tilde{\Phi}_{\ell,i}^{(t,s)} + \tilde{\Phi}_{\ell,i}^{(u,t)} \\ \tilde{\Phi}_{\ell,i}^{(t,s)} + \tilde{\Phi}_{\ell,i}^{(u,t)} \\ \tilde{\Phi}_{\ell,i}^{(t,s)} - \tilde{\Phi}_{\ell,i}^{(u,t)} \end{bmatrix}, \quad i = 1, 2 \quad (8.12)$$

$$\Phi_{\ell,i}^I = \begin{bmatrix} \Phi_{\ell,i}^0 \\ \Phi_{\ell,i}^1 \\ \Phi_{\ell,i}^2 \end{bmatrix} = \begin{bmatrix} 3\Phi_{\ell,i}^{(s)} + \Phi_{\ell,i}^{(t)} + \Phi_{\ell,i}^{(u)} \\ \Phi_{\ell,i}^{(t)} + \Phi_{\ell,i}^{(u)} \\ \Phi_{\ell,i}^{(t)} - \Phi_{\ell,i}^{(u)} \end{bmatrix}, \quad i = 1, 2 \quad (8.13)$$

as well as the coefficient to multiply the constant T_0

$$\hat{\Phi}_\ell^I = \begin{bmatrix} \hat{\Phi}_{\ell,i}^0 \\ \hat{\Phi}_{\ell,i}^1 \\ \hat{\Phi}_{\ell,i}^2 \end{bmatrix} = \frac{\delta_{l0}}{2} \begin{bmatrix} (N+2) \\ 0 \\ 2 \end{bmatrix} \quad (8.14)$$

The combinations here can be understood directly from the combinations in (2.2) for defining amplitudes with fixed isospins. Integrating the constant T_0 , spectral densities $\sigma_{1,2}$ and $\rho_{1,2}$ according to (8.1) give the analytic partial waves with definite isospins.

8.2 Mapping to the circle

For numerically computing the above integrals, we map the cut plane of ν (standing for s, t, u) onto a unit disk

$$z(\nu) = \frac{\sqrt{4-\nu_0} - \sqrt{4-\nu}}{\sqrt{4-\nu_0} + \sqrt{4-\nu}} \quad (8.15)$$

where the point $\nu = \nu_0$ is mapped to the center of the unit z disk.⁸ The region $x \in (4, \infty)$ is mapped to the upper half circle of $z = e^{i\phi}$, $\phi \in [0, \pi]$:

$$x(\phi) = \nu_0 + \frac{8 - 2\nu_0}{1 + \cos(\phi)}, \quad x \in (4, \infty) \quad (8.16)$$

Under this map, the integrals in (8.1) simply become

$$\int_4^\infty dx \rightarrow \int_0^\pi x'(\phi) d\phi \quad (8.17)$$

where

$$x'(\phi) = \frac{2(4 - \nu_0) \sin \phi}{(1 + \cos \phi)^2} \quad (8.18)$$

The variables x, y in the kernels (8.6) can be simply replaced by $x(\phi_1), y(\phi_2)$. We will rename the spectral densities $\sigma_{1,2}(\phi_1), \rho_{1,2}(\phi_1, \phi_2)$ accordingly.

⁸this is the same map used in the ρ variable parametrization of the S-matrix bootstrap [6]

Under the map (8.15), the region above the cut is mapped to the upper half circle of z and below the cut mapped to the lower half circle of z . Let us now look at the kernel \mathcal{K} which has a jump across the cut $s > 4$. Under this map, we can then replace

$$\int_4^\infty dx \mathcal{K}(\nu, x) \rightarrow \int_0^\pi d\phi K(z, \phi) \quad (8.19)$$

with

$$K(z, \phi) = \frac{2z \sin \phi}{\pi + \pi z^2 - 2\pi z \cos \phi} \quad (8.20)$$

where we absorbed (8.18) into the definition of K . The kernel K allows to compute analytic functions on the unit disk of z (and vanishes at $z = 0$) using their imaginary part on the upper half circle:

$$g(z) = \int_0^\infty d\phi K(z, \phi) \text{Im}g(\phi) \quad (8.21)$$

Evaluating the real part $\text{Re}g(\phi)$ on the upper half circle requires computing a principal part integral

$$\text{Reg}(\phi) = \oint_0^\pi d\phi_1 \hat{K}(\phi, \phi_1) \text{Im}g(\phi_1) = \frac{1}{\pi} \oint_0^\pi d\phi_1 \frac{\sin \phi_1}{\cos \phi - \cos \phi_1} \text{Im}g(\phi_1) \quad (8.22)$$

To perform this integral we extend $\text{Im}g(\phi_1)$ to the range $-\pi \leq \phi_1 \leq \pi$ by assuming that it is anti-symmetric $\text{Im}g(-\phi_1) = -\text{Im}g(\phi_1)$ so that the integrand is symmetric. For the spectral densities $\sigma_{1,2}(\phi_1)$, $\rho_{1,2}(\phi_1, \phi_2)$ this agrees with them being the imaginary part of an amplitude that changes sign across the cut.

The expression (8.1) for computing the physical partial waves now becomes ($I = 0, 1, 2$)

$$\begin{aligned} f_\ell^I(s) = & \hat{\Phi}_\ell^I(s) T_0 + \int_0^\pi d\phi_1 \Phi_{\ell,1}^I(s, \phi_1) \sigma_1(\phi_1) + \int_0^\pi d\phi_1 \Phi_{\ell,2}^I(s, \phi_1) \sigma_2(\phi_1) \\ & + \int_0^\pi d\phi_1 d\phi_2 \tilde{\Phi}_{\ell,1}^I(s, \phi_1, \phi_2) \rho_1(\phi_1, \phi_2) + \int_0^\pi d\phi_1 d\phi_2 \tilde{\Phi}_{\ell,2}^I(s, \phi_1, \phi_2) \rho_2(\phi_1, \phi_2) \end{aligned} \quad (8.23)$$

where we just renamed the kernels as $\Phi, \tilde{\Phi}$ when using variables ϕ_1, ϕ_2 and absorb the Jacobian (8.18) into the definitions of Φ and $\tilde{\Phi}$.

Consider now the analytic form factor (2.7) which can be parameterized by its imaginary part $\text{Im}F(x)$ (neglecting the indices for now) above the cut $s > 4$. The

same map (8.15) and (8.16) applies and we can write its real part $\text{Re}F(s)$ in the physical region $s > 4$ (denoted as $\text{Re}F(\phi)$) using the above dispersion relation (8.22)

$$\text{Re}F(\phi) = 1 + \oint_0^\pi d\phi_1 \hat{K}(\phi, \phi_1) \text{Im}F(\phi_1) + \int_0^\pi K_0(\phi_1) \text{Im}F(\phi_1) \quad (8.24)$$

with

$$K_0(\phi) = \frac{\nu_0 \sin \phi}{\pi(8 - \nu_0 + \nu_0 \cos \phi)} \quad (8.25)$$

computing the difference between subtracting at $s = 0$ and $s = \nu_0$.⁹

Furthermore, we can also use the map (8.16) to rewrite the spectral density ρ_ℓ^I as

$$\rho_\ell^I(x) \rightarrow \rho_\ell^I(\phi) \quad (8.26)$$

When implementing the sum rules, we need to perform integrals of the type (2.17g), (2.18g) and (2.19g), which become

$$\int_0^{\phi_0} x'(\phi) d\phi \rho_\ell^I(\phi) x(\phi)^n, \quad s_0 = x(\phi_0) \quad (8.27)$$

To summarize, after mapping to the circle, all our bootstrap variables (2.9) are parameterized by the angles $\phi_1, \phi_2 \in (0, \pi)$: (where $\rho_2(\phi_1, \phi_2) = \rho_2(\phi_2, \phi_1)$)

$$\{T_0, \sigma_{\alpha=1,2}(\phi_1), \rho_{\alpha=1,2}(\phi_1, \phi_2), \text{Im}F_\ell^I(\phi_1), \rho_\ell^I(\phi_1)\} \quad (8.28)$$

which we will discretize in the next subsection.

8.3 Interpolation points

To discretize the bootstrap variables $\{T_0, \sigma_1, \sigma_2, \rho_1, \rho_2, \text{Im}F_\ell^I, \rho_\ell^I\}$, we choose equally spaced M points in the range $\phi \in (0, \pi)$:

$$\phi_j = \left(j - \frac{1}{2}\right) \Delta_\phi, \quad j = 1, 2, \dots, M, \quad \Delta_\phi = \frac{\pi}{M} \quad (8.29)$$

The index j is shifted to avoid taking the point exactly at threshold¹⁰. This corresponds to a set of points in the region $(4, \infty)$

$$x_j = x(\phi_j), \quad j = 1, \dots, M \quad (8.30)$$

⁹recall the normalization $F(0) = 1$ and that the point $s = \nu_0$ is mapped to the center of the disk where the kernel (8.20) vanishes

¹⁰Note that according to the map (8.16), the discrete set of angles (8.29) correspond to different distributions of $x_j \in (0, 4)$ depending on the center ν_0 for the map. We have tested the convergence of the numerics for a few values of ν_0 and the results in this paper are obtained using $\nu_0 = -20$.

which is also the set of points where we will evaluate the partial waves in the physical region. We thus have the discrete set of bootstrap variables (where $\rho_{2,j_1j_2} = \rho_{2,j_2j_1}$)

$$\{T_0, \sigma_{1,j_1}, \sigma_{2,j_1}, \rho_{1,j_1j_2}, \rho_{2,j_1j_2}, \text{Im}F_{\ell,j_1}^I, \rho_{\ell,j_1}^I\}, \quad j_1, j_2 = 1, 2, \dots, M \quad (8.31)$$

For the bootstrap procedure, we also have to evaluate the partial waves at an unphysical point s_* (can be complex in general) $f_\ell^I(s_*)$. This will be used for both defining functionals of the type (2.20), as well as for the requirement of matching with the tree level partial waves (2.16) in the low energy unphysical region $s \in (0, 4)$.

The partial waves evaluation at a generic point s_* (away from the cut $s > 4$) can be done directly by taking an unphysical point s_* and replacing the integrals in (8.23) with sums:

$$f_\ell^I(s_*) = fT_0 + f_{1,j_1}\sigma_{1,j_1} + f_{2,j_1}\sigma_{2,j_1} + f_{1,j_1j_2}\rho_{1,j_1j_2} + f_{2,j_1j_2}\rho_{2,j_1j_2} \quad (8.32)$$

where

$$\begin{aligned} f &= \hat{\Phi}_\ell^I(s_*), \quad f_{1,j_1} = \Delta_\phi \Phi_{\ell,1}^I(s_*, \phi_{j_1}), \quad f_{2,j_1} = \Delta_\phi \Phi_{\ell,2}^I(s_*, \phi_{j_1}), \\ f_{1,j_1j_2} &= \Delta_\phi^2 \tilde{\Phi}_{\ell,1}^I(s_*, \phi_{j_1}, \phi_{j_2}), \quad f_{2,j_1j_2} = \Delta_\phi^2 \tilde{\Phi}_{\ell,2}^I(s_*, \phi_{j_1}, \phi_{j_2}) \end{aligned} \quad (8.33)$$

The evaluation of the partial waves in the physical region $s > 4$ above the cut is slightly trickier since the kernel \mathcal{K} (or equivalently K in (8.20)) has real and imaginary parts in the physical region. In this case, we can write the discretized version of the kernel K (8.20) (evaluated on the upper half circle) as

$$K(\phi_j, \phi_{j_1}) = \hat{K}_{jj_1} + \frac{i}{2\pi} \delta_{jj_1} \quad (8.34)$$

where the principal integral (8.22) becomes the sum

$$\text{Reg}(\phi_j) = \sum_{j_1=-M}^M \hat{K}_{jj_1} \text{Im}g(\phi_{j_1}) \quad (8.35)$$

and

$$\hat{K}_{j_1j_2} = -\frac{1}{2M} (1 - (-)^{j_1-j_2}) \cot\left(\frac{\pi}{2M}(j_1 - j_2)\right) \quad (8.36)$$

namely the discretized kernel that relates the real and imaginary part of an analytic function at the boundary of the unit disk.

With this, we can now evaluate the partial waves in the physical region. In practice, for imposing the unitarity constraints, we evaluate the rescaled partial waves

$$h_\ell^I(s) = \pi \sqrt{\frac{s-4}{s}} f_\ell^I(s) \quad (8.37)$$

at discrete points $s_j = x(\phi_j) \in (4, \infty)$. This is given by

$$h_{\ell,j}^I = h_{\ell,j}^I T_0 + h_{\ell,1;j,j_1}^I \sigma_{1,j_1} + h_{\ell,2;j,j_1}^I \sigma_{2,j_1} + h_{\ell,1;j,j_1,j_2}^I \rho_{1,j_1,j_2} + h_{\ell,2;j,j_1,j_2}^I \rho_{2,j_1,j_2} \quad (8.38)$$

where

$$\begin{aligned} h_{\ell,j}^I &= \omega_j \hat{\Phi}_\ell^I(s_j), \quad h_{\ell,1;j,j_1}^I = \omega_j \Delta_\phi \Phi_{\ell,1}^I(s_j, \phi_{j_1}), \quad h_{\ell,2;j,j_1}^I = \omega_j \Delta_\phi \Phi_{\ell,2}^I(s_j, \phi_{j_1}), \\ h_{\ell,1;j,j_1,j_2}^I &= \omega_j \Delta_\phi^2 \tilde{\Phi}_{\ell,1}^I(s_j, \phi_{j_1}, \phi_{j_2}), \quad h_{\ell,2;j,j_1,j_2}^I = \omega_j \Delta_\phi^2 \tilde{\Phi}_{\ell,2}^I(s_j, \phi_{j_1}, \phi_{j_2}) \end{aligned} \quad (8.39)$$

with

$$\omega_j = \pi \sqrt{\frac{s_j - 4}{s_j}} \quad (8.40)$$

from the factor in 8.37. For evaluating the sum (8.38), one simply uses their original definition in section 8.1, and take the values of s_j at discrete points (8.30) (keep in mind that the Jacobian has been absorbed into the redefinitions of $\Phi, \tilde{\Phi}$). In particular, for the kernels that involve \mathcal{K} , one has to use the expressions (8.34), (8.36) that perform the numerical principal integral which gives rise to the real and imaginary part of the partial waves in the physical region $s > 4$.

As an additional numerical comment, due to the symmetry of the spectral density $\rho_{2,j_1 j_2} = \rho_{2,j_2 j_1}$, in practice we symmetrize the numerical matrices that multiply ρ_2 , namely $f_{2,j_1 j_2}$ and $\Phi_{\ell,2;j,j_1,j_2}^I$ with respect to the j_1, j_2 indices thus reducing the number of variables.

The numerical computation of the form factors is completely analogous. The form factor is parametrized by its imaginary part on the physical region at discretized points $\text{Im}F(s_j) \rightarrow \text{Im}F(\phi_j)$. According to (8.24), the real part can be computed with

$$\text{Re}F_j = 1 + (\hat{K}_{j,j_1} + K_{0,j_1}) \text{Im}F_{j_1} \quad (8.41)$$

where

$$K_{0,j_1} = K_0(\phi_{j_1}) \quad (8.42)$$

Finally, for implementing the sum rules that involve the integral (8.27), we compute the discrete sum:

$$\int_0^{\phi_0} x'(\phi) d\phi \rho_\ell^I(\phi) x(\phi)^n \rightarrow \sum_{i=1}^{n_0} \Delta_\phi x'(\phi_i) x(\phi_i)^n \rho_\ell^I(\phi_i) \quad (8.43)$$

where n_0 denotes the cutoff angle ϕ_0 (i.e. the energy scale s_0).

The numerical matrices involved in the above computations ((8.33), (8.39), (8.41), (8.43)) are all included in the Mathematica notebook `GTB_numerics.nb` we provide with this paper.

8.4 Numerical gauge theory bootstrap

With the above numerical setup, let us now describe the concrete implementation of the gauge theory bootstrap. We provide a matlab code `GTB_numerics.m` that implements this procedure. Interested readers can simply download the file, install the CVX package together with the MOSEK solver to run the program and reproduce the results in this paper. This section may serve as a guide to help understand the numerical code.

S-matrix/form factor bootstrap In the numerical procedure, we have a discrete set of variables (ρ_{2,j_1j_2} has only symmetric part)

$$v_a = \{T_0, \sigma_{1,j_1}, \sigma_{2,j_1}, \rho_{1,j_1j_2}, \rho_{2,j_1j_2}, \text{Im}F_{\ell,j_1}^I, \rho_{\ell,j_1}^I\}. \quad (8.44)$$

Taking into account the symmetry of ρ_{2,j_1j_2} , we have total number of variables (in our case we take $M = 50$ and $\mathbf{M} = 4176$)

$$\mathbf{M} = 1 + 2M + M^2 + \frac{M(M+1)}{2} + 3M + 3M \quad (8.45)$$

As described above, the $\{T_0, \sigma_{1,2}, \rho_{1,2}\}$ parameterize the amplitude and we compute the rescaled partial waves (8.38) in the physical region at discrete points s_j (corresponding to (8.30)) up to a maximal spin $\ell = L$ ($=19$ in our paper). In appendix B, we analyze the sensitivity of the results to the numerical parameters M, L . Denoting

$$\text{Re}h_n = A_{n,a}v_a, \quad \text{Im}h_n = B_{n,a}v_a \quad (8.46)$$

where n summarizes the indices I, ℓ, s_j , we impose the unitarity condition

$$\text{Re}h_n^2 + \text{Im}h_n^2 \leq 2\text{Im}h_n, \quad \forall n \quad (8.47)$$

While (8.47) describes the standard constraint in a pure S-matrix bootstrap, we make two technical improvements in our numerical computation. The first one involves a rescaling of the unitarity cone condition (8.47) on both sides with a factor Λ_n^2 to improve the machine precision optimization. To do this, we define

$$\text{Re}\tilde{h}_n = \Lambda_n^{-1}A_{n,a}v_a, \quad \text{Im}\tilde{h}_n = \Lambda_n^{-1}B_{n,a}v_a, \quad \text{Im}\hat{h}_n = \Lambda_n^{-2}B_{n,a}v_a \quad (8.48)$$

such that we have a rescaled version of (8.47)

$$\text{Re}\tilde{h}_n^2 + \text{Im}\tilde{h}_n^2 \leq 2\text{Im}\hat{h}_n, \quad \forall n \quad (8.49)$$

The rescaling factor Λ_n here is given by

$$\Lambda_\ell(s) = \left(\frac{\sqrt{s} - 2}{\sqrt{s} + 1} \right)^{\frac{\ell}{2}} \quad (8.50)$$

and characterizes the typical scale of the partial waves depending on the energy s and the angular momentum ℓ . In the numerical computations (in `GTB_numerics.nb`), we compute the linear transformations matrices $\Lambda_n^{-1}A_{n,a}$, $\Lambda_n^{-1}B_{n,a}$, $\Lambda_n^{-2}B_{n,a}$ with high precision before importing them into the optimization program and multiplying them with the machine precision variables v_a . The purpose of this rescaling is so that we can use our machine precision variables v_a to describe a set of unitarity cones of similar scale, avoiding potential numerical instability.

A second technical improvement is the regularization procedure we introduced in [71] by requiring a bound on the norm of the double spectral density with a large regulator M_{reg}

$$||[\rho_{1,j_1,j_2}, \rho_{2,j_1,j_2}]||_4 \leq M_{reg} \quad (8.51)$$

The detail motivation of the regularization is explained in [71] and is related to the feasibility of the dual formulation of the problem. The value of the M_{reg} is tested with the pure S-matrix bootstrap to ensure convergence. In producing the results in this paper, we take it to be $M_{reg} = 10^2$. For different numerical problems, one would need to test this to ensure convergence.

Let us move on to the inclusion of the form factors and spectral densities. In this paper, we consider only the $S0$, $P1$, $D0$ form factors to compute the positive semidefinite matrix (2.8). This can of course be done for generic ℓ (for example, to higher energy one would be interested in including $F1$ to search for the ρ_3 meson, which would requires more numerical resolution than our current setup). The numerical computation including more form factors is however more time consuming.

The form factors are parametrized by the imaginary part $\text{Im}F(s_j)$. Using (8.41), we can compute the real part $\text{Re}F(s_j)$ on the physical line. The rescaled form factors $\mathcal{F}_\ell^I(s_j)$ are then obtained by multiplying with the rescaling factors as given in (2.17e), (2.18e), (2.19e).

To impose the positivity condition (2.8), we choose $s_0 \simeq 2\text{GeV}$, and impose the positive semidefinite conditions in the range $s \in (4, s_0)$. We denote n_0 the highest index in the list of points s_j (8.30) whose value is below 2GeV. Denoting:

$$S_\ell^I(s_j) \rightarrow S_{\ell,j}^I, \quad \mathcal{F}_\ell^I(s_j) \rightarrow \mathcal{F}_{\ell,j}^I, \quad \rho_\ell^I(s_j) \rightarrow \rho_{\ell,j}^I, \quad j = 1, \dots, n_0 \quad (8.52)$$

we impose the positivity condition:

$$B_{\ell,j}^I = \begin{pmatrix} 1 & S_{\ell,j}^I & \mathcal{F}_{\ell,j}^I \\ S_{\ell,j}^{I*} & 1 & \mathcal{F}_{\ell,j}^{I*} \\ \mathcal{F}_{\ell,j}^{I*} & \mathcal{F}_{\ell,j}^I & \rho_{\ell,j}^I \end{pmatrix} \succeq 0 \quad (8.53)$$

$$\{I, \ell\} \in \{S0, P1, D0\}, \quad j = 1, \dots, n_0$$

Chiral symmetry breaking The implementation of the chiral symmetry breaking condition is straightforward. Using (8.38), we can evaluate the first six partial waves

$$f_0^0, f_2^0, f_0^2, f_2^2, f_1^1, f_3^1 \quad (8.54)$$

at four unphysical points

$$s_{*,i} = \{1/2, 1, 3/2, 2\} \quad (8.55)$$

The tree level partial waves (2.15) define the following ratios of the $S0, P1, S2$ waves:

$$R_{01}^{\text{tree}}(s) = \frac{3(2s-1)}{s-4}, \quad R_{21}^{\text{tree}}(s) = \frac{3(2-s)}{s-4} \quad (8.56)$$

and all the higher tree level partial waves vanish. Let us define

$$\begin{aligned} \mathbf{f}_{01}^X &= f_0^0(s_{*,i}) - R_{01}^{\text{tree}}(s_{*,i})f_1^1(s_{*,i}) \\ \mathbf{f}_{21}^X &= f_2^0(s_{*,i}) - R_{21}^{\text{tree}}(s_{*,i})f_1^1(s_{*,i}) \\ \mathbf{f}_2^0 &= f_2^0(s_{*,i}), \quad \mathbf{f}_2^2 = f_2^2(s_{*,i}), \quad \mathbf{f}_1^1 = f_1^1(s_{*,i}), \quad s_{*,i} = \{1/2, 1, 3/2, 2\} \end{aligned} \quad (8.57)$$

where the bold face letter should be interpreted as a vector of four components corresponding to the evaluations at the points (8.55). We then require

$$||[\mathbf{f}_{01}^X, \mathbf{f}_{21}^X]|| \leq \epsilon^X, \quad ||[\mathbf{f}_2^0, \mathbf{f}_2^2, \mathbf{f}_1^1]|| \leq \epsilon^X, \quad (8.58)$$

Namely we are matching these quantities with the tree level partial waves at very low energy (the four points (8.55)) up to a tolerance ϵ^X .

In producing the results of this paper, we take the tolerance to be $\epsilon^X = 3 \times 10^{-2}$. This choice follows from the explorations done in our previous paper [1]. To briefly summarize the idea, we have previously tested imposing the constraints (8.58) with a series of tolerances ϵ^X . Such tolerance for the matching should not be too small or too large: if it is too small, the theory we are studying with the physical $f_\pi = 92$

MeV would be excluded; if it is too large, there would be a large deviation from the tree level behavior at very low energy. Through such exploration, we numerically fix a tolerance $\epsilon^\chi = 3 \times 10^{-2}$ which best approximate the tree level partial waves at very low energy. See section 4.2 in our previous paper [1] for discussion. It is of course desirable to improve this procedure, which we leave for future work.

SVZ sum rules To include the QCD information at high energy, we first impose the finite energy SVZ sum rule for $S0, P1, D0$ spectral densities ρ_ℓ^I as summarized in (2.17g), (2.18g) and (2.19g). In practice, we take the first three moments for each spectral density:

$$S0 : n = 0, 1, 2, \quad P1 : n = -1, 0, 1, \quad D0 : n = -2, -1, 0 \quad (8.59)$$

This amounts to the following explicit sum rules:

$$\begin{aligned} \int_4^{s_0} \frac{\rho_0^0(x) dx}{s_0^2} &\simeq 3.1 \times 10^{-7}, \quad \int_4^{s_0} \frac{\rho_0^0(x) x dx}{s_0^3} \simeq 2.1 \times 10^{-7}, \quad \int_4^{s_0} \frac{\rho_0^0(x) x^2 dx}{s_0^4} \simeq 1.6 \times 10^{-7} \\ \int_4^{s_0} \frac{\rho_1^1(x) dx}{s_0^2} &\simeq 5.6 \times 10^{-5}, \quad \int_4^{s_0} \frac{\rho_1^1(x) x dx}{s_0^3} \simeq 2.8 \times 10^{-5}, \quad \int_4^{s_0} \frac{\rho_1^1(x) x^2 dx}{s_0^4} \simeq 1.8 \times 10^{-5} \\ \int_4^{s_0} \frac{\rho_2^0(x) dx}{s_0^2} &\simeq 5.1 \times 10^{-5}, \quad \int_4^{s_0} \frac{\rho_2^0(x) x dx}{s_0^3} \simeq 2.6 \times 10^{-5}, \quad \int_4^{s_0} \frac{\rho_2^0(x) x^2 dx}{s_0^4} \simeq 1.7 \times 10^{-5} \end{aligned} \quad (8.60)$$

The numerical implementation replaces the integrals with discrete sum as given above in (8.43). To be more specific, we take the integral up to the highest discrete numerical points below s_0 , namely the point n_0 , and we use the value $x(\phi_{n_0})$ as the s_0 in (8.60). In practice purposes, the sum rule that has the most influence on the result is the $P1$ wave although the others are needed to compute the corresponding form factors and the spectral densities themselves.

As given in (2.17g), (2.18g) and (2.19g), the sum rules we are using contain the identity operator contribution in the SVZ expansion and only up to order α_s in the perturbative QCD expansion (see section 7 for the perturbative QCD computations). To estimate the error from the higher order α_s corrections, we use the contribution from the order α_s term to set an error in implementing the sum rules (8.60). Note that this error is of the same order of magnitude for different moments of the same spectral density. Defining the error for various moments as

$$w_{\ell,n}^I = \sum_{i=1}^{n_0} \frac{x'(\phi_i)}{x(\phi_0)^{n+n_\ell}} \Delta_\phi x(\phi_i)^n \rho_\ell^I(\phi_i) - \text{RHS of (8.60)}, \quad n_\ell = \begin{cases} 2, & S0, P1 \\ 3, & D0 \end{cases} \quad (8.61)$$

This leads to the following sum rule numerical constraints

$$\begin{aligned}
|| (w_{0,n=0}^0, w_{0,n=1}^0, w_{0,n=2}^0) || &\lesssim 1 \times 10^{-7} \\
|| (w_{1,n=-1}^1, w_{1,n=0}^1, w_{1,n=1}^1) || &\lesssim 5 \times 10^{-6} \\
|| (w_{2,n=-2}^0, w_{2,n=-1}^0, w_{2,n=0}^0) || &\lesssim 6 \times 10^{-6}
\end{aligned} \tag{8.62}$$

Form factor asymptotics Finally, we also have the asymptotic behavior of the form factors at large momentum transfer (denoted as s). It was already noted in [1] that it is crucial to require that the form factors become small at large energies as follows from generic QCD arguments [17, 18].

The computation of such asymptotic forms is explained in section 6.2 and we have summarized the expressions for $S0, P1, D0$ in (2.17h), (2.18h) and (2.19h). To implement this asymptotic behavior, we take the rescaled form factor \mathcal{F}_ℓ^I at discrete points at high momentum transfer $s > s_0$ (i.e, above the energy scale we use the SVZ sum rules):

$$\mathcal{F}_\ell^I(s_j), \quad j = n_0 + 1, \dots, M \tag{8.63}$$

and require that its values at each of these points are bounded by a small number ϵ^{FF} :

$$|\mathcal{F}_\ell^I(s_j)|^2 \leq \epsilon_{\ell,I}^{FF} \tag{8.64}$$

An initial estimate of the small number $\epsilon_{\ell,I}^{FF}$ for each form factor can be made using the expressions (2.19h) and (2.18h) evaluated at s_0 and then use the same number for all the high s points for the same form factor. Namely, we neglect the precise s dependence of the asymptotic form and simply require the values to be small. As mentioned before, we do not know the precise asymptotic constant for the scalar form factor so we make an estimate based on relative charge in the scalar current as compared with the vector current. In any case, the $\epsilon_{s_0}^{FF}$ does not affect the results. It is interesting to note however that the $D0$ form factor asymptotics turns out to be too stringent. If we use the estimated value based on the asymptotic expression (2.19h), the program becomes infeasible. This suggests that at 2 GeV where we take s_0 , the $D0$ form factor may not be quite in the asymptotic region. Numerically, we then gradually raise the $D0$ asymptotic bound ϵ_{D0}^{FF} until the program just becomes feasible. The final $\epsilon_{\ell,I}^{FF}$'s we use for each form factor are:

$$\begin{aligned}
|\mathcal{F}_0^0(s_j)|^2 &\leq 3 \times 10^{-8} \\
|\mathcal{F}_1^1(s_j)|^2 &\leq 2 \times 10^{-6} \\
|\mathcal{F}_2^0(s_j)|^2 &\leq 4 \times 10^{-2}, \quad \forall j = n_0 + 1, \dots, M
\end{aligned} \tag{8.65}$$

It actually turns out that the estimate from (2.18h) for the $P1$ form factor is 1.89×10^{-6} showing that at 2 GeV, the $P1$ channel is numerically consistent with the asymptotics.

Maximization With the above input, the final step is maximizing linear functionals whose results give extremal scattering amplitudes. In this paper, we consider the two functionals (2.20), whose projection gives rise to the space fig. 3 where we can identify the points (blue, red) closest to the black dots as our theory. The evaluation of these functionals involves only computing the partial waves in the unphysical region $s = 3$ which can be done as described above. In practice, the plot of the shape 3 is done by scanning one functional \mathfrak{F}_0 and maximize/minimize the other one \mathfrak{F}_1 .

8.5 Unitarization

In obtaining the results we show in this paper, we perform an extra step of unitarization. While this was not necessary in our previous work [1] with $s_0 = 1.2$ GeV (unitarity is close to being saturated there), the current computation with $s_0 = 2$ GeV includes more physical constraints and higher energies and as a result, has more unitarity unsaturation after the initial maximization of the functionals (2.20). One point is that we are not interested in the maximal values of these functionals, but only using such a maximization as a tool to compute amplitudes/form factors non-perturbatively. Therefore, once we are done with the initial optimization, we could carry out a step to further unitarize the obtained amplitudes.

The unitarization step uses a technique we introduced previously in [37] for constructing an optimization functional by linearizing unitarity constraints. Consider again the rescaled unitarity cone in (8.49):

$$\text{Re}\tilde{h}_n^2 + \text{Im}\tilde{h}_n^2 \leq 2\text{Im}\hat{h}_n, \quad \forall n$$

Now, suppose that after an initial maximization of the functionals (2.20), we have obtained a set of partial waves denoted as \tilde{h}_n which may not saturate unitarity. Using these $\text{Re}\tilde{h}_n, \text{Im}\tilde{h}_n$, we can then construct a new linear functional that acts on the partial waves in the physical region as

$$\mathcal{F} \left[\{\text{Re}\tilde{h}_n, \text{Im}\tilde{h}_n, \text{Im}\hat{h}_n\} \right] = \text{Re}\tilde{h}_n \text{Re}\tilde{h}_n + \text{Im}\tilde{h}_n \text{Im}\tilde{h}_n - \sum_n \text{Im}\hat{h}_n \quad (8.66)$$

which simply arise from linearizing the unitarity (8.49). Maximizing this linear functional leads to further improving the unitarity saturation.

Recall now the linear transformation from the variables to the rescaled partial waves (8.48)

$$\text{Re}\tilde{h}_n = \tilde{A}_{n,a}v_a, \quad \text{Im}\tilde{h}_n = \tilde{B}_{n,a}v_a, \quad \text{Im}\hat{h}_n = \hat{B}_{n,a}v_a \quad (8.67)$$

with

$$\tilde{A}_{n,a} \equiv \Lambda_n^{-1}A_{n,a}, \quad \tilde{B}_{n,a} \equiv \Lambda_n^{-1}B_{n,a}, \quad \hat{B}_{n,a} = \Lambda_n^{-2}B_{n,a}v_a \quad (8.68)$$

where v_a are the bootstrap variables (8.44). Then the unitarization functional (8.66) is constructed as

$$V_a^{\text{uni}} = \text{Re}\tilde{h}_n\tilde{A}_{n,a} + \text{Im}\tilde{h}_n\tilde{B}_{n,a} - \sum_n \text{Im}\tilde{B}_{n,a} \quad (8.69)$$

where we maximize

$$\mathcal{F} = V_a^{\text{uni}}v_a \quad (8.70)$$

In this paper, we focus on the first 6 partial waves up to the energy scale s_0 and the index n in (8.69) takes values

$$n : I, \ell \in \{S0, D0, P1, F1, S2, D2\}, \quad s_{j=1,\dots,n_0} \quad (8.71)$$

Note that the unitarization step only modifies the optimization functional, with all the bootstrap constraints remaining the same. The result of this step is to get partial waves that saturate unitarity as much as the bootstrap allows. It is worth commenting that in a pure S-matrix bootstrap, such unitarization usually leads to unitarity saturation at all energy. In our case, it is then interesting that we observe possible particle production (in $D0$ wave around f_2 meson and in $P1$ wave around $\rho(1450)$) as indicated in fig. 4, hinting that the unitarity cannot be fully saturated within the GTB framework. This perhaps should not come as a total surprise. After all, we are including constraints to compute for a physical theory which necessarily includes particle production. It would be interesting to further investigate this production in a future work.

9 Conclusions

In a previous paper [1] we proposed the Gauge Theory Bootstrap, a method to study the strongly coupled QCD dynamics of pions at energies where the low energy effective field theory is no longer applicable. The idea was to find the most general S-matrix consistent with bootstrap constraints that matches the low and high energy theories. In particular we matched the gauge theory at an energy $\sqrt{s_0} = 1.2 \text{ GeV}$. The results of [1] were encouraging: we obtained phase shifts in agreement with

experiment and, in particular, the ρ vector meson. However one obvious question was if this agreement would persist if we increased s_0 . In fact one might have suspected that the mass of the ρ and other features of the phase shifts were due to the scale s_0 . In part motivated by this we apply here the same method but using a matching energy $\sqrt{s_0} = 2 \text{ GeV}$ roughly doubling the energy range. We also compute six partial waves instead of just three as before. The results are even better. The phase shifts agree with the ones found before, showing that s_0 is not introducing a scale. Moreover, in the new range of energies we find one strong resonance, the $f_2(1270)$ in the $D0$ channel and a weak new resonance in the $P1$ channel that we identified with the $\rho(1450)$. We even found a hint of particle production happening at the resonance energies suggesting a promising way to incorporate particle production through the resonance (*e.g.* $\pi\pi \rightarrow f_2 \rightarrow \pi\pi\pi\pi$) instead of bootstrapping the more general $\pi\pi \rightarrow \pi\pi\pi\pi$ amplitude. Overall, the new results are a strong indication that the method works and successfully locks into the correct amplitudes. Although this is very encouraging a lot of work remains to be done. In QCD we should include axial and pseudoscalar currents to introduce more constraints. Moreover, improvements need to be done for better identifying the point corresponding to the low energy QCD S-matrix perhaps even computing the value of f_π . Even more interesting could be to start exploring the space of gauge theories and see what happens if we change the number of colors or flavors, or if we take the pion lighter or more massive.

In summary, if we assume chiral symmetry breaking and confinement we can argue that the strongly coupled physics of gauge theories is dominated by pions and nucleons. However, effective field theory methods based on symmetry considerations alone do not allow us to solve the theory since even at moderate energies we need a large number of couplings (or Wilson coefficients) that we do not know how to compute from the gauge theory. We believe the Gauge Theory Bootstrap we proposed is a way to build a bridge between the low and high energy theories and allows to solve the strongly coupled QCD dynamics.

10 Acknowledgements

We want to thank all the colleagues that provided us with many comments, suggestions and encouragement after we published the previous paper and that we tried to reflect in this new publication. In particular we are grateful to B. Bellazini, F. Boudjema, L. Córdova, C. Delaunay, V. Gorbenko, K. Häring, J. Henriksson, A. Herderschee, C. Herzog, D. Karateev, Z. Komargodski, L. Lellouch, H. Osborn, M. Paulos, J. Peláez, J. Penedones, J. Qiao, F. Riva, S. Rychkov, A. Shapere, N. Su, P. Tourkine, A. Vainshtein, A. Vichi, S. Zhiboedov, and J.B. Zuber.

This work was supported in part by DOE through grant DE-SC0007884 and under the QuantiSED Fermilab consortium.

A Scattering lengths from chiral Lagrangian coefficients

In [31] Gasser and Leutwyler computed the scattering lengths in terms of the low energy parameters \bar{l}_j using one-loop chiral perturbation theory obtaining the result:

$$a_0^{(0)} = \frac{7m_\pi^2}{32\pi f_\pi^2} \left\{ 1 + \frac{5m_\pi^2}{84\pi^2 f_\pi^2} \left(\bar{l}_1 + 2\bar{l}_2 - \frac{3}{8}\bar{l}_3 + \frac{21}{10}\bar{l}_4 + \frac{21}{8} \right) \right\} \quad (\text{A.1})$$

$$b_0^{(0)} = \frac{1}{4\pi f_\pi^2} \left\{ 1 + \frac{m_\pi^2}{12\pi^2 f_\pi^2} \left(2\bar{l}_1 + 3\bar{l}_2 + \frac{3}{2}\bar{l}_4 - \frac{13}{16} \right) \right\} \quad (\text{A.2})$$

$$a_0^{(2)} = -\frac{m_\pi^2}{16\pi f_\pi^2} \left\{ 1 - \frac{m_\pi^2}{12\pi^2 f_\pi^2} \left(\bar{l}_1 + 2\bar{l}_2 - \frac{3}{8}\bar{l}_3 - \frac{3}{2}\bar{l}_4 + \frac{3}{8} \right) \right\} \quad (\text{A.3})$$

$$b_0^{(2)} = -\frac{1}{8\pi f_\pi^2} \left\{ 1 - \frac{m_\pi^2}{12\pi^2 f_\pi^2} \left(\bar{l}_1 + 3\bar{l}_2 - \frac{3}{2}\bar{l}_4 - \frac{5}{16} \right) \right\} \quad (\text{A.4})$$

$$a_1^{(1)} = \frac{1}{24\pi f_\pi^2} \left\{ 1 - \frac{m_\pi^2}{12\pi^2 f_\pi^2} \left(\bar{l}_1 - \bar{l}_2 - \frac{3}{2}\bar{l}_4 + \frac{65}{48} \right) \right\} \quad (\text{A.5})$$

$$b_1^{(1)} = \frac{1}{288\pi^3 f_\pi^4} \left(-\bar{l}_1 + \bar{l}_2 + \frac{97}{120} \right) \quad (\text{A.6})$$

$$a_2^{(0)} = \frac{1}{1440\pi^3 f_\pi^4} \left(\bar{l}_1 + 4\bar{l}_2 - \frac{53}{8} \right) \quad (\text{A.7})$$

$$a_2^{(2)} = \frac{1}{1440\pi^3 f_\pi^4} \left(\bar{l}_1 + \bar{l}_2 - \frac{103}{40} \right) \quad (\text{A.8})$$

Notice that we rewrote their formulas in terms of renormalized parameters and used the physical pion mass and f_π . It makes sense then to recompute the scattering lengths using the low energy parameters obtained in table 3 (we set $\bar{l}_3 = 0$ since we are not able to evaluate it independently). The results are presented in table 8. They agree reasonably well with the direct extraction as given in table 1 (denoted as GTB here).

	GTB	GTBII	PY
$a_0^{(0)}$	0.178, 0.182	0.21, 0.21	0.230 ± 0.010
$a_0^{(2)}$	-0.0369, -0.0378	-0.044, -0.044	-0.0422 ± 0.0022
$b_0^{(0)}$	0.287, 0.290	0.26, 0.25	0.268 ± 0.010
$b_0^{(2)}$	-0.064, -0.066	-0.080, -0.082	-0.071 ± 0.004
$a_1^{(1)}$	28.0, 28.4	35.8, 35.6	$38.1 \pm 1.4 \times 10^{-3}$
$b_1^{(1)}$	2.86, 3.37	2.35, 2.31	$4.75 \pm 0.16 \times 10^{-3}$
$a_2^{(0)}$	12.6, 12.3	12.6, 12.3	$18.0 \pm 0.2 \times 10^{-4}$
$a_2^{(2)}$	2.87, 2.81	2.9, 2.8	$2.2 \pm 0.2 \times 10^{-4}$

Table 8: Scattering lengths, units of m_π , consistency check. GTBII are computed using in (A.1)–(A.8) the values from table 3. There is reasonable agreement between the three columns including phenomenological data from PY [19].

B Test on numerical parameters M, L

As described in section 8.4, to carry out the numerical computation, we discretize the bootstrap variables (8.44) by taking $M = 50$. In addition, we impose the unitarity constraints in the physical region for partial waves up to angular momentum $L = 19$. In this section, we present a brief test on how sensitive the results are when changing M, L .

In figure 17, we show the results on the phase shifts δ_ℓ^I and inelasticity η_ℓ^I (as in fig. 4) for three choice of numerical parameters: $M = 50, L = 19$ (red), $M = 50, L = 23$ (green), $M = 60, L = 19$ (purple). It is clear that at $M = 50, L = 19$ the results have attained a good convergence in the sense that by increasing M, L the phase shifts do not change much. The only subtlety is that in $D0$ wave, the phase rise identified with $f_2(1270)$ is slightly shifted for $M = 60, L = 10$. This is likely due to the fact that at 2 GeV, the $D0$ form factor is not quite in the asymptotic region: since changing M shifts the point n_0 slightly, the bounds on the asymptotic behavior (8.65) (which we keep fixed in this test) is slightly different for $M = 60$ and $M = 50$.

C Form factors asymptotics

The computation of asymptotic form factors is standard in QCD. However, for completeness we compute in this appendix the Feynman diagram (a) of fig.13. The diagram is computed as a tree level diagrams with external quark states giving what is called the kernel that has to be inserted between pion states:

$$\begin{aligned} \mathbb{T}_{1\text{-diag}}^{(a)} &= (ig)^2 \left(\bar{u}_{k'}^{s'_1} \gamma^\mu \frac{i(\not{k} + \not{p}' - \not{p})}{(k + p' - p)^2} \not{A} u_k^{s_1} \right) \left(\bar{v}_{p-k}^{s_1} \gamma_\mu v_{p'-k'}^{s'_1} \right) \frac{(-i)}{(p - k - p' + k')^2} \times \\ &\quad (-ik\Delta)^{\ell-1} t_{ca}^{\hat{D}} t_{ac}^{\hat{D}} \delta_{AB'} \delta_{A'C} \delta_{BD} \end{aligned} \quad (\text{C.1})$$

Writing $k = xp + k_\perp$ and $k' = x'p' + k'_\perp$ and taking the high energy limit where $s = (p - p')^2 \simeq -2pp' \rightarrow \infty$ is the only term we keep, we perform the replacements

$$(k + p' - p)^2 \rightarrow (1 - x)s, \quad (p - k - p' + k')^2 \rightarrow (1 - x)(1 - x')s, \quad (k\Delta) \rightarrow x(p\Delta), \quad (\text{C.2})$$

$$\bar{u}_{k'}^{s'_1} \rightarrow \sqrt{x'} \bar{u}_{p'}^{s'_1} \quad u_k^{s_1} \rightarrow \sqrt{x} u_p^{s_1} \quad \bar{v}_{p-k}^{s_1} \rightarrow \sqrt{1-x} \bar{v}_p^{s_1} \quad v_{p'-k'}^{s'_1} \rightarrow \sqrt{1-x'} v_{p'}^{s'_1} \quad (\text{C.3})$$

We can now further simplify the result with the identities (valid since we choose $v_p^s = -\gamma_5 u_p^s$):

$$v_{p'}^s \bar{u}_{p'}^s = -\gamma_5 (\not{p}' + m_q), \quad u_p^s \bar{v}_p^s = (\not{p} + m_q) \gamma_5 \quad (\text{C.4})$$

we find, using, $t_{ca}^{\hat{D}} t_{ac}^{\hat{D}} = C_2(N_c) = \frac{N_c^2 - 1}{2}$, the result

$$\mathbb{T}_{1\text{-diagram}}^{(a)} = \sqrt{x(1-x)x'(1-x')} \delta_{AB'} \delta_{A'C} \delta_{BD} \frac{8ig^2 C_2(N_c)}{s} (-ip\Delta)^{\ell-1} \frac{x^{\ell-1}}{(1-x)(1-x')} \quad (\text{C.5})$$

which is used in the main text. There we included the other three diagrams of the same form where the current is inserted in the other fermionic lines.

D Some integrals

In this appendix we include some integrals that can be done by standard methods and that we find useful in the main text.

D.1 Feynman type integrals

$$\int \frac{d^d k}{(2\pi)^d} \frac{k^{2\ell}}{(k^2 - \tilde{\Delta} + i\epsilon)^n} = i \frac{(-1)^{\ell+n}}{(4\pi)^{\frac{d}{2}}} \frac{\Gamma(\frac{d}{2} + \ell) \Gamma(n - \frac{d}{2} - \ell)}{\Gamma(n) \Gamma(\frac{d}{2}) (\tilde{\Delta} - i\epsilon)^{n - \frac{d}{2} - \ell}} \quad (\text{D.1})$$

$$\int \frac{d^d k}{(2\pi)^d} \frac{(ik\Delta)^\ell (ik\bar{\Delta})^\ell}{(k^2 - \tilde{\Delta} + i\epsilon)^n} = i \frac{(-1)^n}{2^\ell (4\pi)^{\frac{d}{2}}} \frac{\ell! (\Delta\bar{\Delta})^\ell \Gamma(n - \frac{d}{2} - \ell)}{\Gamma(n) (\tilde{\Delta} - i\epsilon)^{n - \frac{d}{2} - \ell}} \quad (\text{D.2})$$

where $\Delta^2 = 0 = \bar{\Delta}^2$. These are useful to compute current correlators.

D.2 Multi-ball integrals

In the case of four particle states it is useful to compute integrals of the form

$$\int \prod_{j=1}^4 d^3 k_j \delta(\sum_{j=1}^4 |\vec{k}_j| - 1) \delta^{(3)}(\sum_{j=1}^4 \vec{k}_j) = \frac{11\pi^3}{26880} \quad (\text{D.3})$$

$$\int \prod_{j=1}^4 d^3 k_j \delta(\sum_{j=1}^4 |\vec{k}_j| - 1) \delta^{(3)}(\sum_{j=1}^4 \vec{k}_j) (1 - \hat{k}_1 \hat{k}_2)(1 - \hat{k}_3 \hat{k}_4) = \frac{\pi^3}{1440} \quad (\text{D.4})$$

that measures in some way the phase space available to four massless particles at given energy and in the center of mass. As an example, one way to compute these integrals is ($\lambda > 0$ is an arbitrary constant)

$$\begin{aligned} & \int \prod_{j=1}^4 d^3 k_j \delta(\sum_{j=1}^4 |\vec{k}_j| - 1) \delta^{(3)}(\sum_{j=1}^4 \vec{k}_j) \\ &= e^\lambda \int \frac{d^4 x}{(2\pi)^4} e^{-ix_0} \prod_{j=1}^4 d^3 k_j e^{-(\lambda - ix_0)|\vec{k}_j| + i\vec{k}_j \vec{x}} \\ &= 2^{12} \pi^4 \int \frac{d^4 x}{(2\pi)^4} e^{\lambda - ix_0} \frac{(\lambda - ix_0)^4}{((\lambda - ix_0)^2 + x^2)^8} \\ &= \frac{2^{12} \pi^4 \Gamma(\frac{13}{2})}{\Gamma(8) (4\pi)^{\frac{3}{2}}} \int \frac{dx_0}{2\pi} \frac{e^{\lambda - ix_0}}{(\lambda - ix_0)^9} \\ &= \frac{11\pi^3}{26880} \end{aligned} \quad (\text{D.5})$$

References

- [1] Y. He and M. Kruczenski, “Bootstrapping gauge theories,” [arXiv:2309.12402](#) [[hep-th](#)].
- [2] G. Chew, *The Analytic S Matrix: A Basis for Nuclear Democracy*.
- [3] R. J. Eden, P. V. Landshoff, D. I. Olive, and J. C. Polkinghorne, *The analytic S-matrix*. Cambridge Univ. Press, Cambridge, 1966.

- [4] M. F. Paulos, J. Penedones, J. Toledo, B. C. van Rees, and P. Vieira, “The S-matrix bootstrap. Part I: QFT in AdS,” *JHEP* **11** (2017) 133, [arXiv:1607.06109 \[hep-th\]](#).
- [5] M. F. Paulos, J. Penedones, J. Toledo, B. C. van Rees, and P. Vieira, “The S-matrix bootstrap II: two dimensional amplitudes,” *JHEP* **11** (2017) 143, [arXiv:1607.06110 \[hep-th\]](#).
- [6] M. F. Paulos, J. Penedones, J. Toledo, B. C. van Rees, and P. Vieira, “The S-matrix bootstrap. Part III: higher dimensional amplitudes,” *JHEP* **12** (2019) 040, [arXiv:1708.06765 \[hep-th\]](#).
- [7] M. Kruczenski, J. Penedones, and B. C. van Rees, “Snowmass White Paper: S-matrix Bootstrap,” [arXiv:2203.02421 \[hep-th\]](#).
- [8] D. Karateev, S. Kuhn, and J. a. Penedones, “Bootstrapping Massive Quantum Field Theories,” *JHEP* **07** (2020) 035, [arXiv:1912.08940 \[hep-th\]](#).
- [9] S. Weinberg, “Pion scattering lengths,” *Phys. Rev. Lett.* **17** (1966) 616–621.
- [10] M. Shifman, A. Vainshtein, and V. Zakharov, “Qcd and resonance physics. theoretical foundations,” *Nuclear Physics B* **147** no. 5, (1979) 385–447.
- [11] M. Shifman, A. Vainshtein, and V. Zakharov, “Qcd and resonance physics. applications,” *Nuclear Physics B* **147** no. 5, (1979) 448–518.
- [12] M. A. Shifman, A. I. Vainshtein, and V. I. Zakharov, “QCD and Resonance Physics. The rho-omega Mixing,” *Nucl. Phys. B* **147** (1979) 519–534.
- [13] V. A. Novikov, L. B. Okun, M. A. Shifman, A. I. Vainshtein, M. B. Voloshin, and V. I. Zakharov, “Charmonium and Gluons: Basic Experimental Facts and Theoretical Introduction,” *Phys. Rept.* **41** (1978) 1–133.
- [14] L. J. Reinders, “SPECTROSCOPY WITH QCD SUM RULES,” 9, 1981.
- [15] L. J. Reinders, H. Rubinstein, and S. Yazaki, “Hadron Properties from QCD Sum Rules,” *Phys. Rept.* **127** (1985) 1.
- [16] P. Gubler and D. Satow, “Recent Progress in QCD Condensate Evaluations and Sum Rules,” *Prog. Part. Nucl. Phys.* **106** (2019) 1–67, [arXiv:1812.00385 \[hep-ph\]](#).

- [17] G. Peter Lepage and S. J. Brodsky, “Exclusive processes in quantum chromodynamics: Evolution equations for hadronic wavefunctions and the form factors of mesons,” *Physics Letters B* **87** no. 4, (11, 1979) .
- [18] B. Pire, “Exclusive reactions in QCD,” in *Les Houches Summer School on Theoretical Physics, Session 66: Trends in Nuclear Physics, 100 Years Later*, pp. 567–591. 7, 1996. [arXiv:nucl-th/9612009](#).
- [19] J. R. Pelaez and F. J. Yndurain, “The Pion-pion scattering amplitude,” *Phys. Rev. D* **71** (2005) 074016, [arXiv:hep-ph/0411334](#).
- [20] F. J. Yndurain, “Low-energy pion physics,” [arXiv:hep-ph/0212282](#).
- [21] G. Colangelo, J. Gasser, and H. Leutwyler, “ $\pi\pi$ scattering,” *Nucl. Phys. B* **603** (2001) 125–179, [arXiv:hep-ph/0103088](#).
- [22] A. Guerrieri, J. Penedones, and P. Vieira, “S-matrix Bootstrap for Effective Field Theories: Massless Pions,” [arXiv:2011.02802 \[hep-th\]](#).
- [23] A. L. Guerrieri, J. Penedones, and P. Vieira, “Bootstrapping QCD Using Pion Scattering Amplitudes,” *Phys. Rev. Lett.* **122** no. 24, (2019) 241604, [arXiv:1810.12849 \[hep-th\]](#).
- [24] J. Albert and L. Rastelli, “Bootstrapping pions at large N ,” *JHEP* **08** (2022) 151, [arXiv:2203.11950 \[hep-th\]](#).
- [25] C. Fernandez, A. Pomarol, F. Riva, and F. Sciotti, “Cornering large- N_c QCD with positivity bounds,” *JHEP* **06** (2023) 094, [arXiv:2211.12488 \[hep-th\]](#).
- [26] J. Albert and L. Rastelli, “Bootstrapping Pions at Large N . Part II: Background Gauge Fields and the Chiral Anomaly,” [arXiv:2307.01246 \[hep-th\]](#).
- [27] T. Ma, A. Pomarol, and F. Sciotti, “Bootstrapping the chiral anomaly at large N_c ,” *JHEP* **11** (2023) 176, [arXiv:2307.04729 \[hep-th\]](#).
- [28] J. Albert, J. Henriksson, L. Rastelli, and A. Vichi, “Bootstrapping mesons at large N : Regge trajectory from spin-two maximization,” [arXiv:2312.15013 \[hep-th\]](#).
- [29] A. Keshavarzi, K. S. Khaw, and T. Yoshioka, “Muon $g-2$: A review,” *Nuclear Physics B* **975** (2022) 115675.

- [30] M. Davier, Z. Fodor, A. Gerardin, L. Lellouch, B. Malaescu, F. M. Stokes, K. K. Szabo, B. C. Toth, L. Varnhorst, and Z. Zhang, “Hadronic vacuum polarization: comparing lattice QCD and data-driven results in systematically improvable ways,” [arXiv:2308.04221 \[hep-ph\]](#).
- [31] J. Gasser and H. Leutwyler, “Chiral perturbation theory to one loop,” *Annals of Physics* **158** no. 1, (1984) 142–210.
- [32] J. Gasser, “Chiral perturbation theory and effective lagrangians,” *Nuclear Physics B* **279** no. 1, (1987) 65–79.
- [33] S. Scherer, “Introduction to chiral perturbation theory,” *Adv. Nucl. Phys.* **27** (2003) 277, [arXiv:hep-ph/0210398](#).
- [34] B. Martin, D. Morgan, and G. Shaw, *Pion-Pion Interactions in particle physics*. Academic Press, 1976.
- [35] J. F. Donoghue, E. Golowich, and B. R. Holstein, *Dynamics of the Standard Model*. Cambridge Monographs on Particle Physics, Nuclear Physics and Cosmology. Cambridge University Press, 2 ed., 2014.
- [36] L. Córdova, Y. He, M. Kruczenski, and P. Vieira, “The O(N) S-matrix Monolith,” *JHEP* **04** (2020) 142, [arXiv:1909.06495 \[hep-th\]](#).
- [37] Y. He, A. Irrgang, and M. Kruczenski, “A note on the S-matrix bootstrap for the 2d O(N) bosonic model,” *JHEP* **11** (2018) 093, [arXiv:1805.02812 \[hep-th\]](#).
- [38] S. D. Protopopescu, M. Alston-Garnjost, A. Barbaro-Galtieri, S. M. Flatte, J. H. Friedman, T. A. Lasinski, G. R. Lynch, M. S. Rabin, and F. T. Solmitz, “Pi pi Partial Wave Analysis from Reactions $\pi^+ p \rightarrow \pi^+ \pi^- \Delta^{++}$ and $\pi^+ p \rightarrow K^+ K^- \Delta^{++}$ at 7.1-GeV/c,” *Phys. Rev. D* **7** (1973) 1279.
- [39] M. Losty, V. Chaloupka, A. Ferrando, L. Montanet, E. Paul, D. Yaffe, A. Zieminski, J. Alitti, B. Gandois, and J. Louie., “A study of $\pi\pi$ scattering from $\pi - p$ interactions at 3.93 gev/c,” *Nuclear Physics B* **69** (1974) 185–204.
- [40] B. Hyams *et al.*, “A Study of All the pi pi Phase Shift Solutions in the Mass Region 1.0-GeV to 1.8-GeV from $\pi^- p \rightarrow \pi^- \pi^+ n$ at 17.2-GeV,” *Nucl. Phys. B* **100** (1975) 205–224.

- [41] J. F. Donoghue, J. Gasser, and H. Leutwyler, “The decay of a light higgs boson,” *Nuclear Physics B* **343** no. 2, (1990) 341–368.
- [42] S. Amendolia and Others, “A measurement of the space-like pion electromagnetic form factor,” *Nuclear Physics B* **277** (1986) 168–196.
- [43] J. Bijnens, G. Colangelo, and P. Talavera, “The Vector and scalar form-factors of the pion to two loops,” *JHEP* **05** (1998) 014, [arXiv:hep-ph/9805389](#).
- [44] J. Bijnens, G. Colangelo, G. Ecker, J. Gasser, and M. E. Sainio, “Pion-pion scattering at low energy,” *Nucl. Phys. B* **508** (1997) 263–310, [arXiv:hep-ph/9707291](#).
- [45] J. Bijnens, G. Colangelo, and J. Gasser, “K(l4) decays beyond one loop,” *Nucl. Phys. B* **427** (1994) 427–454, [arXiv:hep-ph/9403390](#).
- [46] G. J. Gounaris and J. J. Sakurai, “Finite width corrections to the vector meson dominance prediction for $\rho \rightarrow e^+e^-$,” *Phys. Rev. Lett.* **21** (1968) 244–247.
- [47] M. E. Peskin and D. V. Schroeder, *An Introduction to quantum field theory*. Addison-Wesley, Reading, USA, 1995.
- [48] F. Halzen and A. Martin, *Quarks and Leptons*. John Wiley and Sons, New York, 1984.
- [49] **Particle Data Group** Collaboration, R. L. Workman and Others, “Review of Particle Physics,” *PTEP* **2022** (2022) 083C01.
- [50] C. Ewerz, M. Maniatis, and O. Nachtmann, “A model for soft high-energy scattering: Tensor pomeron and vector odderon,” *Annals of Physics* **342** (2014) 31–77.
- [51] J. Sakurai, *current and mesons*. The University of Chicago Press, Chicago, London, 1973.
- [52] B. Ananthanarayan, I. Caprini, G. Colangelo, J. Gasser, and H. Leutwyler, “Scalar form factors of light mesons,” *Physics Letters B* **602** no. 3-4, (Nov, 2004) 218–225.
- [53] X.-B. Tong, J.-P. Ma, and F. Yuan, “Gluon gravitational form factors at large momentum transfer,” *Physics Letters B* **823** (Dec., 2021) 136751.

- [54] K. Raya, Z.-F. Cui, L. Chang, J. M. Morgado, C. D. Roberts, and J. Rodríguez-Quintero, “Revealing pion and kaon structure via generalised parton distributions *,” *Chinese Physics C* **46** no. 1, (Jan, 2022) 013105.
- [55] S. Kumano, Q.-T. Song, and O. V. Teryaev, “Hadron tomography by generalized distribution amplitudes in the pion-pair production process $\gamma^*\gamma \rightarrow \pi^0\pi^0$ and gravitational form factors for pion,” *Phys. Rev. D* **97** (Jan, 2018) 014020.
- [56] X.-B. Tong, J.-P. Ma, and F. Yuan, “Perturbative calculations of gravitational form factors at large momentum transfer,” *Journal of High Energy Physics* **2022** no. 10, (Oct., 2022) .
- [57] P. Hoodbhoy, X.-d. Ji, and F. Yuan, “Probing quark distribution amplitudes through generalized parton distributions at large momentum transfer,” *Phys. Rev. Lett.* **92** (2004) 012003, [arXiv:hep-ph/0309085](#).
- [58] K. Tanaka, “Operator relations for gravitational form factors of a spin-0 hadron,” *Physical Review D* **98** no. 3, (Aug., 2018) .
- [59] D. Karateev, “Two-point functions and bootstrap applications in quantum field theories,” *JHEP* **02** (2022) 186, [arXiv:2012.08538 \[hep-th\]](#).
- [60] H. Chen, A. L. Fitzpatrick, and D. Karateev, “Bootstrapping 2d ϕ^4 theory with Hamiltonian truncation data,” *JHEP* **02** (2022) 146, [arXiv:2107.10286 \[hep-th\]](#).
- [61] M. Correia, J. Penedones, and A. Vuignier, “Injecting the UV into the bootstrap: Ising Field Theory,” *JHEP* **08** (2023) 108, [arXiv:2212.03917 \[hep-th\]](#).
- [62] L. Cordova, M. Correia, A. Georgoudis, and A. Vuignier, “The O(N) monolith reloaded: sum rules and Form Factor Bootstrap,” *JHEP* **01** (2024) 093, [arXiv:2311.03031 \[hep-th\]](#).
- [63] S. Narison, *QCD as a Theory of Hadrons: From Partons to Confinement*. Cambridge Monographs on Particle Physics, Nuclear Physics and Cosmology. Cambridge University Press, 2004.
- [64] S. Caron-Huot, A. Pokraka, and Z. Zahraee, “Two-point sum-rules in three-dimensional Yang-Mills theory,” *JHEP* **01** (2024) 195, [arXiv:2309.04472 \[hep-th\]](#).

- [65] M. F. Zoller and K. G. Chetyrkin, “Ope of the energy-momentum tensor correlator in massless qcd,” *Journal of High Energy Physics* **2012** no. 12, (Dec., 2012) .
- [66] J. I. Latorre and P. Pascual, “QCD Sum Rules and the $\bar{q}q\bar{q}q$ System,” *J. Phys. G* **11** (1985) L231.
- [67] M. Grant and S. Boyd, “CVX: Matlab software for disciplined convex programming, version 2.1.” <http://cvxr.com/cvx>, Mar., 2014.
- [68] M. Grant and S. Boyd, “Graph implementations for nonsmooth convex programs,” in *Recent Advances in Learning and Control*, V. Blondel, S. Boyd, and H. Kimura, eds., Lecture Notes in Control and Information Sciences, pp. 95–110. Springer-Verlag Limited, 2008.
- [69] S. Boyd, L. Vandenberghe, and C. U. Press, *Convex Optimization*. No. pt. 1 in Berichte über verteilte messsysteme. Cambridge University Press, 2004.
- [70] M. ApS, *The MOSEK optimization toolbox for MATLAB manual. Version 10.1.*, 2024. <http://docs.mosek.com/latest/toolbox/index.html>.
- [71] Y. He and M. Kruczenski, “S-matrix bootstrap in 3+1 dimensions: regularization and dual convex problem,” *JHEP* **08** (2021) 125, [arXiv:2103.11484](https://arxiv.org/abs/2103.11484) [hep-th].

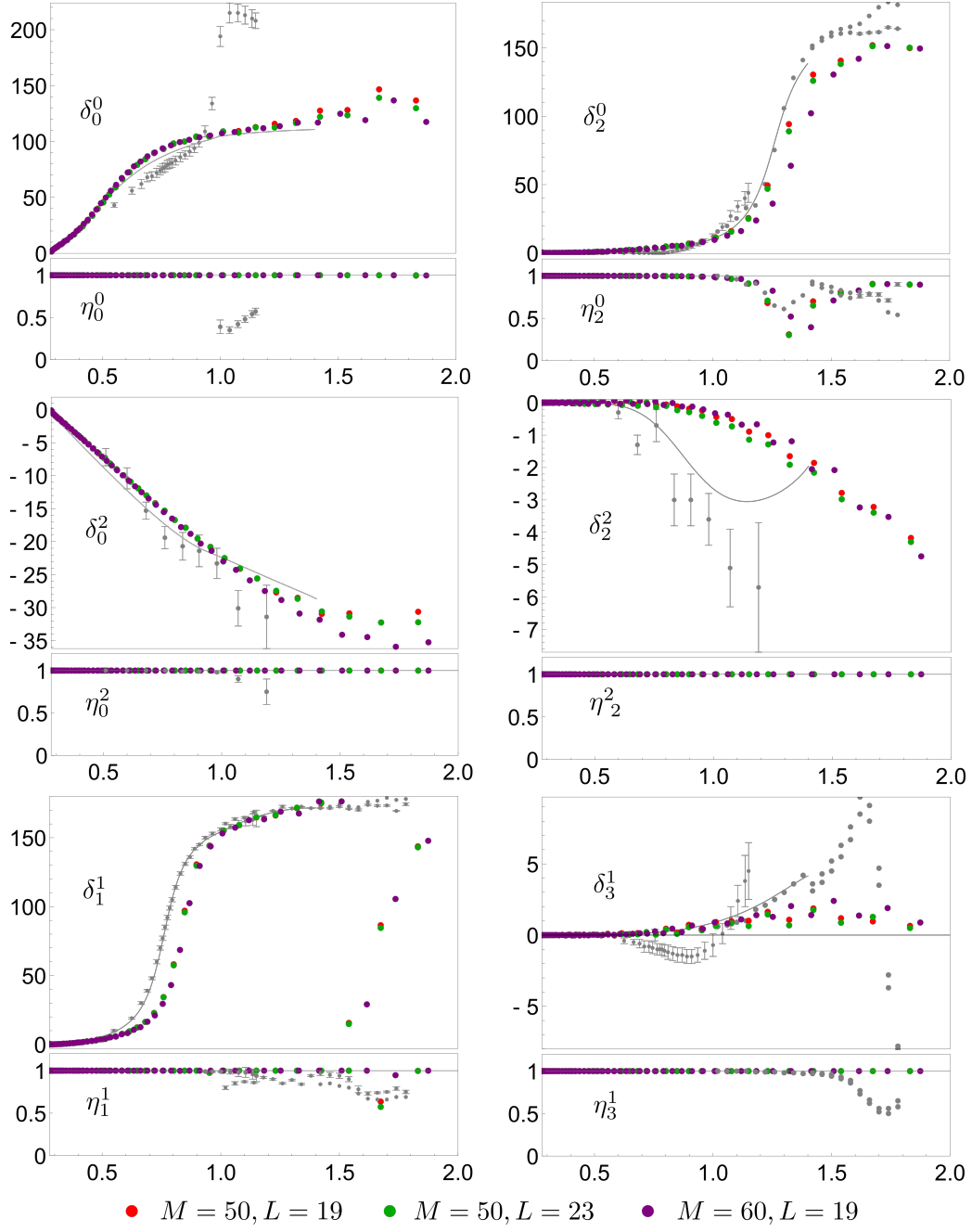


Figure 17: Phase shifts δ_ℓ^I and inelasticity η_ℓ^I from GTB with different numerical parameters M, L .